MULTI-H PHASE CODING

By

ANNE TRØYM LEREIM, siv.ing.

A Thesis

Submitted to the Faculty of Graduate Studies

in Partial Fulfilment of the Requirements

for the Degree

Master of Engineering

McMaster University

June, 1978

MULTI-H PHASE CODING

MASTER OF ENGINEERING (1978)
(Electrical Engineering)

McMASTER UNIVERSITY
Hamilton, Ontario

TITLE: Multi-h-phase coding

AUTHOR: Anne Trøym Lereim, sivilingeniør (N.T.H., Norway)

SUPERVISOR: Professor D.P. Taylor

NUMBER OF PAGES: viii, 121

ABSTRACT

The main objective of this thesis is to investigate the spectral properties of Multi-h phase coding and to consider the trade-offs between error performance and bandwidth occupancy for this modulation method.

There are multi-h phase codes which allow for a wide range of trade-offs. For example, there is a bandwidth-efficient code which occupies 23% less bandwidth than Fast Frequency Shift Keying (Fast FSK) but requires 2.4 dB more power to give the same noise immunity. There is also a code that needs 40% more bandwidth than Fast FSK but yields the same transmission quality with a 3.7 dB savings in power.

The power spectrum of a multi-h code is line-free and the tail of the spectrum rolls off as $1/f^4$ as in Fast FSK.

Three different methods for spectral analysis are presented and compared. We have found that approaches based upon the Wiener-Khinchin Theorem are to be preferred.

Pelchat's analysis of binary FSK with continuous phase is extended to the general multi-index case.

A multi-h code can be modelled as a Markov chain and the auto-correlation function can be calculated using the theory for such processes. We have devised a simple procedure for identifying the states of the Markov chain.

ACKNOWLEDGEMENT

The author gratefully acknowledges the support and guidance given by her supervisor, Dr. D.P. Taylor, throughout this study of phase coding. She would also like to thank Dr. J.B. Anderson for the many helpful discussions.

This work was supported by the National Research Council of Canada.

TABLE OF CONTENTS

TABLE OF CONTENTS (continued)

LIST OF FIGURES

LIST OF FIGURES (continued)

CHAPTER 1

INTRODUCTION

The growing need for digital transmission demands efficient utilization of the allocated radio spectrum, [1], [2]. In order to conserve spectrum, the band occupancy of the chosen modulation scheme must be small so that many channels can be accommodated in a given band.

This has lead to the search for spectrally efficient modulation methods for use in satellite communications and on heavy traffic terrestrial links.

Amplitude modulation techniques are seldom used over satellite channels because the non-linear effects of the channel tend to destroy or mutilate any amplitude information carried by the transmitted signal. Less sensitive to the non-linear media effects are constant-envelope signals which convey the information in their phase or frequency. For satellite communications, therefore, Phase Shift Keying (PSK) and Frequency Shift Keying (FSK) are the forms of modulation to be used.

Unfortunately, neither binary coherent PSK nor conventional orthogonal FSK are suited for high-speed data transmission because of their large bandwidth requirements. However, the band occupancy may be reduced by modifying the transmitted sequence of waveforms. This is known as Spectrally Efficient Modulation [2].

The modifications can be done in two ways. First, shaping of the transmitted waveforms may reduce the bandwidth needs in order to maximize the transmission rate for a given bandwidth. Second, we can introduce changes in the nature of the sequence by using m-ary signalling. Blocks of m binary data are then represented by a single symbol carrying m bits of information, and thus data are transmitted at a higher rate provided the length of the symbol interval, T, is kept constant.

The main objective of spectral efficient modulation is to maximize the transmitted data rate through a given bandwidth and the bandwidth efficiency is defined by

$$\eta = \frac{m/T}{W} \text{ [bits per sec per Hz]}$$

where W is the band occupancy of the transmitted signal.

Multilevel coherent phase shift keying illustrates how the modification of the sequence characteristics can reduce the bandwidth needs.

Four phase PSK (QPSK) is the most widely used modulation method for data transmission. This technique conserves bandwidth as well as power, and the constant envelope makes the signal relatively immune to non-linear effects of the channel. However, it only achieves a theoretical efficiency of $\eta = 0.1$ bits per sec. per Hz. This result assumes that 99% of the energy in the modulated signal is passed through the bandwidth W [3].

When the receiver has to distinguish between more phases, the system is inevitably more sensitive to noise and interference, and as a result the power per symbol must be increased if the error rate is to be kept at an acceptable level. We can say that m-ary modulation schemes use power to save bandwidth.

Pulse shaping is employed in the socalled Fast FSK (or Minimum Shift Keying, MSK), [4]-[9], which is a special case of FSK with modulation index h equal to 0.5. The pulse shaping makes the phase of the signal continuous at the transitions and so the power spectrum exhibits very rapid roll-off characteristics. Fast FSK has the same error performance as QPSK and it tends to be less sensitive to narrow-band filtering. The theoretical efficiency of Fast FSK is η = 0.8 bits per sec per Hz.

Another and more complex continuous-phase FSK (CPFSK) scheme has recently been proposed by Miyakawa et al [10]. The modulation method is called Multi-mode binary CPFSK since the modulation index is varied cyclically from baud to baud. Anderson and deBuda [11] have shown that the demodulation may be simplified by placing certain restrictions on the set of low modulation indices, and they call their modified multi-mode CPFSK Multi-h phase <u>coding</u> to emphasize that the continuous phase introduces memory into the signal.

The error performance of multi-h phase codes have been investigated by Anderson and Taylor [12]-[14], who found that there are codes which for a given error rate require 2-4 dB less power than Fast FSK. However, coding is said to use bandwidth to save power. The question is, therefore, whether the penalty - in terms of band occupancy

- to be paid for the improvement in error performance is such that the codes do not meet the requirement of bandwidth economy.

We have seen that spectrally efficient modulation uses power to save bandwidth. So if there are bandwidth efficient codes, what is the degradation in transmission quality to be paid for the savings in bandwidth?

Are multi-h phase codes of any use for high-quality, high-speed data transmission?

The main objective of this work is to answer the above questions. One remarkable answer is: Compared to Fast FSK, the improvement in noise immunity is obtained at no or a small expense of bandwidth. Another interesting result is that some multi-h phase codes are very bandwidth efficient. While codes with the same error performance as Fast FSK require 12% less bandwidth, there are codes which can be passed through a 25% narrower band than Fast FSK and require only 2.4 dB more power for a given error rate. Those latter codes have an efficiency of 1.1 bits per sec per Hz.

The multi-h phase codes and their error performance are presented in Chapter 2. Their power spectra are developed in Chapter 4, and the spectral properties are discussed in detail. Chapter 5 deals with the trade-off between power conservation and bandwidth economy.

The spectral analysis follows two approaches. The first is based on the Wiener-Khinchin Theorem which states that the autocorrelation function and the power spectrum of a signal form a Fourier transform pair. The other approach is more direct and approximates the power spectrum by the energy distribution of a truncated version of the signal. The different methods are described and compared in Chapter 3.

CHAPTER 2

MULTI-H PHASE CODING

This chapter presents briefly the multi-h phase codes and their error performance properties. A broader presentation is given in [10]-[14].

2.1 Conventional CPFSK

Multi-h phase codes are, as we shall see, essentially frequency shift keyed signals where the phase is constrained to be continuous during a symbol transition. In order to introduce some notation, we will therefore first consider a simple conventional CPFSK signal of the form

$$s(t) = \sqrt{\frac{2E}{T}} \cdot \cos\left(2\pi f_c t + \phi(t) + \alpha\right) \qquad (1)$$

where the constant-envelope signal s(t) has symbol energy E, the signalling interval is of duration T and α is an arbitrary initial phase of the carrier.

The time-varying phase $\phi(t)$ is related to the modulating signal x(t) by

$$\phi(t) = \int_0^t x(t') \, dt' \qquad (2)$$

We will assume the modulating signal $x(t)$ to be a train of non-overlapping, rectangular pulses, with the pulse $x_i(t)$ corresponding to the digital data symbol a_i in baud no. i. Thus $\phi(t)$ is a continuous and piecewise linear function, representing the phase of the modulated signal referred to the carrier term's linearly increasing phase, and so $\phi(t)$ will be called the excess phase function.

The pulse train $x(t)$ may be written

$$x(t) = \sum_{i=0}^{\infty} x_i(t - iT) \tag{3}$$

If we separate the shape of $x_i(t)$ from its weighting coefficient, $x_i(t)$ may be expressed as

$$x_i(t) = a_i \omega g(t) \tag{4}$$

where a_i is the binary data (± 1) in baud no. i, $g(t)$ is a rectangular pulse of unit height defined on $[0, T]$, and ω is defined by

$$\omega = \frac{\pi \cdot h}{T} \tag{5}$$

Here, h is the modulation index or the deviation ratio as defined in Fig. 2.

The signal $s(t)$ in baud no. i is ($\alpha = 0$)

$$s(t) = \sqrt{\frac{2E}{T}} \cos(2\pi f_c t \pm \frac{\pi h}{T} (t-iT) + \phi(iT)), \tag{6}$$

$$iT \leq t < (i+1)T$$

Fig. 1 shows the signals $x(t)$, $\phi(t)$, and $s(t)$ for a particular sequence of binary data. The excess phase function in Fig. 1 is a particular path along the phase trellis of possible paths shown in Fig. 2a. Since phase occurs modulo-2π, the phase trellis actually lies on a cylinder, not on a plane, and Fig. 2b and 2c show the phase trellises for signals with modulation index $h = 1/2$ (Fast FSK) and $h = 2/3$ respectively. The broken lines indicate phase transitions along the back of the cylinder.

Unless otherwise stated, we shall in the following reserve the name phase trellis for trellises mapped on a cylinder.

When the modulation index h is a rational number, the phase trellis is periodic with period T or 2T [Appendix A].

2.2 Multi-h Phase Coding

Let us now return to the multi-h phase coded signals.

Multi-h phase coding may be considered as a generalization of CPFSK where the modulation index is varied cyclically from baud to baud. If $\{h_1, h_2, \ldots, h_K\}$ is the set of indices available to the modulator, the index in baud i equals the index in baud i+K. In order to get a periodic phase trellis, we consider only rational indices, and we will assume that the modulation is narrowbanded, i.e. $h \leq 1$. Further, we will require the phase trellis to have constraint length K. This means that two trellis paths remain separated over at least K+1 bauds. The phase trellis has constraint length K if no two subsets of the K indicies have the same sum, modulo 1 [12], [13], [14].

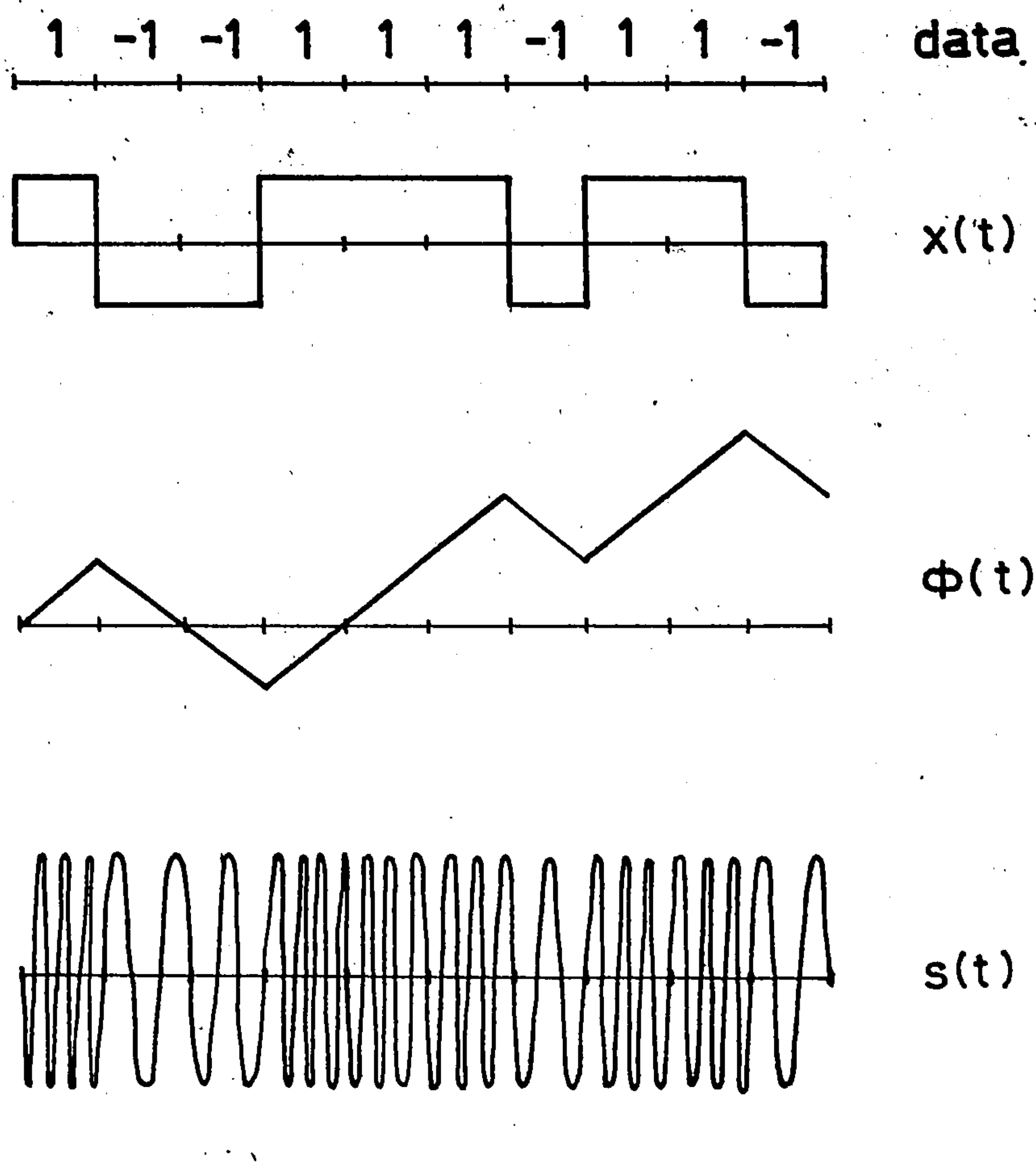

Fig. 1. CONVENTIONAL CPFSK.

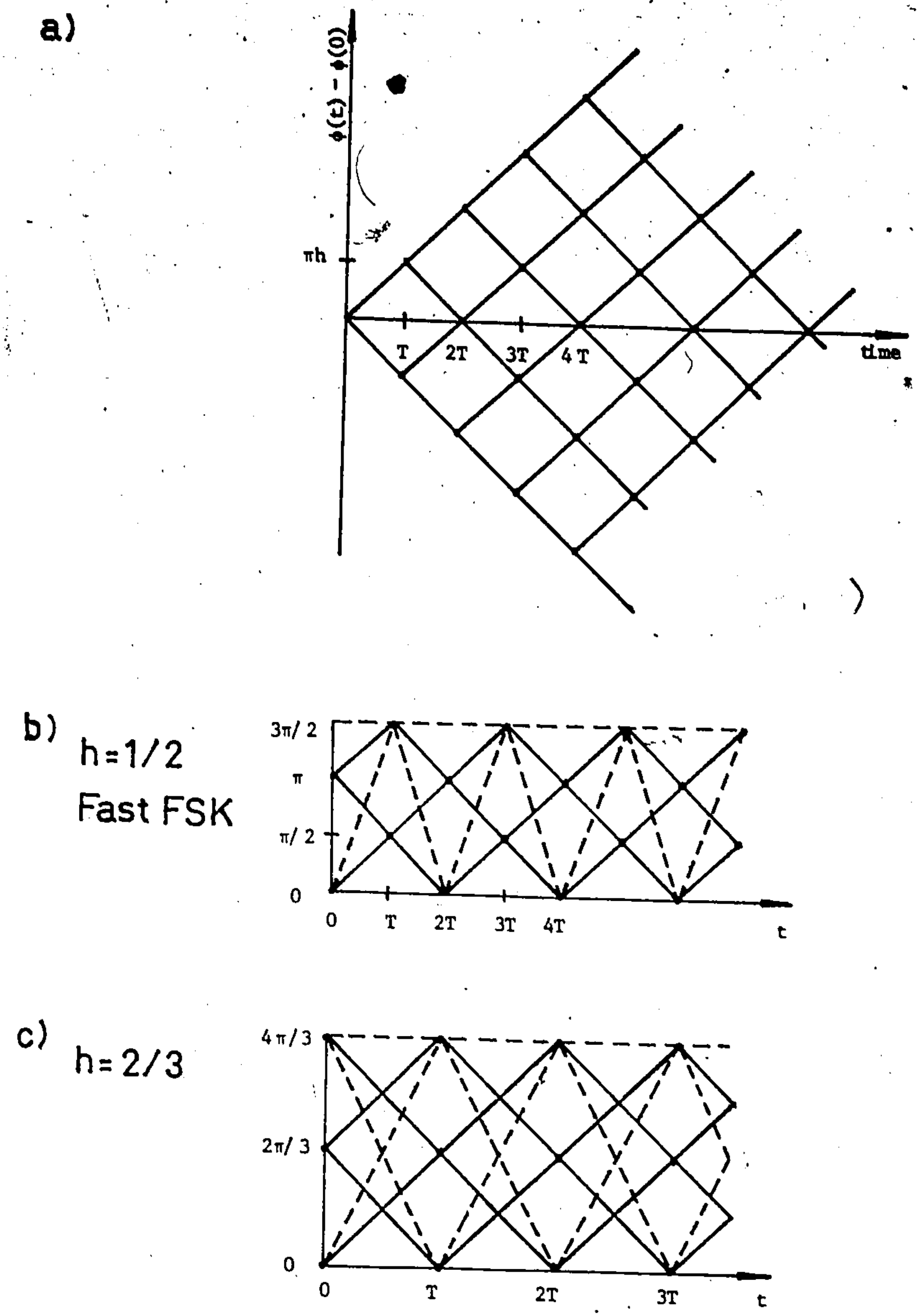

Fig. 2. PHASE TRELLISES, CONVENTIONAL CPFSK.

For example, the set $\{h_1 = 1/4,\ h_2 = 2/4,\ h_3 = 3/4\}$ will not give a constraint 3 trellis since $h_1 = (h_2 + h_3)$, modulo 1.

We will say that the set of indices

$$C = \{h_1 = \frac{L_1}{S},\ h_2 = \frac{L_2}{S},\ \ldots,\ h_K = \frac{L_K}{S}\},$$

where S and L_i (i=1, ..., K) are integers, forms a constraint K code, and the code will be written in the shorter form

$$C = S/L_1, L_2, \ldots, L_K \tag{7}$$

Fig. 3a shows the possible phase sequences vs time for the constraint 2 code 4/1,2. The excess phase function is continuous and piecewise linear, and as expected, any pair of paths in the phase trellis in Fig. 3b will merge after 3 or more bauds.

Why do we call the considered modulation method for Multi-h phase coding? Coding is the process of building redundancy or memory into a message, and this is exactly what the continuous phase does to our signal. If the transmitted signal is known in baud i-1 and in baud i+1, it is also known in baud i.

A particular data sequence corresponds to a particular path through the phase trellis. This path may be viewed as a codeword in phase and time since the codeword is a sequence of sinusoidal waveforms rather than a sequence of non-physical symbols. We can therefore say that coding and modulation are done in one operation.

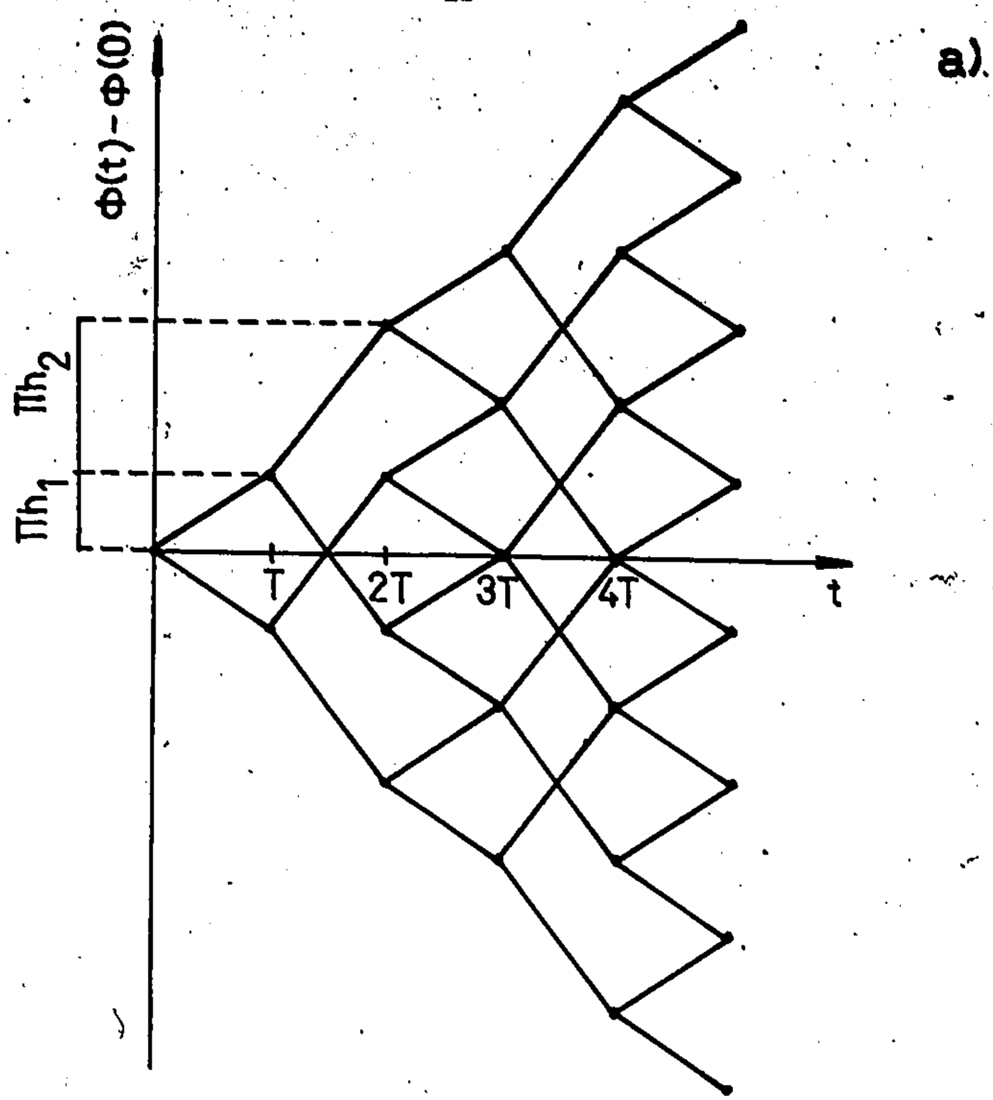

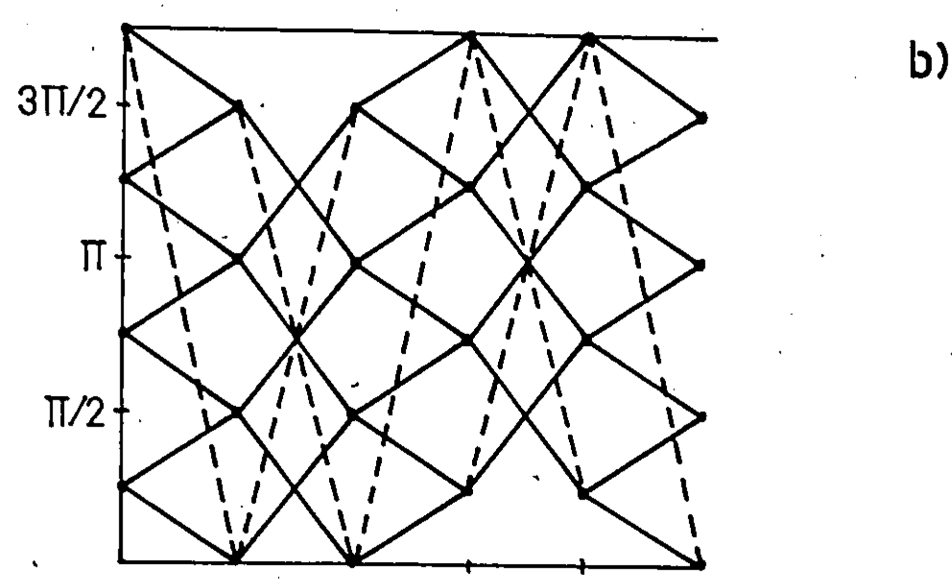

Fig . 3. PHASE TRELLIS, MULTI-H PHASE CODE.
The code is 4/ 1 2.

2.3 Mathematical Model

A codeword is essentially a frequency modulated signal of the form of eqn. (1). As we will see later on, we can without loss of generality let $\alpha = \phi(0) = 0$.

The signal in baud i may be written as

$$s(t) = \frac{2E}{T} \cos(2\pi f_0 t + a_i \omega_i (t-iT) + \phi(iT)), \qquad iT \leq t < (i+1)T \tag{8}$$

where $\omega_i = \pi h_i/T$ and h_i is the modulation index in baud i. The index is varied periodically, thus

$$\omega_i = \omega_{i+K} \tag{9}$$

The continuity of the phase gives

$$\phi(iT) = \sum_{j=0}^{i-1} a_j \omega_j T \tag{10}$$

The signalling interval of duration $T_K = K{:}T$ will be called a superbaud. Let $y_r(t)$ be the waveform transmitted in superbaud r. Then, making use of (3),

$$x(t) = \sum_{r=0}^{\infty} y_r(t - rT_K)$$

$$= \sum_{r=0}^{\infty} \sum_{k=0}^{K-1} X_{rK+k} (t - (rK+k)T) \tag{11}$$

Alternatively, the signal s(t) in the ith baud may be written (cfr. Fig. 4)

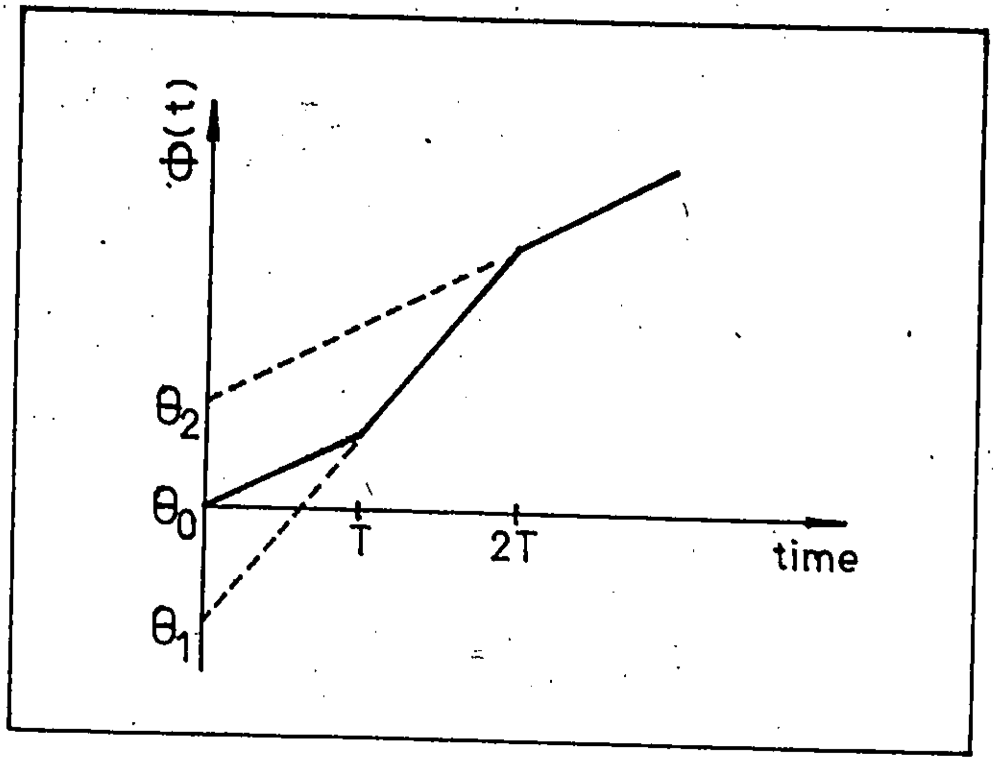

Figure 4 Definition of θ_i

$$s(t) = \sqrt{\frac{2E}{T}} \cos(2\pi f_c t + a_i \omega_i t + \theta_i), \qquad iT \leq t < (i+1)T \tag{12}$$

By comparison with eqn. (8),

$$\theta_i = \phi(iT) - a_i \omega_i iT$$

$$= \sum_{j=0}^{i-1} a_j \omega_j T - a_i \omega_i iT \tag{13}$$

Similarly,

$$\theta_{i-1} = \sum_{j=0}^{i-2} a_j \omega_j T - a_{i-1} \omega_{i-1} (i-1)T \tag{14}$$

We can then obtain a recursive formula for θ_i by combining eqn. (13) and (14) to obtain:

$$\theta_i = \theta_{i-1} + iT\,(a_{i-1}\,\omega_{i-1} - a_i\,\omega_i) \tag{15}$$

2.4 The Concept of Minimum Distance

The continuous phase not only offers spectral advantages [16], but it introduces memory into the signal which makes it possible to reduce the probability of error by observing the received signal over several bauds in order to decide which data was transmitted in a given interval.

Any codeword is a point in a signal space [12], [13]. The receiver will compare the received signal and the possible codewords and decide that the "closest" codeword is the signal transmitted. However, in the case when this codeword is close to another codeword, a wrong decision is easily made since then the received signal is close to two codewords. This means that the error performance of a multi-h phase code depends on the distances between the codewords.

When the signal-to-noise ratio is large, the probability of making a wrong decision is dominated by the distance between the closest codewords in the code, d^2_{min} [13].

Consequently, the codewords should be selected such that the minimum distance is large in order to improve the error performance or, if the transmission quality is better than required, to save power. Since the probability of error is a function of the product $d^2_{min}E$, an increase in d^2_{min} is seen to give a rough indication of the power savings - or coding gain - for a given error rate.

The distance between the codewords s_i and s_k is defined by

$$d^2 = \int_{-\infty}^{\infty} |s_i(t) - s_k(t)|^2 \, dt \qquad (16)$$

When the two paths are separated for L bauds, eqn. (16) can be written [12], [13], [14], [17]

$$d^2 = \sum_{n=1}^{L} d_n^2(j,k) \qquad (17)$$

where d_n^2 is the distance over baud n. It depends only on the phase difference between the codewords at the beginning and end of the interval, α and $\phi(0)$ will therefore not affect the distance properties.

Since the distance cumulates from baud to baud, we should expect the performance to improve if we can delay the merging of the paths in the phase trellis. This is the idea behind multi-h codes. By increasing the constraint length K, we can hopefully increase the minimum distance d^2_{min}. However, two paths merging after a few bauds may have a larger distance than two paths which remain separated over more intervals. In other words, a code with good error performance has necessarily a long constraint length, but a code with long constraint length does not necessarily have a large minimum distance.

The minimum distance for several constraint 2, 3 and 4 codes are computed by Anderson [18], following the procedure presented in [12] and [13].

Fig. 5 shows, as a function of the mean index

$$\bar{h} = \frac{1}{K} \sum_{i=1}^{K} h_i ,$$

d^2_{min} for the codes with the largest coding gain. For $0.5 \leq \bar{h} \leq 0.75$, one can obtain a substantial coding gain by introducing more complexity (increasing the constraint length). The best constraint 4, 3 and 2 codes give an improvement compared to Fast FSK (or binary PSK) of 3.7 dB, 3.4 dB, and 2.7 dB respectively. For other mean indices, the coding gain does not depend on the constraint length as long as $K \geq 2$.

Only codes with $S \leq 16$ are considered. We note that there are no codes with $K \geq 5$ having $S = 16$ since a constraint K code has $S_{min} = 2^K$ [12], [13].

2.5 Decoding of Multi-h Phase Codes

A maximum likelihood receiver performs coherent detection and a phase reference for the incoming signal is needed.

The function of the decoder/demodulator is to match the received signal to the possible codewords and decide which codeword was most likely transmitted. When timing information is available (i.e. the receiver has baud lock and superbaud lock), this matching operation requires the receiver to distinguish between the possible phases at the end of a signalling interval. In Appendix A we show that there are S possible phases for a multi-h code with rational indices of the form h_i

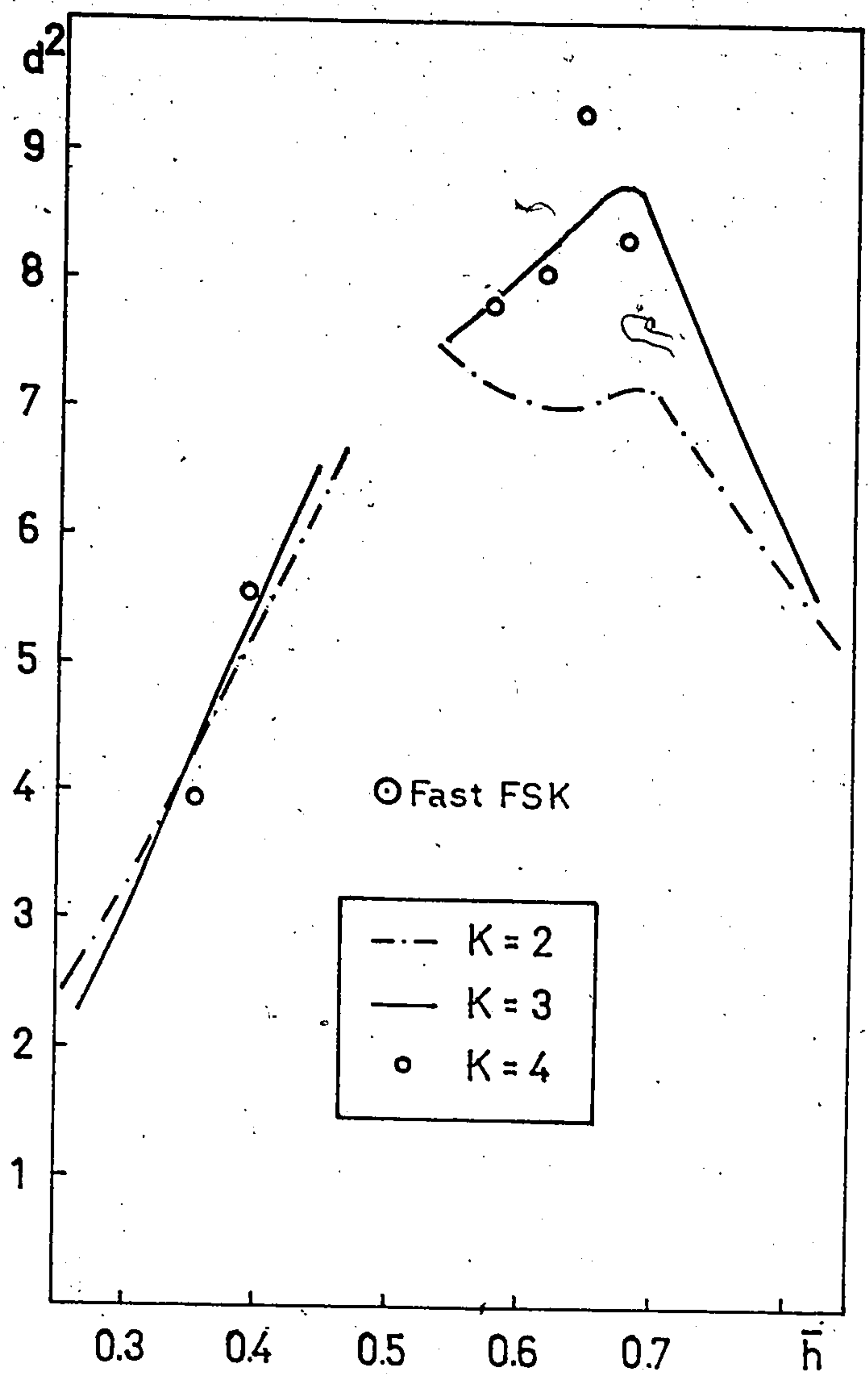

Fig. 5. MINIMUM DISTANCE VERSUS MEAN INDEX.
S ≤ 16.

$= L_i/S$. If the indices are not ratios of small integers, the phase trellis will be complicated and lead to a difficult decoding. Miyakawa et al [10] have proposed a multi-h code with this drawback.

A decoder observes the received signal for several bauds in order to make a correct decision. It is obvious that once two paths merge, future received data cannot help resolve which one of those paths was transmitted. But as long as some paths remain separated, the decoder will do a better job by observing for a longer interval. In general, maximum likelihood decoding requires an infinitely long observation interval because there are some paths that will never merge.

A practical decoder, however, will observe for only a finite time and then it is forced to make a decision. How will this degrade the performance? If two unmerged paths have an observed distance d_0^2 less than d_{min}^2, we expect a degradation of the error performance since it is then dominated by d_0^2. Now, eqn. (17) says that the distance is additive. We can therefore reduce the probability of making a wrong decision by increasing the observation interval and thereby increase d_0^2. Evidently, there exists a finite observation interval such that any pair of unmerged paths have an observed distance equal to or greater than d_{min}^2. Then the probability of error is dominated by d_{min}^2 and further observation will give only a negligible improvement of the performance. We shall call this interval the decision depth. The decision depth tends to grow with K ands S [12], [13].

Anderson and deBuda [11] have pointed out that when K and S are kept small, the periodic phase trellis structure allows simple maximum likelihood decoding of multi-h phase codes by employing the Viterbi algorithm [19].

A practical Viterbi decoder will perform only a truncated search and thereby make errors [12], [13].

CHAPTER 3

SPECTRAL ANALYSIS OF MULTI-H PHASE CODES

The power spectrum provides an estimate of the band occupancy of a signal.

In this chapter we shall derive expressions for the power spectra of multi-h phase codes. Three different analytical approaches are presented and compared.

First, let us make clear which assumptions the analysis is based upon.

Substituting for eqn. (2), (3), (4), and (5) into eqn. (8), we obtain an expression for the multi-h coded signal s(t),

$$s(t) = \sqrt{\frac{2E}{T}} \cdot \cos(2\pi f_c t + \phi(t) + \alpha), \qquad iT \leq t \leq (i+1)T \tag{18}$$

where the excess phase function $\phi(t)$ is given by

$$\begin{aligned}\phi(t) &= \int_0^t x(t') \, dt' + \phi(0) \\ &= \int_0^t \sum_{i=0}^{\infty} a_i \frac{\pi h_i}{T} \cdot g(t'-iT) \, dt' + \phi(0)\end{aligned}$$

and h_i (i mod. K) is the modulation index in the ith signalling interval.

We have made the following assumptions:

(i) The initial carrier phase α is arbitrary.

(ii) The sequence of binary data can be modelled by a sequence of binary random variables a_i. The variables are statistically independent and they are identically distributed.

(iii) The modulation index h is varied cyclically from baud to baud. The cycle has period $T_K = K \cdot T$.

(iv) The modulation is narrowbanded, i.e. $h \leq 1$ and $f_c >> 1/T$.

(v) g(t) is a rectangular pulse of unit height defined on [0, T].

(vi) The excess phase function $\phi(t)$ is continuous.

We shall also without loss of generality assume that $\alpha = \phi(0) = 0$.

3.1 The Power Spectrum of the Modulated Signal

We shall analyse the power distribution of the signal s(t) defined in eqn. (18).

The general method of attack is to obtain the autocorrelation function $K(t_1; \tau)$ of the signal and hence the power spectrum W(f) which is related to the autocorrelation function by a Fourier transform.

Let u(t) be the complex representation of s(t). Then s(t) is the real part of u(t),

$$s(t) = \text{Re}\,\{u(t)\} \tag{19}$$

where

$$u(t) = \sqrt{\frac{2E}{T}} \cdot e^{j(2\pi f_c t + \phi(t) + \alpha)} \tag{20}$$

The autocorrelation function is given by

$$K(t_1;\tau) = E\,[s(t_1)\,.\,s(t_1+\tau)]$$

$$= \frac{1}{4}\,E\,[\{u(t_1)+u^*(t_1)\}.\{u(t_1+\tau)+u^*(t_1+\tau)\}] \qquad (21)$$

The symbol E[•] denotes ensemble average or expected value. The function $u^*(t)$ is the complex conjugate of u(t).

Since α is uniformly distributed on $[0, 2\pi]$,

$$E[Re\{u(t)\}] = E[Im\{u(t)\}] \qquad (22)$$

Making use of eqn. (22) and the fact that $\phi(t)$ is evenly distributed around zero, we can rewrite eqn. (21)

$$K(t_1;\ \tau) = \frac{1}{2}\,Re\{E[u^*(t_1)\ .\ u(t_1+\tau)]\}$$

$$= \frac{2E}{T}\ .\ \frac{1}{2}\,Re\{E[e^{j2\pi f_c\tau}\ .\ e^{j\phi(t_1+\tau)-j\phi(t_1)}]\}$$

$$= \frac{2E}{T}\ .\ \frac{1}{2}\cos 2\pi f_c\tau\ .\ E[e^{j\phi(t_1+\tau)-j\phi(t_1)}] \qquad (23)$$

For a stationary process, the autocorrelation function does not depend on t_1, and the autocorrelation function and the power spectrum form a Fourier transform pair.

The autocorrelation function of a non-stationary process is a function of t_1, and an accurate representation of the power spectrum cannot in general be found by taking the Fourier transform of the time averaged autocorrelation function [20]. We will instead obtain a probabilistic representation of the spectrum which now defines the distribution of power for a "typical" sequence at a "typical" time.

It can be shown [21], however, that the representation of the spectrum is accurate when the non-stationary process is a constant-envelope signal and it has a periodic phase trellis.

Thus the power spectrum $W(f)$ of the non-stationary multi-h phase coded signal $s(t)$ is the Fourier transform of the time averaged autocorrelation function $K(\tau)$ defined by

$$K(\tau) = M[K(t_1;\tau)] \tag{24}$$

The symbol $M[\cdot]$ denotes the time averaging operator.

It follows from eqn. (23) that $W(f)$ may be found by convolution (denoted by $*$). Let $G(f)$ be the power spectrum of the complex lowpass function

$$v(t) = e^{j\phi(t)} \tag{25}$$

with autocorrelation function

$$R(t_1;\tau) = E[e^{j\phi(t_1+\tau)-j\phi(t_1)}] \tag{26}$$

Then

$$W(f) = \frac{2E}{T}\cdot\frac{1}{2}G(f) * \{\frac{1}{2}\delta(f-f_c) + \frac{1}{2}\delta(f+f_c)\}$$

or

$$W(f) = \frac{2E}{T}\cdot\frac{1}{4}\{G(f-f_c) + G(f+f_c)\} \tag{27}$$

Our problem is therefore reduced to that of finding the lowpass spectrum $G(f)$.

We note that α and $\phi(0)$ cancel out in eqn. (23). Since they do not affect the lowpass spectrum, we will let $\alpha = \phi(0) = 0$.

The relationship between the power spectra of the lowpass

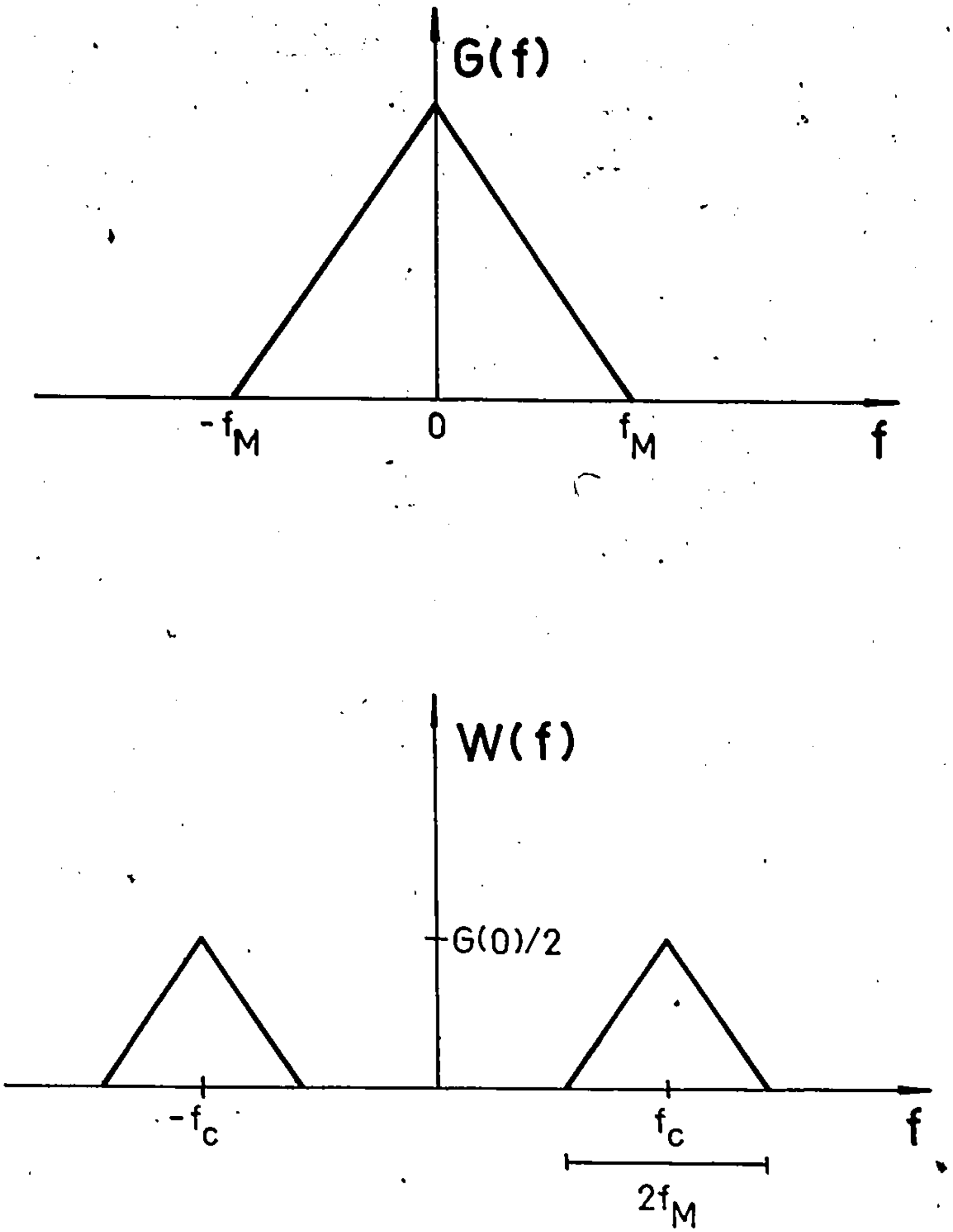

Fig. 6. THE LOWPASS SPECTRUM G(f) AND THE POWER SPECTRUM W(f) OF THE MODULATED SIGNAL.
For normalized power, i.e. $\frac{E}{T} = 1$.

function $v(t)$ and the modulated signal $s(t)$ is illustrated in Fig. 6 for normalized power. The two images do not overlap since the modulation is narrowbanded.

3.2 The Lowpass Spectrum

We have seen that the power spectrum of the modulated signal is uniquely determined by the spectrum of the complex lowpass signal

$$v(t) = e^{j\phi(t)}$$

In the following we present three approaches to the problem of calculating this lowpass spectrum. The methods are known as

- The Transform Technique
- The Markov Chain Approach
- The Direct Method

The Transform Technique [15], [16], [22] makes use of the Wiener-Khinchin Theorem which states that the autocorrelation function and the power spectrum form a Fourier transform pair. Bennett and Rice [16] and Pelchat [15] have calculated the spectrum of conventional binary CPFSK using this method. Our work is in the main an extension of Pelchat's analysis.

In physical situations, the assumption of a linear relationship between the frequency and the modulating signal is an idealization. Wittke [42] has examined the non-linear case for a Gaussian modulating signal.

When the phase trellis is periodic, we can model the lowpass signal $v(t)$ as a Markov chain and evaluate the autocorrelation function using the theory of such random processes [23]-[27]. The Markov Chain

Method is thus a special case of the Transform Technique.

Anderson and Salz [28] introduced the Direct Method in their calculation of the spectrum of M-ary CPFSK. They calculated the average power in a segmented signal v(t) and then evaluated the limit as the length of the segment increased without bounds. The method is also presented in [29].

3.2.1 An Example: Conventional CPFSK

The basic steps in the derivation of an expression for the lowpass spectrum are best illustrated by an example.

We consider the conventional CPFSK with modulation index h and a phase tree as shown in Fig. 2a.

The autocorrelation function of the complex lowpass function v(t) is given by

$$R(t_1;\ \tau) = E[e^{j\phi(t_1+\tau)-j\phi(t_1)}]$$

We suppose that t_1 lies in baud no. i and $t_2 = t_1+\tau$ in baud j. From Fig. 7 it is seen that the phase difference then is

$$\phi(t_1+\tau) - \phi(t_1) = a_i\ \omega((i+1)T-t_1) + a_{i+1}\ \omega T + \dots$$
$$\dots + a_{j-1}\ \omega T + a_j\omega(t_2-jT) \qquad (28)$$

and hence

$$R(t_1;\tau) = E[e^{ja_i\omega((i+1)T-t_1)} \cdot e^{ja_{i+1}\omega T} \ldots$$

$$\ldots e^{ja_{j-1}\omega T} \cdot e^{ja_j\omega(t_2-jT)}] \tag{29}$$

Since the a_is are statistically independent, we may rewrite eqn. (29) as

$$R(t_1;\tau) = E[e^{ja_i\omega((i+1)T-t_1)}] \cdot E[e^{ja_{i+1}\omega T}] \ldots$$

$$\ldots E[e^{ja_{j-1}\omega T}] \cdot E[e^{ja_j\omega(t_2-jT)}] \tag{30}$$

With binary signalling, the two messages, $a = 1$ and $a = -1$, will occur with the same probability. Thus

$$E[e^{ja\omega t}] = \frac{1}{2}\, e^{j\omega t} + \frac{1}{2}\, e^{-j\omega t} = \cos\omega T \tag{31}$$

The autocorrelation function takes the form

$$R(t_1;\tau) = (\cos\omega T)^{j-1-i} \cdot E[e^{ja_i\omega((i+1)T-t_1)}] \cdot E[e^{jaj\omega(t_2-jT)}]$$

$$= (\cos\omega t)^{j-1-i}.\cos\omega((i+1)T-t_1).\cos\omega(t_1+\tau-jT),\ i\neq j \tag{32a}$$

and

$$R(t_1;\tau) = E[e^{ja_i\omega(t_2-t_1)}] = \cos\omega(t_2-t_1) = \cos\omega\tau \quad ,\ i=j \tag{32b}$$

$R(t_1;\tau)$ is a function of τ rather than of the baud numbers. The next step, therefore, is to find the value of τ that will make t_2 fall into baud no. j.

As illustrated in Fig. 8, both the location of t_1 in baud i and the value of τ will determine the location of t_2. Let $\tau = nT + \tau_s$ where $0 \leq \tau_s < T$. By inspection, we have

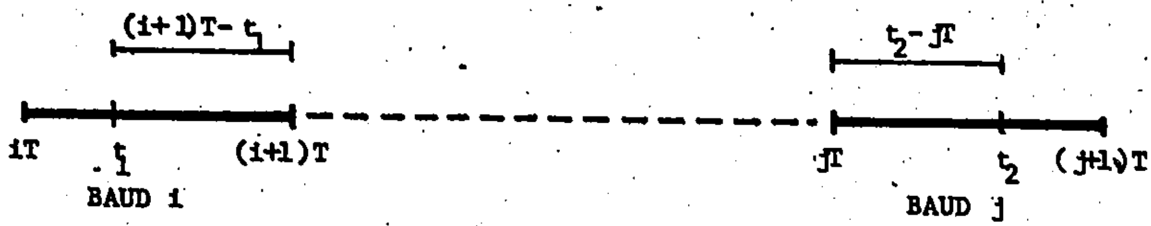

Fig. 7. ILLUSTRATION TO EQN.28.

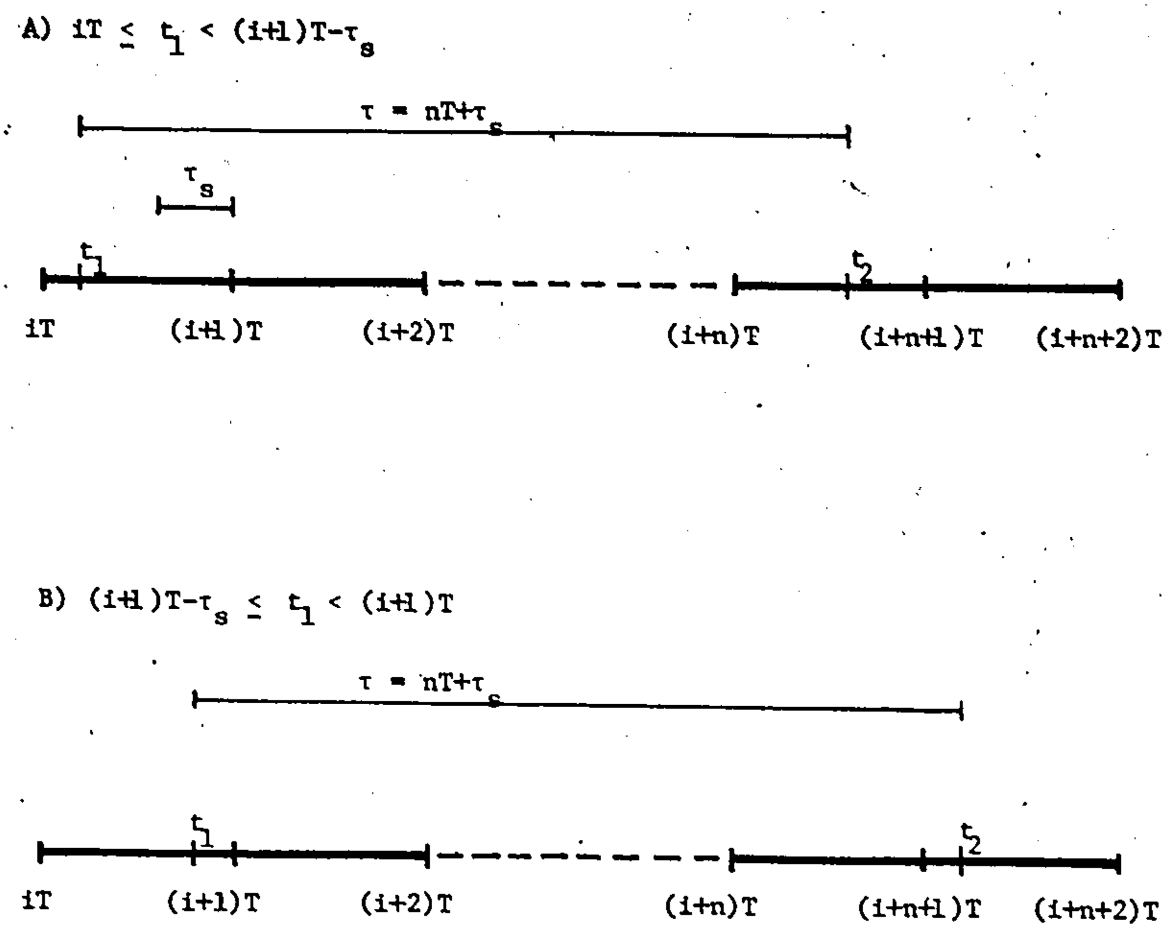

Fig. 8. A MULTI-H PHASE CODE IS A NON-STATIONARY PROCESS.

$$t_2 \in \text{baud } j = i + n \qquad \text{when } iT \leq t_1 < (i+1)T-\tau_s$$
$$t_2 \in \text{baud } j = i+n+1 \qquad \text{when } (i+1)T-\tau_s \leq t_1 < (i+1)T \tag{33}$$

The process $v(t)$ is non-stationary, and $R(t_1;\ \tau)$ is to be time averaged over all possible t_1. We note that the problem of evaluating $R(t_1;\ \tau)$ for a given τ will remain the same if t_1 is increased by $k\cdot T$ where k is any integer. In other words, the autocorrelation function has the property

$$R(t_1;\ \tau) = R(t_1 + kT;\ \tau) \tag{34}$$

The function $R(t_1;\ \tau)$ can therefore be time averaged over only one baud, and we shall without loss of generality assume that t_1 lies in baud 0.

Let $R_n(\tau)$ be the time averaged autocorrelation function for $nT \leq \tau < (n+1)T$. We may then write $R(\tau)$ as the series

$$R(\tau) = \sum_{n=-\infty}^{\infty} R_n(\tau) \tag{35}$$

where the terms $R_n(\tau)$ may be found using eqn. (32) and (33). For n = 0

$$R_o(\tau) = \frac{1}{T}\ \{\int_0^{T-\tau_s} \cos\omega\tau dt_1 + \int_{T-\tau_s}^{T} \cos\omega(T-t_1).\cos\omega(t_1+\tau_s-T)dt_1\} \tag{36a}$$

and for n > 0

$$R_n(\tau) = \frac{1}{T} \int_0^{T-\tau_s} (\cos^{\omega} t)^{n-1}.\cos^{\omega}(T-t_1).\cos^{\omega}(t_1+\tau_s)dt_1$$

$$+ \int_{T-\tau_s}^{T} (\cos^{\omega} t)^{n}.\cos^{\omega}(T-t_1).\cos^{\omega}(t_1+\tau_s-T)dt_1 \qquad (36b)$$

Since the function $\cos^{\omega} t$ is zero outside the interval $0 \leq t \leq T$ (cf. eqn. (4)), the integrands in eqn. (36b) vanish outside the range of integration, and the limits of the integrals may be replaced by $(-\infty,\infty)$.

The power spectrum $G(f)$ can then be found as the Fourier transform of the even autocorrelation function $R(\tau)$

$$G(f) = 2 \text{ Re } \{ \int_0^{\infty} R(\tau)e^{-j2\pi f\tau}d\tau\} \qquad (37)$$

Substituting for $R(\tau)$ from eqn. (35) and (36), we obtain

$$G(f) = 2 \text{ Re } \{\frac{1}{T} \int_0^{T} e^{-j2\pi f\tau}d\tau \int_0^{T-\tau_s} \cos^{\omega}\tau dt_1$$

$$+ \sum_{n=1}^{\infty} \frac{1}{T} \int_{nT}^{(n+1)T} e^{-j2\pi f\tau}d\tau \int_{-\infty}^{\infty} (\cos^{\omega} T)^{n-1}\cos^{\omega}(T-t_1)\cos^{\omega}(t_1+\tau_s)dt_1$$

$$+ \sum_{n=0}^{\infty} \frac{1}{T} \int_{nT}^{(n+1)T} e^{-j2\pi f\tau}d\tau \int_{-\infty}^{\infty} (\cos^{\omega} T)^{n}\cos^{\omega}(T-t_1)\cos^{\omega}(t_1+\tau_s-T)dt_1\} \qquad (38)$$

We shall se that it is possible to simplify this expression by combining the two series, i.e. pairing the last term of $R_n(\tau)$ and the first term of $R_{n+1}(\tau)$.

In the second series, we replace n+1 by n and $\tau_s - T$ by τ_s. Eqn. (38) then takes the form

$$G(f) = 2\mathrm{Re}\{\frac{1}{T}\int_0^T e^{-j2\pi f\tau} d\tau \int_0^{T-\tau_s} \cos\omega\tau \, dt_1$$

$$+ \sum_{n=1}^{\infty} \frac{1}{T} e^{-j2\pi fnT} \int_{-T}^{T} e^{-j2\pi f\tau_s} d\tau_s \int_{-\infty}^{\infty} (\cos\omega T)^{n-1} \ldots \qquad (39)$$

$$\ldots \cos\omega(T-t_1)\cos\omega(T-t_1+\tau_s)dt_1\}$$

The limits (-T, T) may be replaced by $(-\infty, \infty)$ since $|\tau_s| < T$.

We introduce the Fourier transform of the function $\cos\omega t$, $F\{\cos\omega t\}$, and rewrite eqn. (39) as

$$G(f) = 2\mathrm{Re}\{F\{\frac{T-t}{T}\cos\omega t\}$$

$$+ \sum_{n=1}^{\infty} \frac{1}{T} e^{-j2\pi f(n-1)T} . (\cos\omega T)^{n-1} . F\{\cos\omega t\} . F\{\cos\omega t\}\} \qquad (40)$$

In Appendix B it is shown that provided $|\cos\omega T| < 1$, eqn. (40) reduces to the more familiar form [30]

$$G(f) = \frac{4}{T} \frac{\omega^2}{(\omega^2 - 4\pi^2 f^2)^2} \cdot \frac{(\cos\omega T - \cos 2\pi fT)^2}{\cos^2\omega T - 2\cos\omega T\cos 2\pi fT + 1} \qquad (41)$$

This example shows that there are three basic steps in the spectral evaluation.

First, we find the autocorrelation function of the complex lowpass function v(t). It turns out that the process is non-stationary, and this complicates the derivation since the autocorrelation function then is a function of both t and τ. Eqn. (33) is a clue to the solution of this problem.

Second, we calculate the time averaged autocorrelation function and notice that the signal v(t) possesses certain properties which allow us to average over a <u>finite</u> time interval.

Third, the expression for the power spectrum is obtained by taking the Fourier transform of the time averaged autocorrelation function. This is straight forward, but messy. The power spectrum is expressed as a series which can be considerably simplified by combining terms as indicated in eqn. (39).

In this example, the derivation has followed the first approach, namely the Transform Technique. We shall in the next section see how this approach can be extended in order to obtain an expression for the power spectrum of a general multi-h phase code.

3.2.2 Method 1: The Transform Technique

We first calculate the lowpass autocorrelation function over the ensemble at a fixed t_1.

We have shown that $R(t_1;\ \tau)$ may be written (eqn. (26))

$$R(t_1;\ \tau) = E[e^{j\phi(t_1+\tau)-j\phi(t_1)}] = E[e^{j\Delta\phi}]$$

Let $t_2 = t_1+\tau$ where $nT \leq \tau < (n+1)T$, $\tau = nT+\tau_s$. Assume t_1 lies in baud no. i and t_2 in baud no. j. The modulation index varies from baud to baud, so

$$\Delta\phi = a_i\omega_i((i+1)T-t_1) + a_{i+1}\omega_{i+1}T + \ldots$$
$$\ldots + a_{j-1}\omega_{j-1}T + a_j\omega_j(t_2-jT) \qquad (42)$$

Since the a_i.s are i.i.d.

$$R(t_1;\ \tau) = E[\exp ja_i\omega_i((i+1)T-t_1)]\ .\ E[\exp ja_{i+1}\omega_{i+1}T]\ldots$$
$$\ldots E[\exp ja_{j-1}\omega_{j-1}T]\ .\ E[\exp ja_j\omega_j(t_2-jT)] \qquad (43)$$

Eqn. (43) shows that the autocorrelation function can be written as a series

$$R(t_1;\ \tau) = \sum_{j=0}^{\infty} r_{ij}(t_1;\ \tau_s) \quad ,\ i \geq 0 \qquad (44)$$

where we have defined

$$r_{ii}(t_1;\ \tau_s) = \cos\omega_i\tau \qquad ,\ i = j \qquad (45a)$$

$$r_{ij}(t_1;\ \tau_s) = \prod_{k=i+1}^{j-1} \cos\omega_k T\ .$$
$$E[\exp ja_i\omega_i((i+1)T-t_1)]\ .\ E[\exp ja_j\omega_j(t_2-jT)],\ i\neq j \qquad (45b)$$

or, if we define $z = t_1 - iT$

$$r_{ij}(z;\ \tau_s) = \prod_{k=i+1}^{j-1} \cos \omega_k T \ .$$

$$E[\exp\ ja_i\omega_i(T-z)]\ .\ E[\exp\ ja_j\omega_j(z+\tau_s+(n-j+i)T)],\ i \neq j \tag{46}$$

Let us consider the expression E[•] . E[•] in eqn. (45b) and (46). An increase $T_K = K \cdot T$ in τ, where K is the number of modulation indices, will move t_2 from baud j to baud j+K where the modulation index is equal to that of baud j. The value of the expression remains the same, and thus $r_{ij}(t_1;\ \tau_s)$ has the property

$$r_{i,j+K}(t_1;\ \tau_s) = \prod_{k=0}^{K-1} \cos \omega_k T\ .\ r_{ij}(t_1;\ \tau_s),\ i \neq j \tag{47}$$

We now define the characteristic function

$$C(1;\ T_K) = \prod_{k=0}^{K-1} \cos \omega_k T \tag{48}$$

The power spectrum of v(t) will have lines if v(t) is periodic or if a DC-component is present. In both cases, the autocorrelation function will fail to satisfy the condition

$$R(\tau) \rightarrow 0 \qquad \tau \rightarrow \infty \tag{49}$$

By substituting for $C(1;\ T_K)$ in eqn. (47), we therefore have a sufficient and necessary condition for a line-free spectrum, namely

$$|C(1;\ T_K)| < 1 \tag{50}$$

For narrowbanded modulation (i.e. $h \leq 1$), this condition is automatically fulfilled when the set of indices has two or more distinct elements. The condition for absence of spikes in the spectrum, given by eqn. (50), is the same as that presented by Miyakawa [10]. It is a generalization of the more familiar condition $|\cos\pi h| < 1$ for the $K = 1$ case [15], [16], [22], [24], [28], [29].

The autocorrelation function may also be written as a series

$$R(t_1;\ \tau) = \sum_{n=-\infty}^{\infty} R_n(t_1;\ \tau) \tag{51}$$

where $R_n(t_1;\ \tau)$ is the contribution for $nT \leq \tau < (n+1)T$.

What is the relationship between the series in eqn. (44) and (51)? Which value of τ will make t_2 fall into baud no. j?

Let $nT \leq \tau < (n+1)T$. From eqn. (33) we know that

t_2 lies in baud $j = i+n$ when $iT \leq t_1 < (i+1)T-\tau_s$

t_2 lies in baud $j = i+n+1$ when $(i+1)T-\tau_s \leq t_1 < (i+1)T$

Thus

$$R_n(t_1;\ \tau) = \begin{cases} R_n'(t_1;\ \tau) = r_{i,\overline{i+n}}(t_1,\ \tau_s) & ,\ iT \leq t_1 < (i+1)T-\tau_s \\ R_n''(t_1;\ \tau) = r_{i,i+n+1}(t_1;\ \tau_s), & (i+1)T-\tau_s \leq t_1 < (i+1)T \end{cases} \tag{52}$$

The process $v(t)$ is non-stationary, and the power spectrum is the Fourier transform of the time averaged autocorrelation function $R(\tau)$.

We note that the autocorrelation function $R(t_1;\ \tau)$ has the property

$$R(t_1;\ \tau) = R(t_1 + T_K;\ \tau) \tag{53}$$

which means that we can average over one superbaud, say superbaud no. 0. Then

$$R(\tau) = \sum_{n=0}^{\infty} R_n(\tau) = \sum_{n=0}^{\infty} R_n'(\tau) + \sum_{n=0}^{\infty} R_n''(\tau) \tag{54}$$

where

$$R_n'(\tau) = M[R_n'(t_1;\ \tau)]$$

$$= \frac{1}{T_K}\left[\int_0^{T-\tau_s} R_n(t_1;\tau)dt_1 + \int_T^{2T-\tau_s} R_n(t_1;\tau)dt_1 + \right.$$

$$\left. \dots + \int_{(K-1)T}^{T_K-\tau_s} R_n(t_1;\ \tau)\ dt_1\right]$$

$$= \frac{1}{T_K}\left[\int_0^{T-\tau_s} r_{on}(t_1;\tau_s)dt_1 + \int_T^{2T-\tau_s} r_{1,1+n}(t_1;\tau_s)dt_1 + \right.$$

$$\left. \dots + \int_{(K-1)T}^{T_K-\tau_s} r_{K-1,K-1+n}(t_1;\ \tau_s)\ dt_1\right]$$

$$= \frac{1}{T_K}\sum_{m=0}^{k-1} \int_0^{T-\tau_s} r_{m,m+n}(z;\ \tau_s)\ dz \tag{55}$$

and similarly,

$$R_n''(\tau) = M[R_n''(t_1;\ \tau)]$$

$$= \frac{1}{T_K} \sum_{m=0}^{K-1} \int_{T-\tau_s}^{T} r_{m,m+n+1}\,(z;\ \tau_s)\ dz \tag{56}$$

Since the autocorrelation function is even, the power spectrum $G(f)$ is given by eqn. (37)

$$G(f) = 2\text{Re}\{\int_0^{\infty} R(\tau)\ e^{-j2\pi f\tau}\,d\tau\}$$

By using eqn. (54), (55), and (56), we obtain

$$G(f) = 2\text{Re}\{\sum_{n=0}^{\infty} \int_{nT}^{(n+1)T} e^{-j2\pi f\tau}d\tau \cdot \frac{1}{T_K} \sum_{m=0}^{K-1} \int_0^{T-\tau_s} r_{m,m+n}(z;\ \tau_s)dz$$
$$+ \sum_{n=0}^{\infty} \int_{nT}^{(n+1)T} e^{-j2\pi f\tau}d\tau \cdot \frac{1}{T_K} \sum_{m=0}^{K-1} \int_{T-\tau_s}^{T} r_{m,m+n+1}(z;\tau_s)dz\} \tag{57}$$

The integrands $r_{m,m+n}(z;\tau_s)$ and $r_{m,m+n+1}(z;\tau_s)$ are defined in eqn. (46) (assume $n>0$)

$$r_{m,m+n}(z;\tau_s) = \prod_{i=m+1}^{m+n-1} \cos\omega_i T \cdot \cos\omega_m(T-z) \cdot \cos\omega_{m+n}(z+\tau_s)$$
$$r_{m,m+n+1}(z;\tau_s) = \prod_{i=m+1}^{m+n} \cos\omega_i T \cdot \cos\omega_m(T-z) \cdot \cos\omega_{m+n+1}(z+\tau_s-T) \tag{58}$$

The function $\cos\omega_1 t$ is zero outside the interval $0 \leq t \leq T$, so the integrands vanish outside the actual range of integration, and eqn. (57) may be written

$$G(f) = 2\mathrm{Re}\{\sum_{n=0}^{\infty} \int_{nT}^{(n+1)T} e^{-j2\pi f\tau} d\tau \cdot \frac{1}{T_K} \sum_{m=0}^{K-1} \int_{-\infty}^{\infty} r_{m,m+n}(z;\tau_s)dz$$

$$+ \sum_{n=0}^{\infty} \int_{nT}^{(n+1)T} e^{-j2\pi f\tau} d\tau \cdot \frac{1}{T_K} \sum_{m=0}^{K-1} \int_{-\infty}^{\infty} r_{m,m+n+1}(z;\tau_s)dz\} \qquad (59)$$

In the second term we replace n+1 by n and $\tau_s - T$ by τ_s' to obtain

$$G(f) = 2\mathrm{Re}\{\sum_{n=0}^{\infty} e^{-j2\pi fnT} \int_{0}^{T} e^{-j2\pi f\tau_s} d\tau_s \cdot \frac{1}{T_K} \sum_{m=0}^{K-1} \int_{-\infty}^{\infty} r_{m,m+n}(z;\tau_s)dz$$

$$+ \sum_{n=1}^{\infty} e^{-j2\pi fnT} \int_{-T}^{0} e^{-j2\pi f\tau_s'} d\tau_s' \frac{1}{T_K} \sum_{m=0}^{K-1} \int_{-\infty}^{\infty} r_{m,m+n}(z;\tau_s')dz\} \qquad (60)$$

Combining the two terms, eqn. (60) takes the form

$$G(f) = 2\mathrm{Re}\{F\{R_o'(\tau)\}$$

$$+ \sum_{n=1}^{\infty} e^{-j2\pi fnT} \int_{-T}^{T} e^{-j2\pi f\tau_s} d\tau_s \cdot \frac{1}{T_K} \sum_{m=0}^{K-1} \int_{-\infty}^{\infty} r_{m,m+n}(z;\tau_s)dz\} \qquad (61)$$

Since $|\tau_s| < T$, we can replace the limits of the first integral by $\pm\infty$. The series can be written as the sum of K geometric series. By using the property given by eqn. (47) we get

$$e^{-j2\pi fT} \int_{-\infty}^{\infty} e^{-j2\pi f\tau_s} d\tau_s \cdot \frac{1}{T_K} \sum_{m=0}^{K-1} \int_{-\infty}^{\infty} r_{m,m+1}(z;\tau_s)dz$$

$$\cdot \{1 + e^{-j2\pi fT_k} C(1;T_K) + e^{-j4\pi fT_k} \cdot C^2(1;T_K) + \ldots\}$$

$$+ e^{-j4\pi fT} \int_{-\infty}^{\infty} e^{-j2\pi f\tau_s} d\tau_s \cdot \frac{1}{T_K} \sum_{m=0}^{K-1} \int_{-\infty}^{\infty} r_{m,m+2}(z;\tau_s)dz$$

$$\cdot \{1 + e^{-j2\pi fT_K} C(1;T_K) + e^{-j4\pi fT_K} \cdot C^2(1;T_K) + \ldots\}$$

$$+ \ldots$$

$$+ e^{-j2\pi fT_K} \int_{-\infty}^{\infty} e^{-j2\pi f\tau_s} d\tau_s \cdot \frac{1}{T_K} \sum_{m=0}^{K-1} \int_{-\infty}^{\infty} r_{m,m+K}(z;\tau_s)dz \qquad (62)$$

$$\cdot \{1 + e^{-j2\pi fT_K} C(1;T_K) + e^{-j4\pi fT_K} C^2(1;T_K) + \ldots\}$$

The first term of the nth geometric series in eqn. (62) may be written as

$$e^{-j2\pi fnT} \int_{-\infty}^{\infty} e^{-j2\pi f\tau_s} d\tau_s \cdot \frac{1}{T_K} \sum_{m=0}^{K-1} \int_{-\infty}^{\infty} r_{m,m+n}(z;\tau_s)dz$$

$$= \sum_{m=0}^{K-1} \prod_{i=m+1}^{m+n-1} \cos\omega_i T \cdot e^{-j2\pi f(n-1)T} \cdot \frac{1}{T_K}$$

$$\cdot \int_{-\infty}^{\infty} e^{-j2\pi f(T+\tau_s)} d\tau_s \int_{-\infty}^{\infty} \cos\omega_m(T-z).\cos\omega_{m+n}(z+\tau_s)dz$$

$$= \sum_{m=0}^{K-1} \prod_{i=m+1}^{m+n-1} \cos\omega_i T \cdot e^{-j2\pi f(n-1)T} \cdot \frac{1}{T_K}$$

$$\cdot F\{\cos\omega_m t\} \cdot F\{\cos\omega_{m+n} t\} \tag{63}$$

The first term of eqn. (61) may be expressed as

$$F\{R_o'(\tau)\} = \sum_{m=0}^{K-1} \cdot F\{\frac{T-\tau}{T_K} \cdot \cos\omega_m \tau\} \tag{64}$$

By substituting eqn. (63) and (64) into eqn. (61) and replacing the geometric series by their sum (we assume that $|C(1;T_K)| < 1$), we finally obtain

$$G(f) = 2\mathrm{Re}\{ \sum_{m=0}^{K-1} F\{\frac{T-t}{T_K} \cos\omega_m t\}$$

$$+ \sum_{m=0}^{K-1} \sum_{n=1}^{K} \frac{1}{T_K} \frac{1}{1-C(1;T_K)e^{-j2\pi fT_K}} \cdot e^{-j2\pi f(n-1)T}$$

$$\cdot F\{\cos\omega_m t\} \cdot F\{\cos\omega_{m+n} t\}\} \tag{65}$$

where as before the function $\cos\omega_i t$ is zero outside the interval $0 \leq t \leq T$.

3.2.3 Method 2: The Markov Chain Approach

The autocorrelation function of signals which can be modelled as a Markov chain is easily calculated using the well established theory for such processes [25], [26].

However, two main questions arise when employing this method: Can a particular signal be modelled as a Markov chain? If so, what are the states?

There have been no simple answers presented in the literature so far.

We shall show that the two questions can be answered by using the concept of the phase trellis. Any signal with a periodic phase trellis can be modelled as a Markov chain, and the states are easily found by inspection of the trellis.

To show this, we shall investigate the properties of signals with a periodic phase trellis.

As an example, we shall consider the phase code with a single index $h = 0.5$ (Fast FSK). The periodic phase trellis implies a finite number, say b, of different waveforms $\phi_i(t-iT)$. Fig. 9 shows that Fast FSK has $b = 8$.

Consequently, the lowpass waveform $v_i(t-iT) = \exp j\phi_i(t-iT)$ in baud i will be a timeshifted version of one out of b different waveforms. Let $\{q_s(t)\}$, s = 1.2, ..., b, denote this finite set of waveforms defined on [0,T]. Table 1 lists the eight elements $q_s(t)$ for Fast FSK.

If waveform $q_t(t)$ follows $q_s(t)$, we shall say a transition st occurs. The transition diagram defines the transitions which are allowed. In our example, the transition 12 can occur, but the transition 13 is not allowed (see Fig. 9), and this is shown in the diagram in Fig. 10a.

In general, the modulator will decide what to transmit during the next baud from the knowledge about the digital data in that interval and from what is sent in the current baud,

$$v_{i+1}(t-(i+1)T) = f\{v_i(t-iT),\ a_{i+1}\} \tag{66}$$

This leads to the modelling of the random signal v(t) as a Markov process of first order.

The process is said to be in state s if the waveform $q_s(t)$ is transmitted. State s will occur with probability p_s. In Appendix A we show that a multi-h code has maximum b = 4·K·S states.

Say the transition st occurs with probability p_{st}. The transition probability matrix $\underline{P}$ is then obtained from the transition diagram by replacing the dots by the corresponding probabilities p_{st}. The transition matrix for Fast FSK is given in Fig. 10b; only nonzero entries are shown.

The behaviour of the process v(t) is completely described by its set of states and its transition matrix. In other words, a particular signal v(t) is represented by a unique sequence of states, or equivalently, by a unique sequence of transitions. The possible state sequences may be shown in a diagram as done for Fast FSK in Fig. 11. Each node corresponds to a state in a given baud; and each branch represents a transition to some new state. Each branch in Fig. 11 has assigned the transition probability p = 1/2 to it.

From the theory of Markov processes we know that the probability of $q_t(t)$ being transmitted in baud $j = i+n$ when it is given that $q_s(t)$ was transmitted in baud i, is $p_{st}(n)$, the st-th element of the matrix $\underline{P}^n$.

The autocorrelation function can now be expressed in terms of the characteristics of the Markov chain.

Say t_1 lies in baud i and t_2 in baud j. The waveforms transmitted in baud i and j are $q_s(t)$ and $q_t(t)$, respectively. Then

$$r_{ij}(t_1;\tau_s) = \sum_{t=1}^{b} p_s \cdot p_{st}(j-i) \cdot q_s^*(t_1-iT) \cdot q_t(t_2-jT) \quad i \neq j \qquad (67a)$$

and

$$r_{ij}(t_1;\tau_s) = \sum_{t=1}^{b} p_s \cdot q_s^*(t_1-iT) \cdot q_s(t_2-iT) \qquad i=j \qquad (67b)$$

Our Markov chain is regular. This is equivalent to stating that if the process has been running for an infinite long time, the proability of being in state s is independent of the state from which the chain started. Mathematically

$$p_{st}(\infty) = p_t \qquad (68)$$

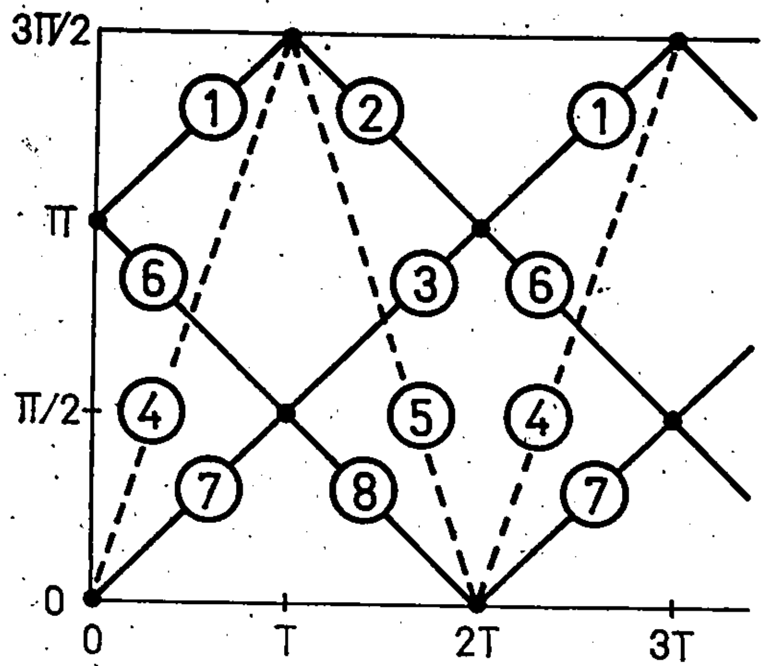

Fig. 9. PHASE TRELLIS, Fast FSK.

Table 1: State waveforms, Fast FSK.

$q_1(t) = \exp j(\frac{\pi}{2T} t + \pi)$	$q_5(t) = \exp j(\frac{\pi}{2T} t + \frac{3\pi}{2})$
$q_2(t) = \exp j(-\frac{\pi}{2T} t + \frac{3\pi}{2})$	$q_6(t) = \exp j(-\frac{\pi}{2T} t + \pi)$
$q_3(t) = \exp j(\frac{\pi}{2T} t + \frac{\pi}{2})$	$q_7(t) = \exp j(\frac{\pi}{2T} t)$
$q_4(t) = \exp j(-\frac{\pi}{2T} t)$	$q_8(t) = \exp j(-\frac{\pi}{2T} t + \frac{\pi}{2})$

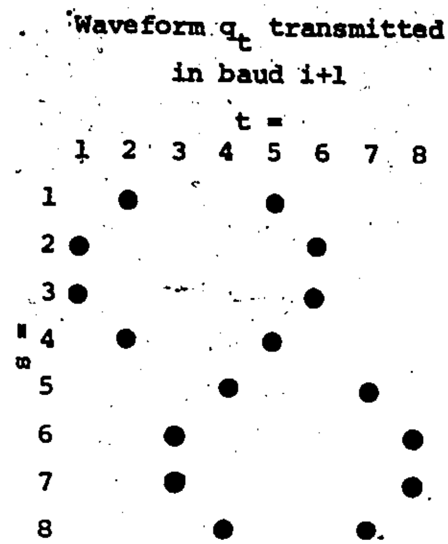

a) Transition diagram, Fast FSK
Dot denotes transition is allowed.

$$
\underline{P} = \begin{bmatrix}
 & \frac{1}{2} & & & \frac{1}{2} & & & \\
\frac{1}{2} & & & & & \frac{1}{2} & & \\
\frac{1}{2} & & & & & \frac{1}{2} & & \\
 & \frac{1}{2} & & & \frac{1}{2} & & & \\
 & & & \frac{1}{2} & & & \frac{1}{2} & \\
 & & \frac{1}{2} & & & & & \frac{1}{2} \\
 & & \frac{1}{2} & & & & & \frac{1}{2} \\
 & & & \frac{1}{2} & & & \frac{1}{2} &
\end{bmatrix}
$$

b) Transition matrix, Fast FSK

Fig. 10. TRANSITION DIAGRAM AND TRANSITION MATRIX, Fast FSK.

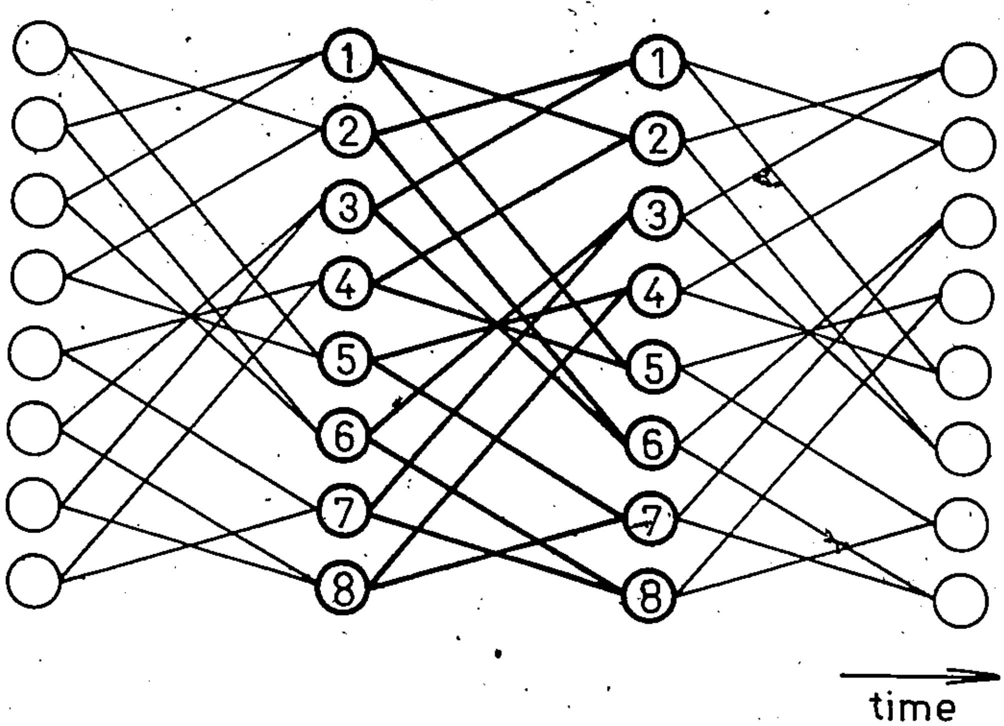

Fig. 11. POSSIBLE STATE SEQUENCES, Fast FSK.

The power spectrum does not have lines if eqn. (49) is satisfied. In the limit, eqn. (67a) takes the form

$$r_{ij}(t_1;\tau_s) = \sum_{t=1}^{b} p_s \cdot p_t \cdot q_s^*(t_1-iT) \cdot q_t(t_2-jT) \;,\; j\to\infty \qquad (69)$$

which implies that a necessary and sufficient condition for the absence of spectral lines is

$$\sum_{s=1}^{b} p_s \cdot q_s(t) = 0 \qquad (70)$$

In Appendix A it is shown that this condition is satisifed for any signal under consideration except for that known as Sunde's CPFSK [31].

In order to express the autocorrelation function as a function of τ rather than of the baud numbers, we define $R(t_1;\tau)$ as in eqn. (44). Assume t_1 lies in baud 0. Then the time averaged $R_n(t_1;\tau)$ is, making use of eqn. (33),

$$R_n(\tau) = \frac{1}{T}\sum_{s=1}^{b}\Big\{\sum_{t=1}^{b}\int_0^{T-\tau_s} p_s p_{st}(n) q_s^*(t_1) \cdot q_t(t_2-nT)dt_1$$

$$+\sum_{t=1}^{b}\int_{T-\tau_s}^{T} p_s p_{st}(n+1) q_s^*(t_1) \cdot q_t(t_2-(n+1)T)dt_1\Big\} \qquad (71)$$

The limits of the integrals can be made infinite because the integrands vanish outside the actual range of integration.

The spectrum G(f) and the time averaged autocorrelation function form a Fourier pair. Hence

$$G(f) = \sum_{n=-\infty}^{\infty} \int_{nT}^{(n+1)T} R_n(\tau) e^{-j2\pi f\tau} d\tau$$

$$= \sum_{n=-\infty}^{\infty} e^{-j\omega nT} \int_{0}^{T} R_n(\tau_s) e^{-j2\pi f\tau_s} d\tau_s$$

$$= \frac{1}{T} \sum_{s=1}^{b} \sum_{t=1}^{b} \sum_{n=-\infty}^{\infty} e^{-j2\pi fnT}$$

$$\{ \int_{0}^{T} \int_{-\infty}^{\infty} p_s p_{st}(n) \cdot q_s^*(t_1) \cdot q_t(t_1+\tau_s) dt_1 e^{-j2\pi f\tau_s} d\tau_s$$

$$+ \int_{0}^{T} \int_{-\infty}^{\infty} p_s p_{st}(n+1) \cdot q_s^*(t_1) \cdot q_t(t_1+\tau_s-T) dt_1 e^{-j2\pi f\tau_s} d\tau_s \} \tag{72}$$

In the second term, we replace n+1 by n and change the variable τ_s to τ_s+T.

Eqn. (72) then simplifies to

$$G(f) = \frac{1}{T} \sum_{s=1}^{b} \sum_{t=1}^{b} \sum_{n=-\infty}^{\infty} e^{-j2\pi fnT}$$

$$\cdot \{ \int_{-T}^{T} [\int_{-\infty}^{\infty} p_s p_{st}(n) \cdot q_s^*(t_1) \cdot q_t(t_1+\tau_s) dt_1 e^{-j2\pi f\tau_s}] d\tau_s \} \tag{73}$$

The expression in the brackets is zero for $|\tau_s| > T$. The limits can therefore be replaced by $\pm\infty$, and it follows that

$$G(f) = \frac{1}{T} \sum_{s=1}^{b} \sum_{t=1}^{b} \sum_{n=-\infty}^{\infty} e^{-j2\pi fnT} p_s p_{st}(n) Q_s^*(f) \cdot Q_t(f) \tag{74}$$

When eqn. (70) is satisfied, the above expression gives the total spectrum. If the total spectrum has lines, however, the continuous part can be found from eqn. (74).

Biglieri [26] shows how eqn. (74) can be given a matrix form and suggests a computational algorithm for the numerical evaluation.

3.2.4 The Direct Method

Rice [32] has defined the power spectrum by

$$G(f) = \lim_{\lambda\to\infty} \frac{2}{\lambda} G_\lambda(f) \qquad f > 0 \tag{75}$$

where

$$G_\lambda(f) = E[| \int_0^\lambda v(t) e^{-j2\pi ft} dt|^2]$$

For convenience, let $\lambda = rT_K = r \cdot K \cdot T$

$$G_\lambda(f) = E[(\sum_{i=0}^{rK-1} \int_{iT}^{(i+1)T} dt_1 \,.\, v(t_1-iT)e^{-j2\pi f t_1})^* \,.$$

$$(\sum_{j=0}^{rK-1} \int_{jT}^{(j+1)T} dt_2 \,.\, v(t_2-jT)e^{-j2\pi f t_2})] \qquad (76)$$

where the asterix denotes the complex conjugate. We observe that

$$I = \int_{jT}^{(j+1)T} dt_2\, v(t_2-jT)e^{-j2\pi f t_2}$$

$$= \int_{jT}^{(j+1)T} dt_2 e^{-j2\pi f t_2} \exp(j \int_0^{t_2} x(t)dt)$$

$$= \int_{jT}^{(j+1)T} dt_2 \,.\, e^{-j2\pi f t_2} \exp(j \int_0^{t_2} \sum_{n=0}^{\infty} x_n(t-nT)dt) \qquad (77)$$

Let $y = t_2-jT$

$$I = \int_0^T dy \,.\, e^{-j2\pi f y}\, e^{-j2\pi f jT} \exp(j \int_0^{y+jT} \sum_{n=0}^{\infty} x_n(t-nT)dt) \qquad (78)$$

Let $t' = t-nT$. Then

$$I = \int_0^T dy e^{-j2\pi f y} \,.\, e^{-j2\pi f jT} \,.\, \exp(j \sum_{n=0}^{\infty} \int_{-nT}^{y-(n-j)T} x_n(t')dt') \qquad (79)$$

We define

$$y' = y-(n-j)T$$

$$P_{nj}(y) = \exp(j \int_{-nT} x_n(t')dt') \qquad (80)$$

The three following situations can occur (Fig. 12):

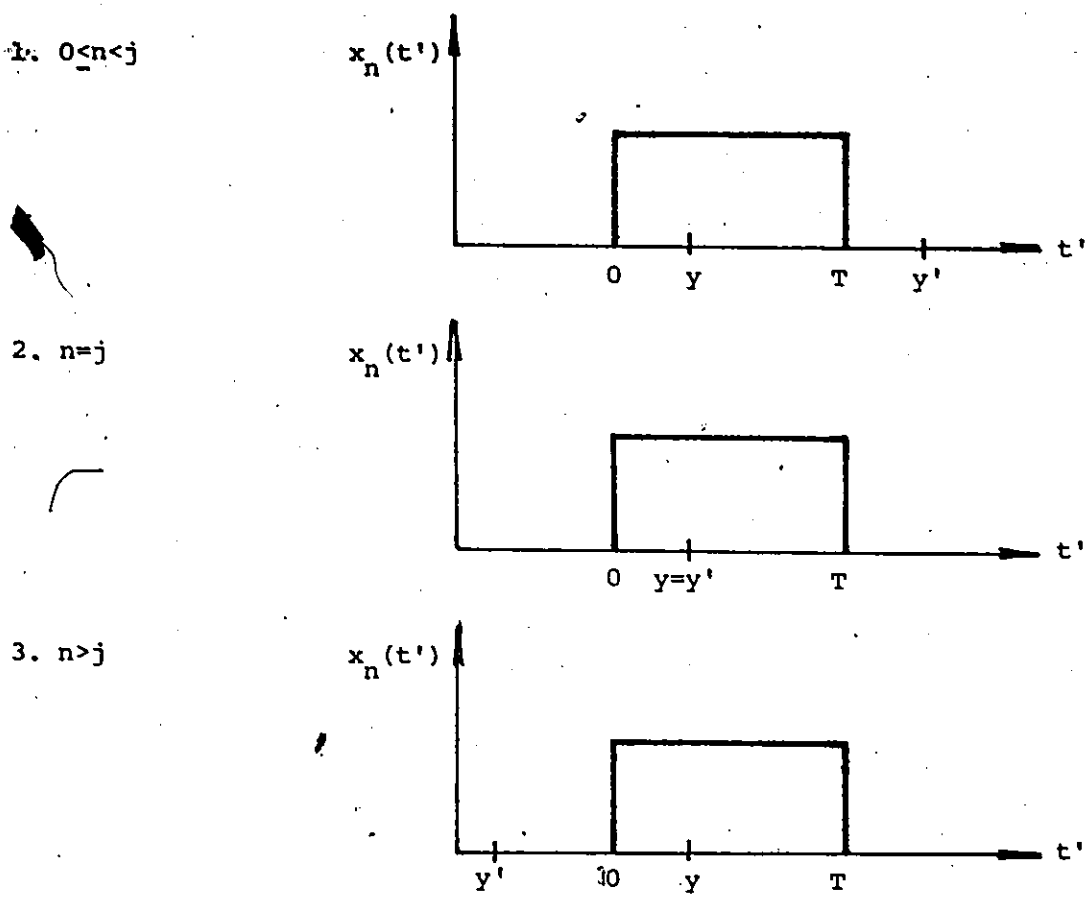

Fig. 12. EVALUATION OF $P_{nj}(y)$.

Such that

$$P_{nj}(y) = \begin{cases} 0 & n < 0 \\ \exp(j \int_0^T x_n(t')dt') & 0 \leq n < j \\ \exp(j \int_0^y x_n(t')dt') & n = j \\ 1 & n > j \end{cases} \tag{81}$$

By substituting for $P_{nj}(y)$ into eqn. (79), we obtain

$$I = \int_0^T dye^{-j2\pi fy} e^{-j2\pi fjT} \exp j \left(\sum_{n=0}^{j-1} \phi_n(T) + \phi_j(y) \right) \tag{82}$$

and eqn. (76) may be written as

$$G_\lambda(f) = E[\sum_{i=0}^{rK-1} \sum_{j=0}^{rK-1} \int_0^T \int_0^T dydz.e^{-j2\pi f(j-i)T} e^{-j2\pi f(y-z)} \\ . \exp j \left(\sum_{n=0}^{j-1} \phi_n(T) - \sum_{n=0}^{i-1} \phi_n(T) \right) . \exp j (\phi_j(y) - \phi_i(z))] \tag{83}$$

We identify the expression

$$E[\exp j \left(\sum_{n=0}^{j-1} \phi_n(T) - \sum_{n=0}^{i-1} \phi_n(T) \right) . \exp j (\phi_j(y) - \phi_i(z))]$$

as the term $r_{ij}(t_1; \tau_s)$ defined in eqn. (45).

Eqn. (83) shows that we can not make use of the periodic properties (cfr. eqn. (47) and eqn. (53)) of the multi-h code in the evaluation of the energy distribution of the truncated signal. This may be easier seen from Fig. C-1. Eqn. (83) states that the summation of contributions to G(f) from the terms $r_{ij}(t_1; \tau)$ shall be done over the square $0 \leq i \leq rK-1$, $0 \leq j \leq rK-1$. But a square is not compatible with the parallelogram shown.

In the limit when the square grows without bounds, however, the Transform Technique and the Direct Method will give equivalent expressions for G(f).

3.2.5 Comparison of the Methods

In this chapter, we have extended the Transform Technique and The Direct Method in order to analyse multi-h phase codes. Although we consider signals with periodic phase trellises, the results are valid for all binary processes with an autocorrelation function $R(t_1; \tau)$ satisfying

$$R(t_1; \tau) = R(t_1 + nT; \tau) \quad , \quad n = 0, 1, 2, \ldots$$

regardless of whether the modulation indices are rational or irrational. However, if some of the indices are irrational, the expression in eqn. (65) is no longer an accurate, but a time averaged, representation of the power spectrum.

On the contrary, we have shown that the Markov Chain Approach assumes rational indices. We have devised a simple procedure for identifying the states of the Markov chain, but we could use the established theory to obtain an expression for the power spectra of multi-h codes. The general final result, given by eqn. (74), is valid for any signal that can be modelled as a Markov process. It clearly shows that the power spectrum is affected by changes either in the nature of the sequence of waveforms or by shaping of the baseband pulses.

We have found two conditions for a line-free spectrum, given by eqn. (50) and eqn. (70). In Appendix A it is shown that they indeed are equivalent.

The Transform Technique and The Direct Method will require the same amount of computation. Of those two, the Transform Technique is intuitively easy to understand and therefore seems to be the preferable one.

The Transform Technique is expected to require less computation than the Markov Chain Approach since the former method makes use of the fact that $R(t_1; \tau)$ is a function of the relative phase difference between $v(t_1)$ and $v(t_2)$ rather than of the absolute signal values at t_1 and t_2.

The Transform Technique assumes rectangular baseband pulses, and the final result has to be slightly modified to cover cases where other pulse shapes are employed.

CHAPTER 4

POWER SPECTRA OF MULTI-H PHASE CODES

The power spectra of multi-h phase codes are computed from eqn. (65).

4.1 Power Spectra of Conventional CPFSK

It turns out that the spectra of conventional CPFSK are useful when describing the spectra of multi-h codes. Since conventional CPFSK may be considered as multi-h phase coding with a single index h, conventional frequency shift keyed signals with continuous phase shall be called single index codes.

Their normalized spectral density W(f) is plotted in Fig. 18 as a function of normalized frequency q where

$$q = (f - f_c)\,T \tag{84}$$

Because of symmetry, we only show values for $q \geq 0$.

The shape of the spectrum changes as the modulation index varies. For very small indices, $h \ll 1$, the carrier is smeared into a spectrum having the shape of a high-Q resonance curve centered on the carrier frequency [15]. For $h = 0.65$ the power spectrum is almost constant over a two-sided bandwidth equal to the bit rate. The spectrum has lines for

$h = 1$, and the spikes occur at half the bit rate [16]. Conventional CPFSK with modulation index $h = 1$ is known as Sunde's CPFSK [31].

The lowest frequency q_o for which the power spectrum goes to zero is given by eqn. (B.9)

$$q_o = 1 - \frac{h}{2} \tag{85}$$

This frequency defines the width of the main lobe. As given by eqn. (85) and illustrated in Fig. 13, the single index code with the lower index will have the wider main lobe.

The band occupancy of an r.f. signal is often defined as the bandwidth that contains a specified fraction of the total power in the modulated signal.

For example, the 99% bandwidth B_{99} passes 99% of the modulated power. In mathematical terms,

$$2 \cdot \int_{f_c-B_{99}/T}^{f_c+B_{99}/T} W(f)df = 0.99 \cdot \int_{-\infty}^{\infty} W(f)df \tag{86}$$

B is given as normalized frequency.

The 75% bandwidth and 99% bandwidth for several single index codes are listed in Table 2. A code with low index is seen to be more bandwidth efficient than a code with high index.

The integration (cfr. eqn. (86)) is done using a combination of Simpson's rule and Newton's 3/8 rule [33] with steplength $\Delta q = 0.0125$.

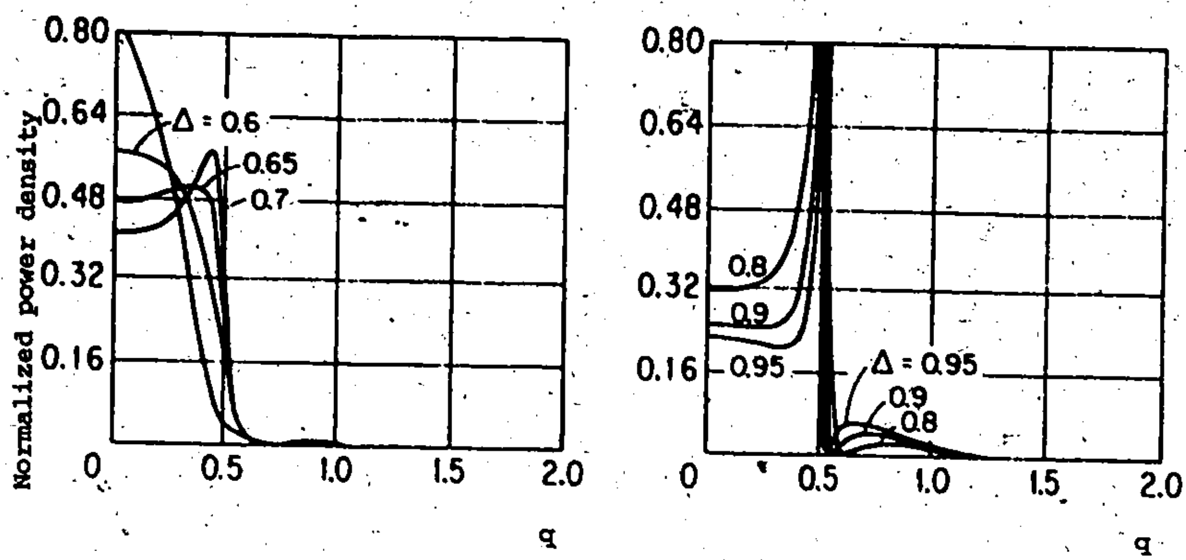

Fig. 13. POWER SPECTRA OF CONVENTIONAL CPFSK.

Δ is the modulation index. From [29].

Table 2: Bandwidth requirements, conventional CPFSK.

Index	B_{75}	B_{99}
0.3	0.14	0.50
0.4	0.21	0.56
0.5	0.29	0.60
0.6	0.35	0.65
0.7	0.43	0.90
0.8	0.48	0.96

4.2 Power Spectra of Multi-h Phase Codes with Small Index Spread

We now return to the multi-h codes with two or more indices. For such codes we shall find it convenient to define the mean index

$$\bar{h} = \frac{1}{K} \sum_{i=1}^{K} h_i \tag{87}$$

and the index spread

$$s^2 = \frac{1}{K-1} \sum_{i=1}^{K} (h_i - \bar{h})^2 \tag{88}$$

When the spread is small, we expect the spectrum to be very close to that of a single index code having modulation index equal to $\bar{h}$ [Appendix C]. This is illustrated in Fig. 14-16 which for three different mean indices show the spectra of codes with a small index spread and constraint length K = 2, 3, and 4 respectively.

In Appendix C we have also shown that in the limit when h_1, h_2, ..., $h_K \rightarrow \bar{h}$, the power spectrum is an average of the K spectra of the single index codes with indices h_1, h_2, ..., h_K. This explains why the spectra of multi-h codes with constraint length $K \geq 2$ do not go to zero, but only have notches were the corresponding single index spectrum with index h goes to zero. The width of the main lobe is defined by $q_o = 1 - h/2$. q_o will be called the notch frequency.

Consider codes with K = 2 and small spread in their indices. Because of the shape of the spectra shown in Fig. 13, we should expect the notchvalue to increase with increasing spread and with increasing mean index as the plot in Fig. 17 shows. We have also found that the notchvalue depends on the constraint length of the code. For low mean indices, the code with the longer constraint length will have the higher notchvalue as illustrated in Fig. 18.

The bandwidth requirements for multi-h phase codes with a small index spread may be found from Fig. 19. Curves for 75%, 95%, 99%, and 99.5% bandwidths are shown.

The curves for 75% and 95% bandwidths flatten out for high indices. This is due to the spectral peak that occurs when $h \to 1$. If the mainlobe does not contain the desired percentage of power, we have to increase the bandwidth substantially because of the notch. This also explains what seems to be a contradiction between Fig. 19 and the statement that Fast FSK has 99.5% of the total power in the main lobe [26]. In fact, our computation shows that the main lobe contains 99.497% of the power, and we have to increase the bandwidth B from 0.75 to 0.80 to include 99.50%.

The curves in Fig. 19 are plotted for codes with K = 2. However, since the single index spectrum is a good approximation for all multi-h codes with the same mean index, regardless of K, Fig. 19 provides good estimates B for the required bandwidth as long as B is less than the notch frequency q_o.

While the distance properties of a multi-h code are found to depend strongly on which code word was transmitted [12], [13], the power spectrum is not affected by which modulation index is made first available to the modulator (see eqn. (55), (56)).

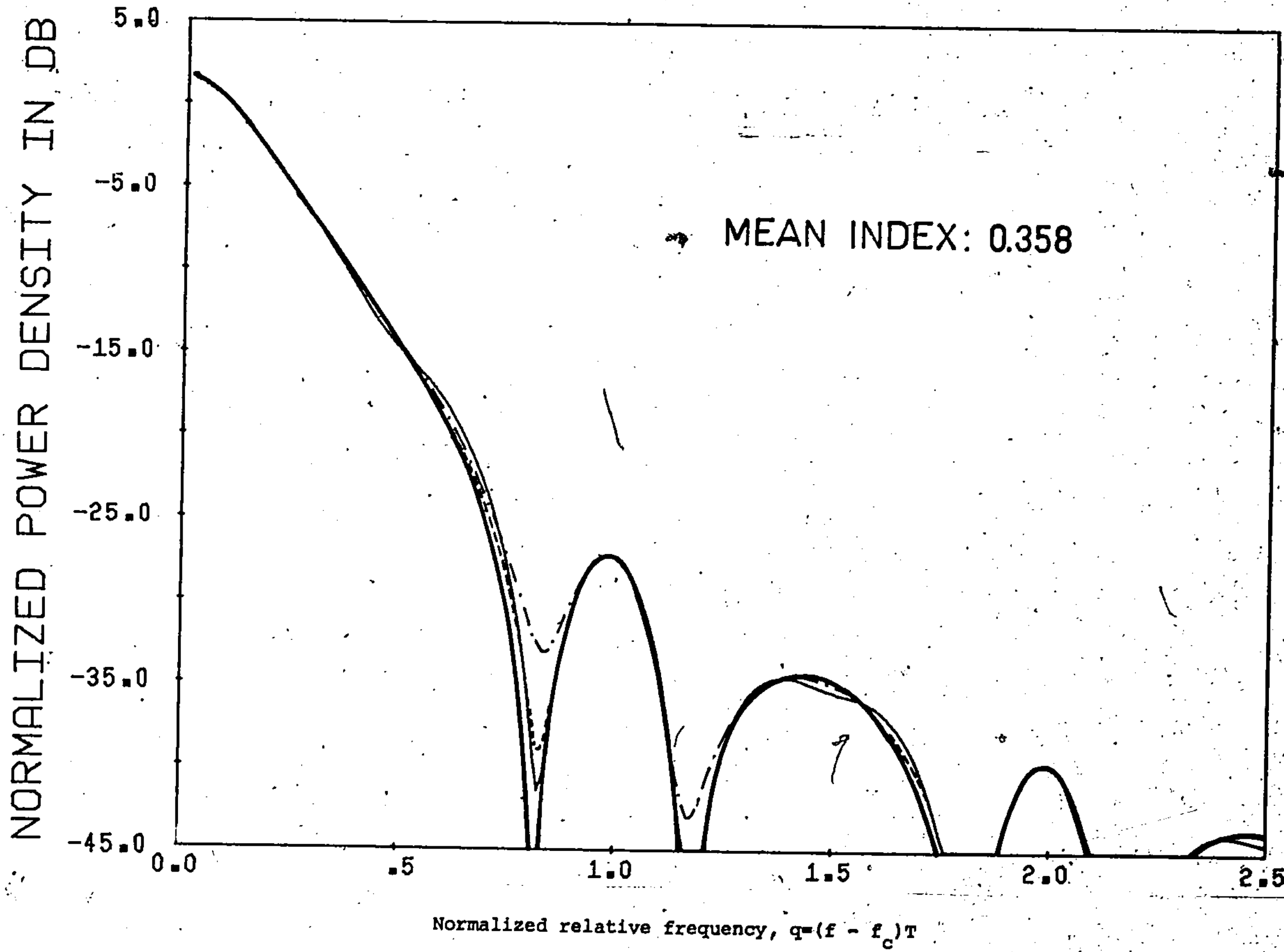

Fig. 14. POWER SPECTRA OF CODES WITH A SMALL INDEX SPREAD AND MEAN INDEX 0.358.

——— $K=1$, $h = 0.358$			
——— $K=2$, $\bar{h} = 0.357$	$s^2 = 0.010$	code	7/ 2 3
- - - - - $K=3$, $\bar{h} = 0.357$	$s^2 = 0.005$	code	14/ 4 5 6
- · - $K=4$, $\bar{h} = 0.359$	$s^2 = 0.011$	code	16/ 4 5 6 8

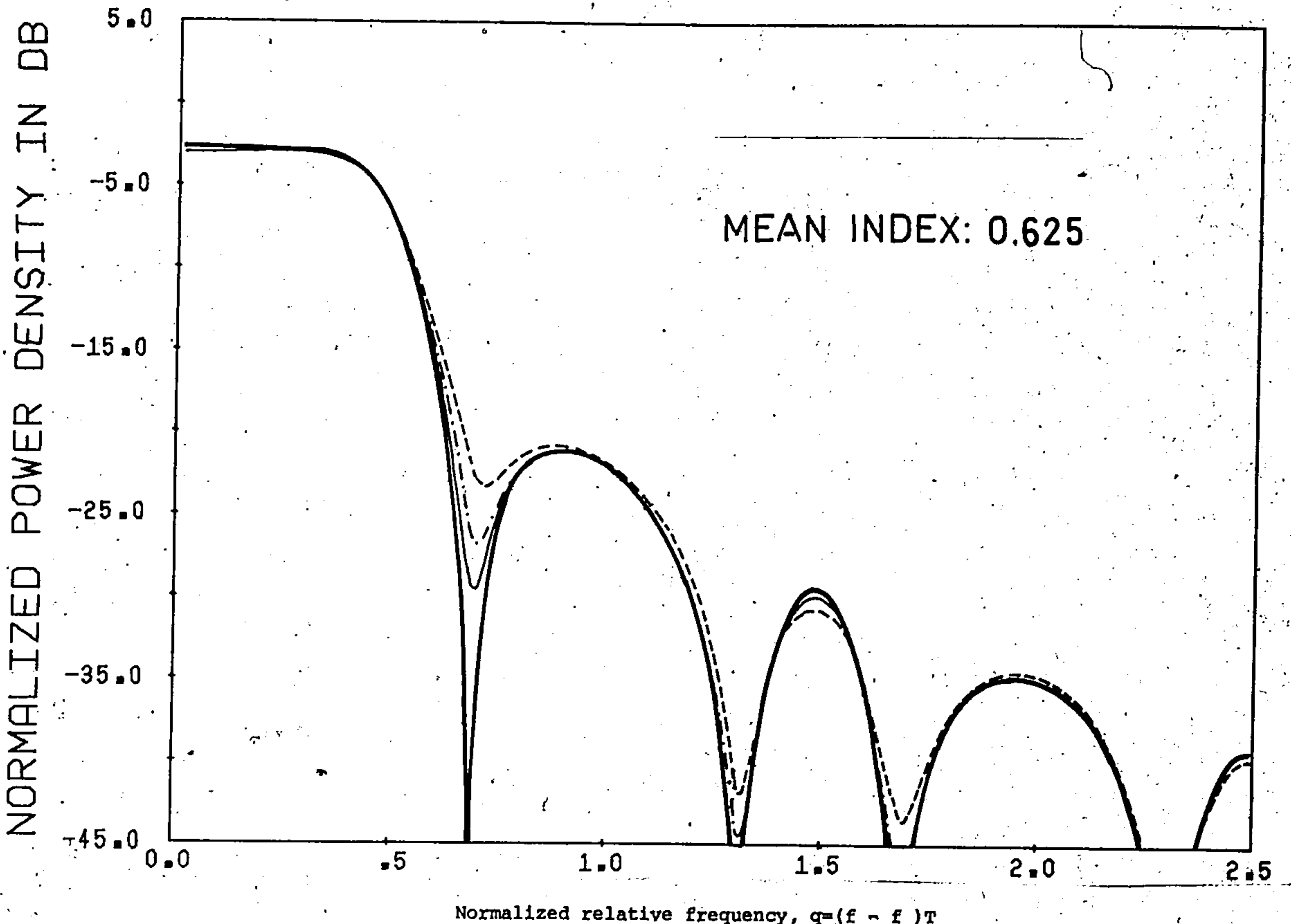

Fig. 15. POWER SPECTRA OF CODES WITH A SMALL INDEX SPREAD AND MEAN 0.625

- K=1, $h = 0.625$
- K=2, $\bar{h} = 0.625$, $s^2 = 0.003$ code 12/ 7 8
- K=3, $\bar{h} = 0.625$ $s^2 = 0.016$ code 8/ 4 5 6
- K=4, $\bar{h} = 0.625$ $s^2 = 0.006$ code 22/12 13 14 16

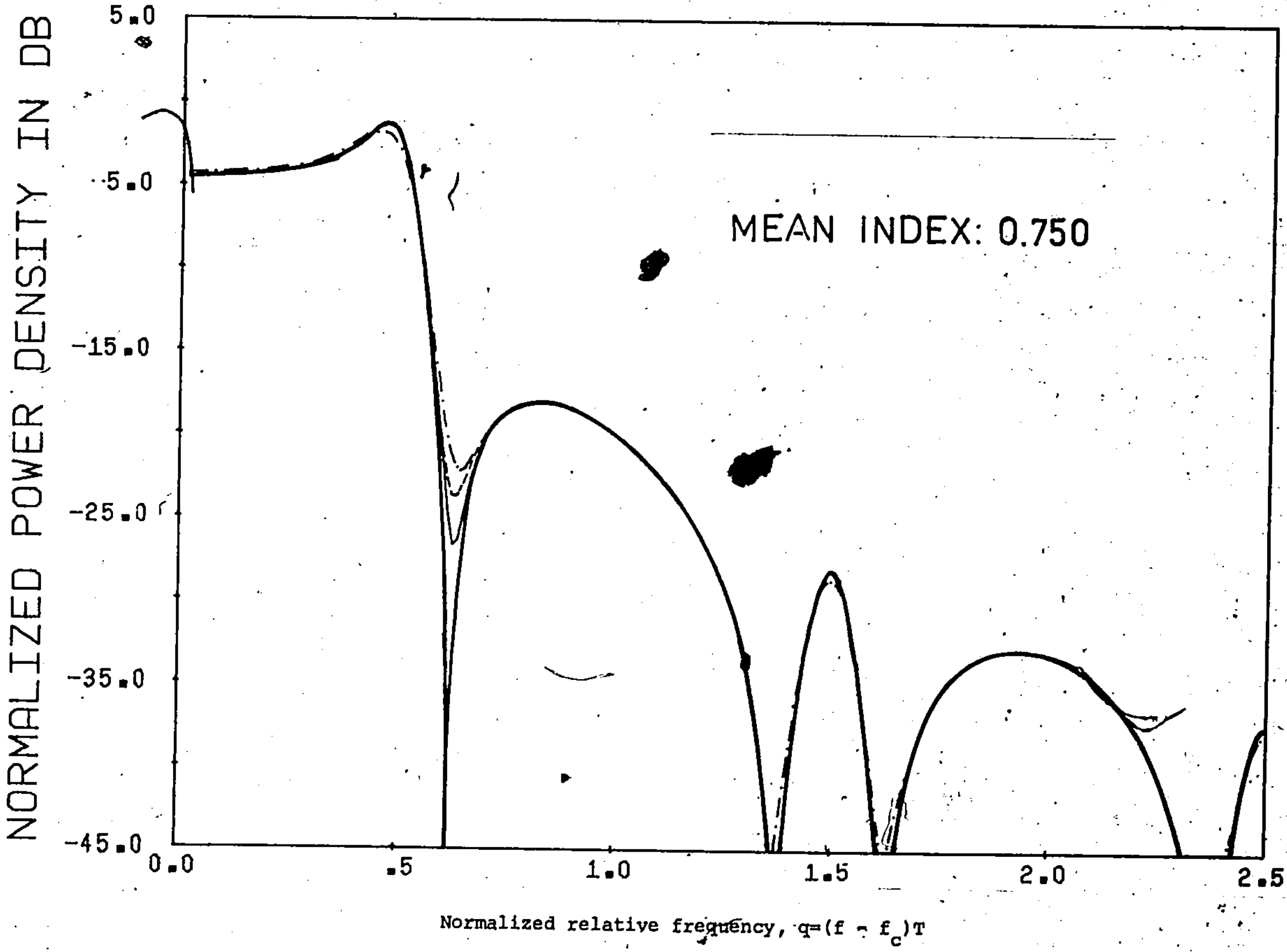

Fig. 16. POWER SPECTRA OF CODES WITH A SMALL INDEX SPREAD AND MEAN 0.750.

——— $K=1$, $h = 0.750$

——— $K=2$, $\bar{h} = 0.750$ $s^2 = 0.003$ code 14/10 11

- - - - - $K=3$, $\bar{h} = 0.750$ $s^2 = 0.004$ code 16/11 12 13

- ' - $K=4$, $\bar{h} = 0.750$ $s^2 = 0.006$ code 22/14 16 17 18

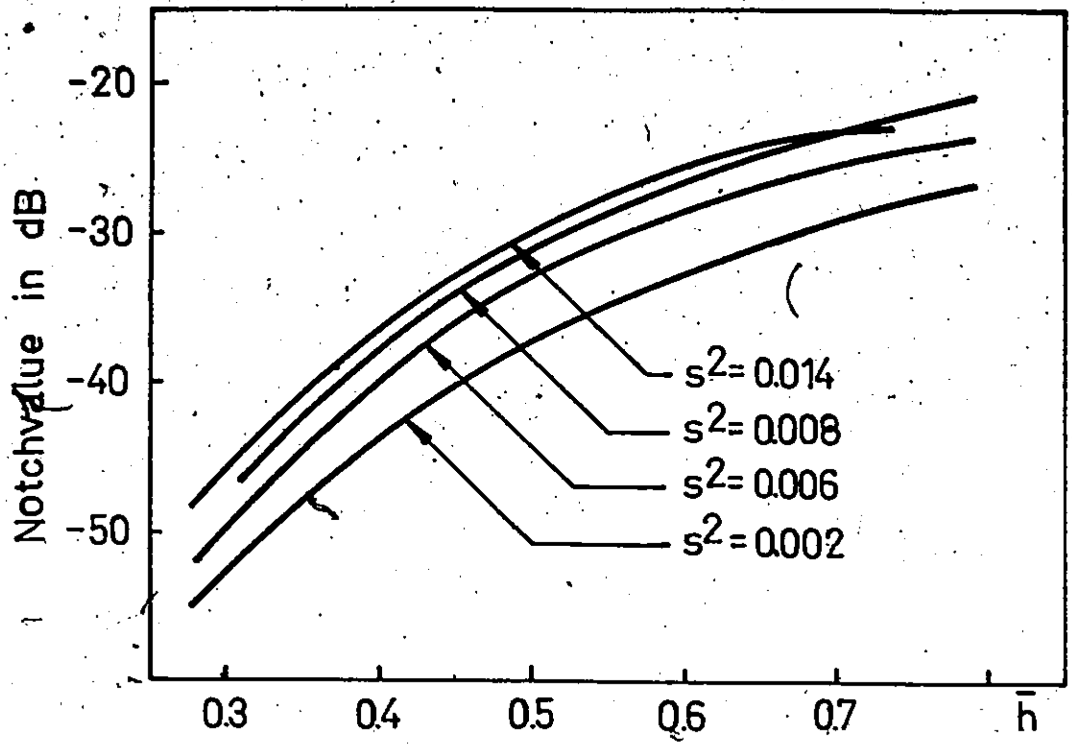

Fig. 17. NOTCHVALUE VERSUS MEAN INDEX AS A FUNCTION OF THE INDEX SPREAD. K = 2.

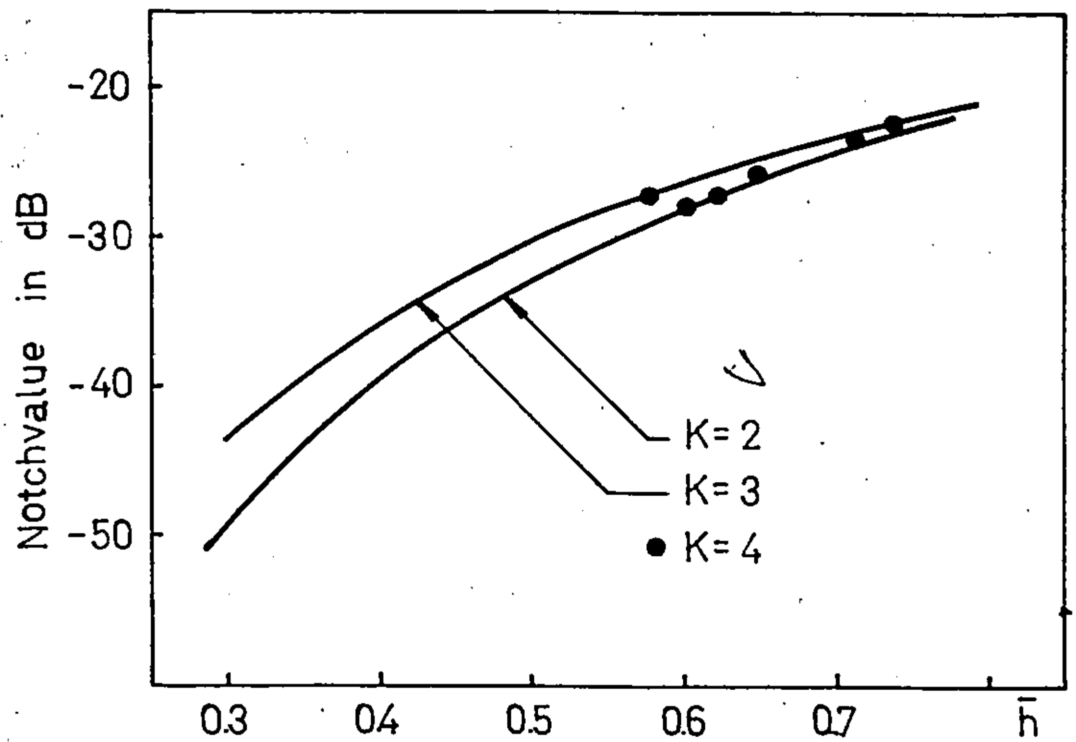

Fig. 18. NOTCHVALUE VERSUS MEAN INDEX AS A FUNCTION OF CONSTRAINT LENGTH. s^2 = 0.006.

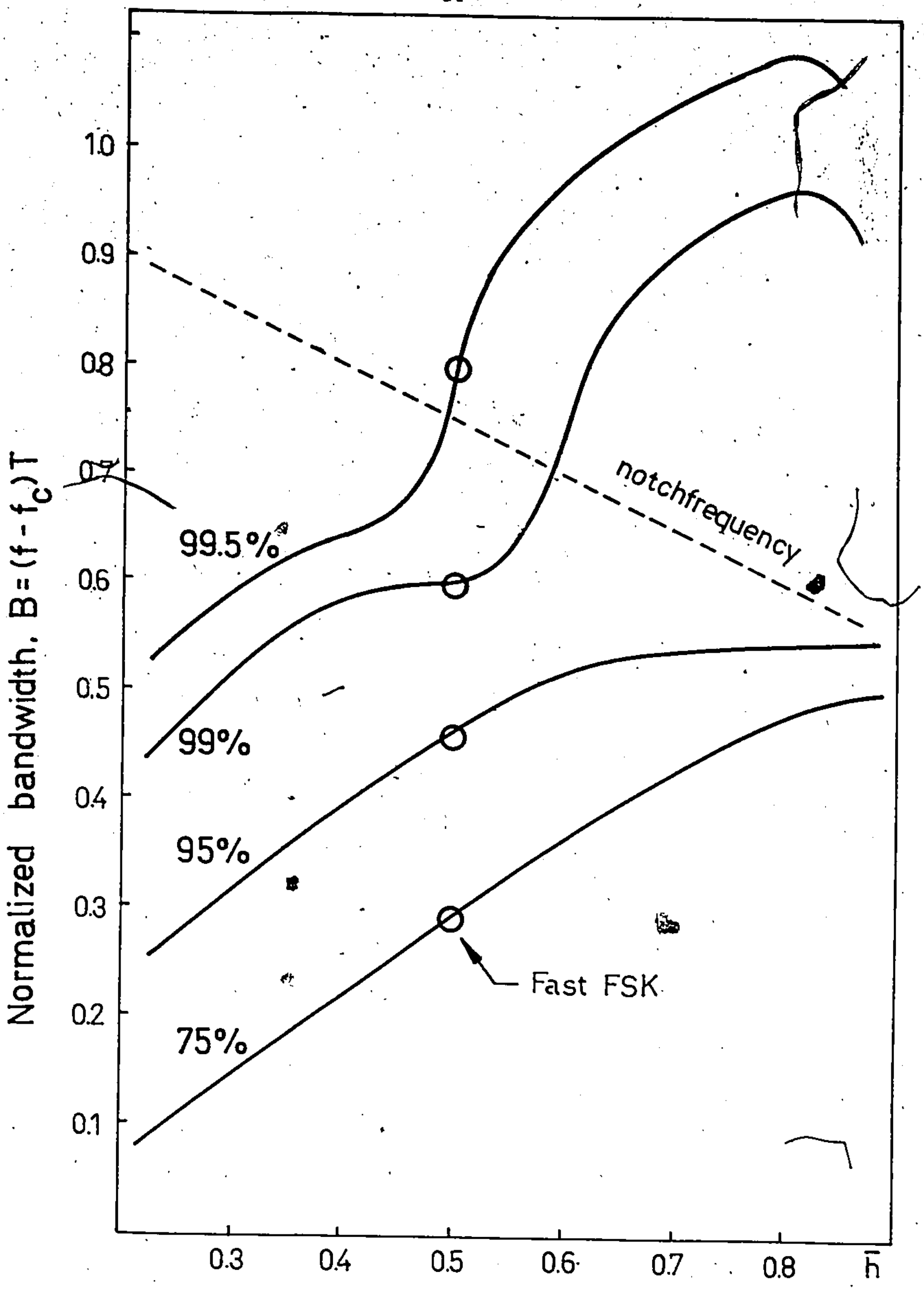

Fig. 19. BANDWIDTH REQUIREMENTS FOR CODES WITH A SMALL INDEX SPREAD. K = 2.

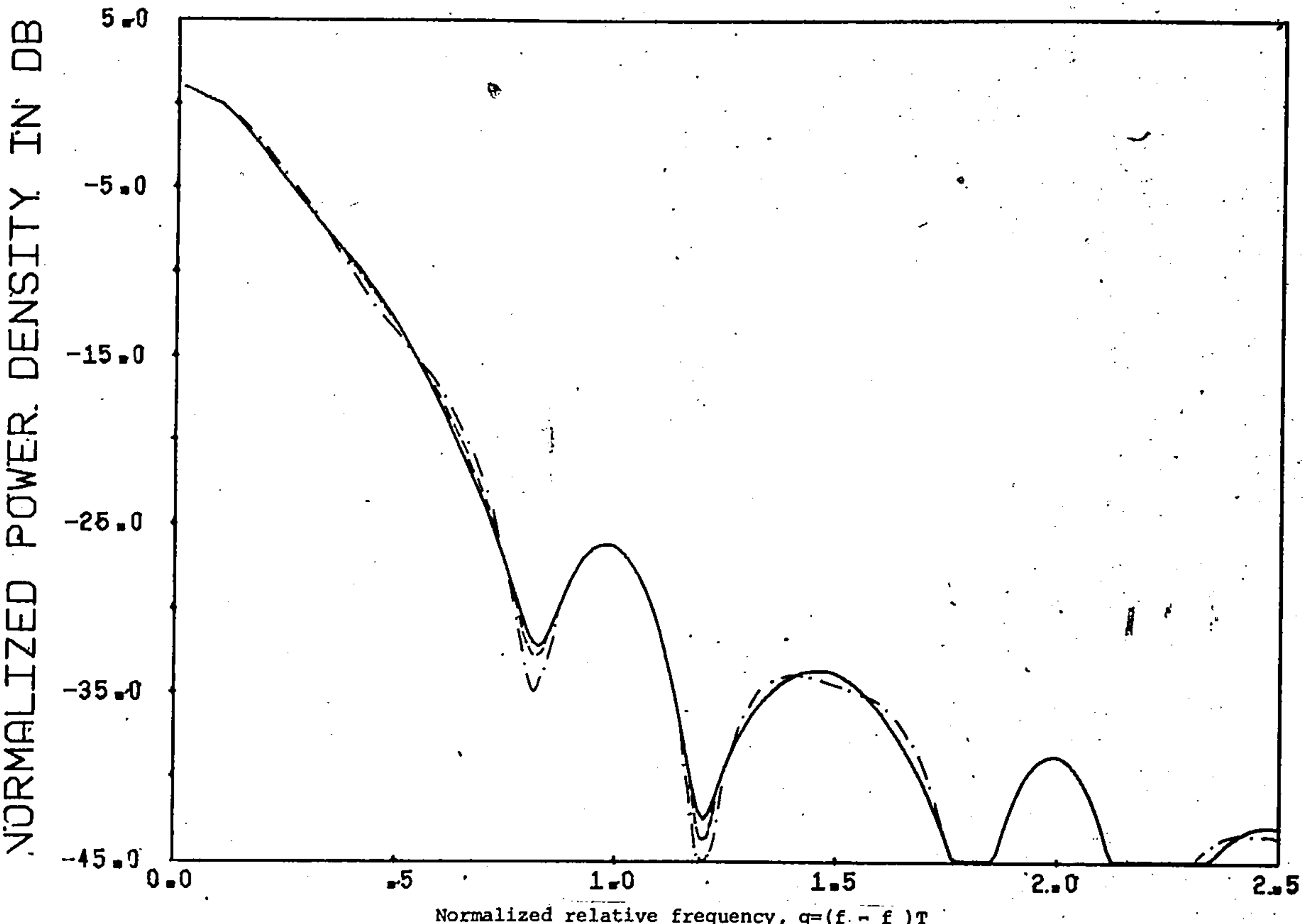

Fig . 20. VARIATIONS IN THE SPECTRUM DUE TO CHANGES IN THE INDEX SEQUENCE. K = 4.

———	16/ 6 4 7 8
-----	16/ 4 6 7 8
- · -	16/ 4 7 6 8

However, a permutation of the indices may influence the spectrum. This is found to be true when $K \geq 4$. Typical variations in the spectrum of a small spread code with constraint length $K = 4$ are shown in Fig. 20. There are three different sequences of the indices, and their corresponding coding gain [18] and bandwidth requirements are given in Table 3.

Table 3: The effects of index permutation

Code	Coding gain	Bandwidths B_{75}	B_{99}
16/4 6 7 8	1.45 dB	0.21	0.58
16/6 4 7 8	1.65 dB	0.21	0.56
16/4 7 6 8	1.21 dB	0.21	0.59

4.3 Power Spectra of Multi-h Phase Codes with Large Index-spread

When the code has a large spread in its indices, the power spectrum may no longer be closely approximated by a linear combination of single index spectra. Figs. 21 and 22 show how the spectrum of a K=2 code with mean index $\bar{h} = 0.375$ and $\bar{h} = 0.625$ respectively, varies with increasing spread.

Table 4 shows that a code with a small index spread is most bandwidth efficient. We know that no code with a large index spread provides a higher coding gain than a small spread code with the same

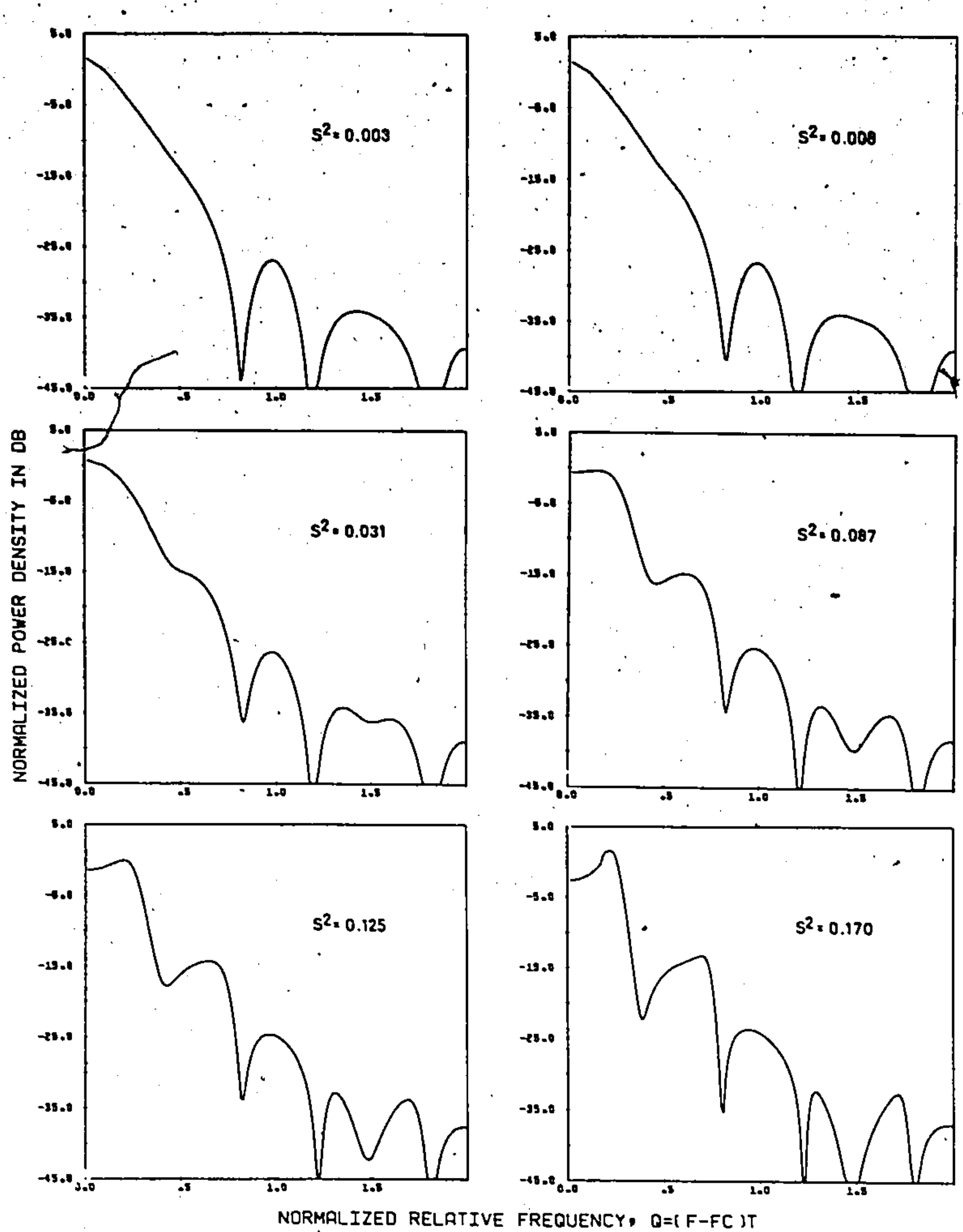

Fig. 21. POWER SPECTRA OF CODES WITH MEAN INDEX 0.375 AND VARYING SPREAD. K = 2.

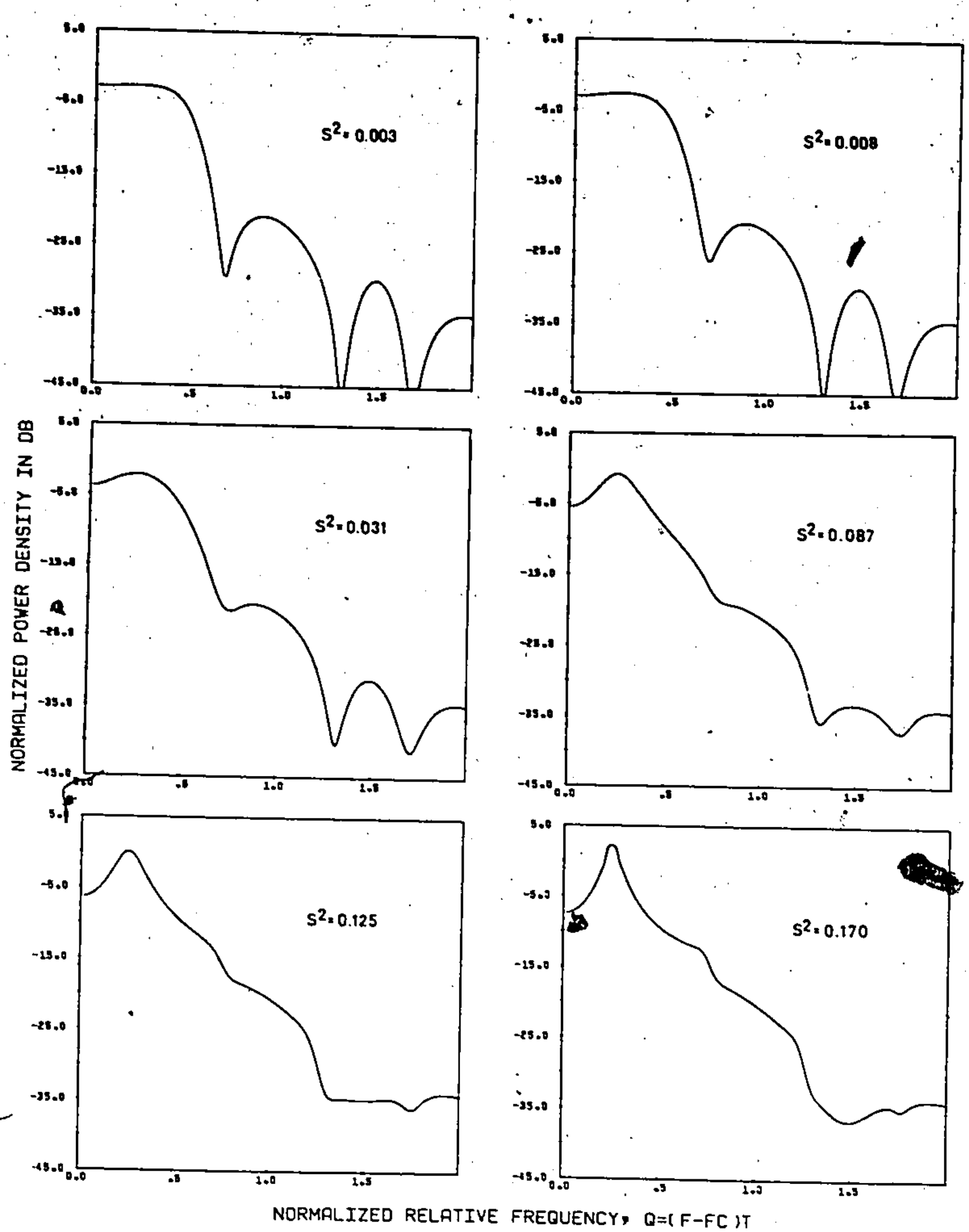

Fig. 22: POWER SPECTRA OF CODES WITH MEAN INDEX 0.625 AND VARYING SPREAD. K = 2.

Table 4: Bandwidth requirements of codes with given mean index and varying spread

	h = 0.375		h = 0.625	
s^2	B_{75}	B_{99}	B_{75}	B_{99}
0.003	0.19	0.55	0.38	0.81
0.008	0.20	0.56	0.38	0.81
0.031	0.20	0.61	0.36	0.85
0.087	0.23	0.68	0.35	0.89
0.125	0.24	0.70	0.35	0.91
0.170	0.24	0.73	0.34	0.94

mean index [18]. Since a good code should combine bandwidth efficiency and a high coding gain, we conclude that the multi-h phase codes of interest are those with a small index spread.

While a code with constraint length K = 2 is uniquely defined by its mean and spread, this is not the case for codes with K > 2. It turns out that two codes with the same mean index and spread may have different spectra as illustrated in Fig. 23. Fig. 24 shows that the constraint length K will also affect the spectrum. The distribution of the indices around the mean value seems to be the dominant effect of those two.

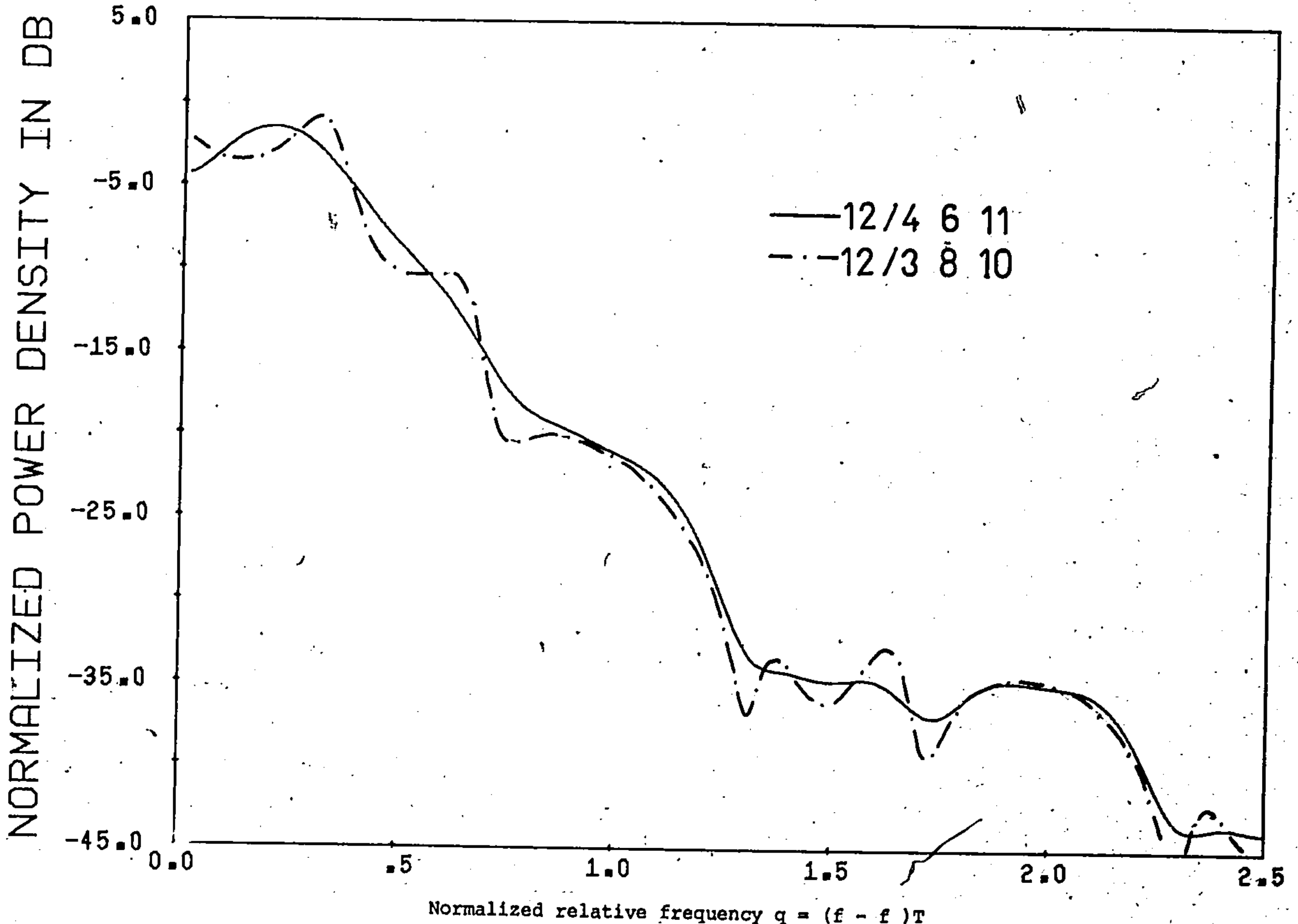

Fig. 23. POWER SPECTRA OF CODES WITH EQUAL MEAN INDEX AND SPREAD BUT DIFFERENT DISTRIBUTION OF THE INDICES. $\bar{h} = 0.583$. $s^2 = 0.09$.

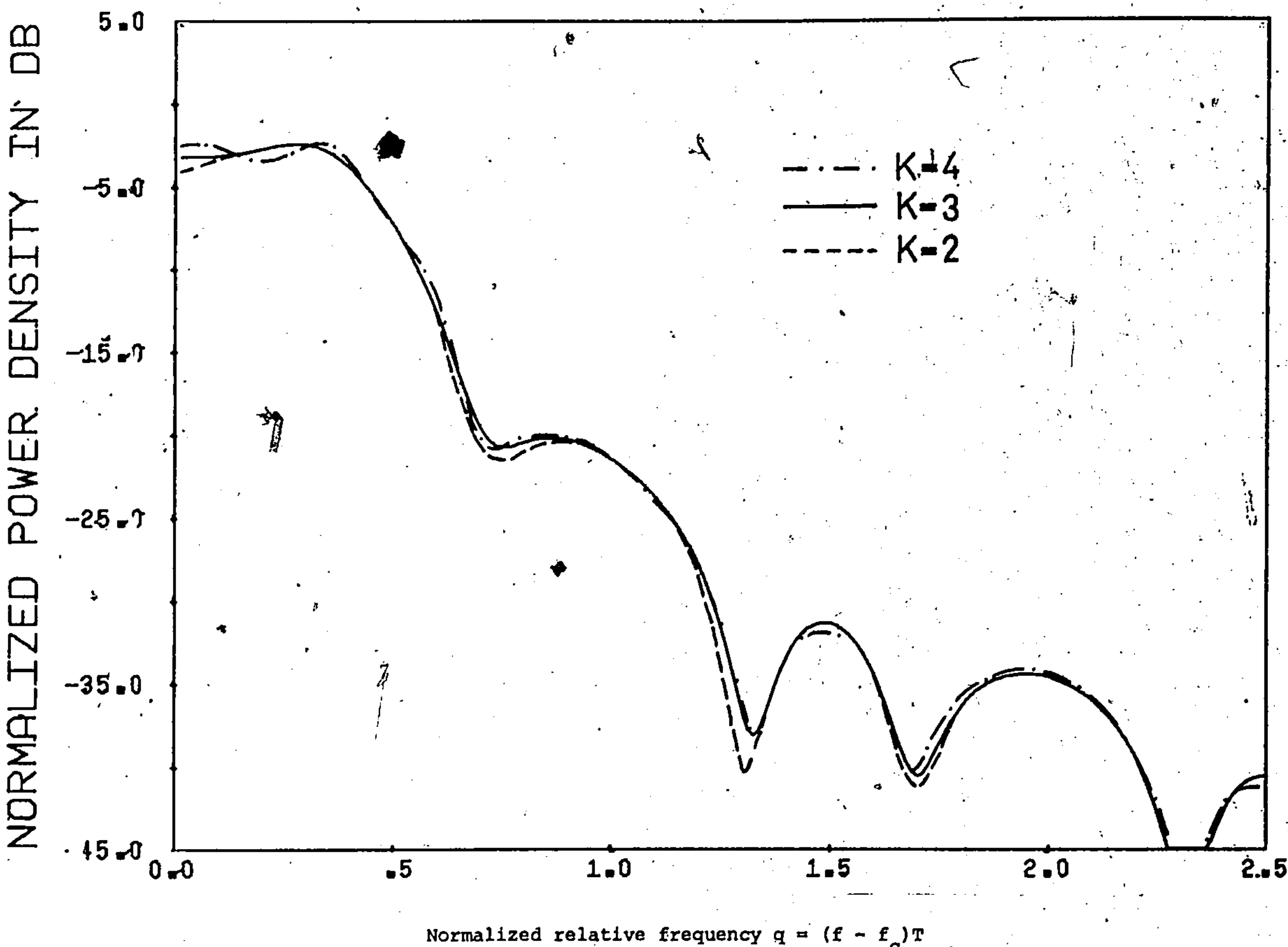

Fig . 24. POWER SPECTRA OF CODES WITH EQUAL MEAN AND SPREAD BUT DIFFERENT CONSTRAINT LENGTH. $\bar{h} = 0.625$. $s^2 = 0.032$.

K = 4: 22/ 16 18 13 8, K = 3: 17/ 8 10 14, K = 2: 4/ 2 3

4.4 Some Remarks

We have seen that the power spectrum provides an estimate of required bandwidth. This estimate, however, is based upon two assumptions.

First, the spectrum shows the distribution of power versus frequency for what the model defines as a "typical" data sequence, i.e. an aperiodic sequence without long strings of ones or zeros. There may exist certain important but "untypical" data sequences for which the spectral analysis is completely misleading.

Second, we have assumed that the power spectrum also defines the distribution of information power. But say the information is carried by frequency components outside the mainlobe. If we filter out the sidelobes, we will still receive most of the total power, but all the information is lost. Laboratory and field testing of a Fast FSK system, however, indicates that our assumption is acceptable [34], [35], and that the information is carried by all frequency components of the signal.

The spectra of multi-h codes are obtained assuming bipolar (±1) signalling and we can thus compare their spectral properties with those of existing modulation schemes such as QPSK and Fast FSK which both require bipolar data. Multi-h codes using unipolar (0, 1) signalling will have a spectrum that is nonsymmetrical around the carrier frequency, and this leads to a complicated spectral analysis [Appendix D].

4.5 Conclusion

Let us sum up the most important spectral results.

The tail of the power spectrum rolls off as $1/f^4$ since a multi-h code is a frequency modulated signal with continuous phase.

The spectrum contains no lines provided the data sequence is random and two or more modulation indices are used in the modulation.

The important subclass of multi-h codes are those with their indices tightly clustered around the mean index $\bar{h}$ ($s^2 < 0.015$). Their spectra may be approximated by the spectrum of the single index code with index $\bar{h}$, or by the linear combination of the K spectra of single index codes with indices $h_1, h_2, \ldots, h_K$. The codes require a bandwidth as given by Fig. 19. In general, codes with a low mean index are more bandwidth efficient.

Such spectra do not go to zero but they have notches where the corresponding single index spectrum has zeros. The notchvalue varies with the index spread and the constraint length of a code.

The spectrum is not affected by which index is used first, but for $K \geq 4$, a permutation of the indices will lead to minor changes in the spectrum.

CHAPTER 5

BAND OCCUPANCY VERSUS ERROR PERFORMANCE

It is desirable to transmit data over a bandlimited channel at as high a speed as possible and with good transmission quality.

We have seen that there exist bandwidth efficient multi-h codes and that there exist codes with better error performance than Fast FSK. Evidently, multi-h coding can be used for high-speed transmission as well as high-quality transmission. Since transmission quality is obtained by trading bandwidth for noise immunity, however, we should ask whether codes exist which combine bandwidth efficiency and high coding gain.

In this chapter we investigate the trade-off between band occupancy and error performance of multi-h phase codes. We have limited ourselves to consider codes with maximum 16 phases ($S \leq 16$) and with a small spread in their indices ($s^2 \lesssim 0.025$).

We define the band occupancy of a code as the bandwidth that contains 99% of the modulated power, as recommended by the Federal Communications Commission [36].

For these codes, the minimum distance is plotted versus the required bandwidth, and Fig. 25 shows the envelope of the plots. For comparison, the data for Fast FSK is plotted on the same figure. It is clear that there are codes which conserve both power and bandwidth

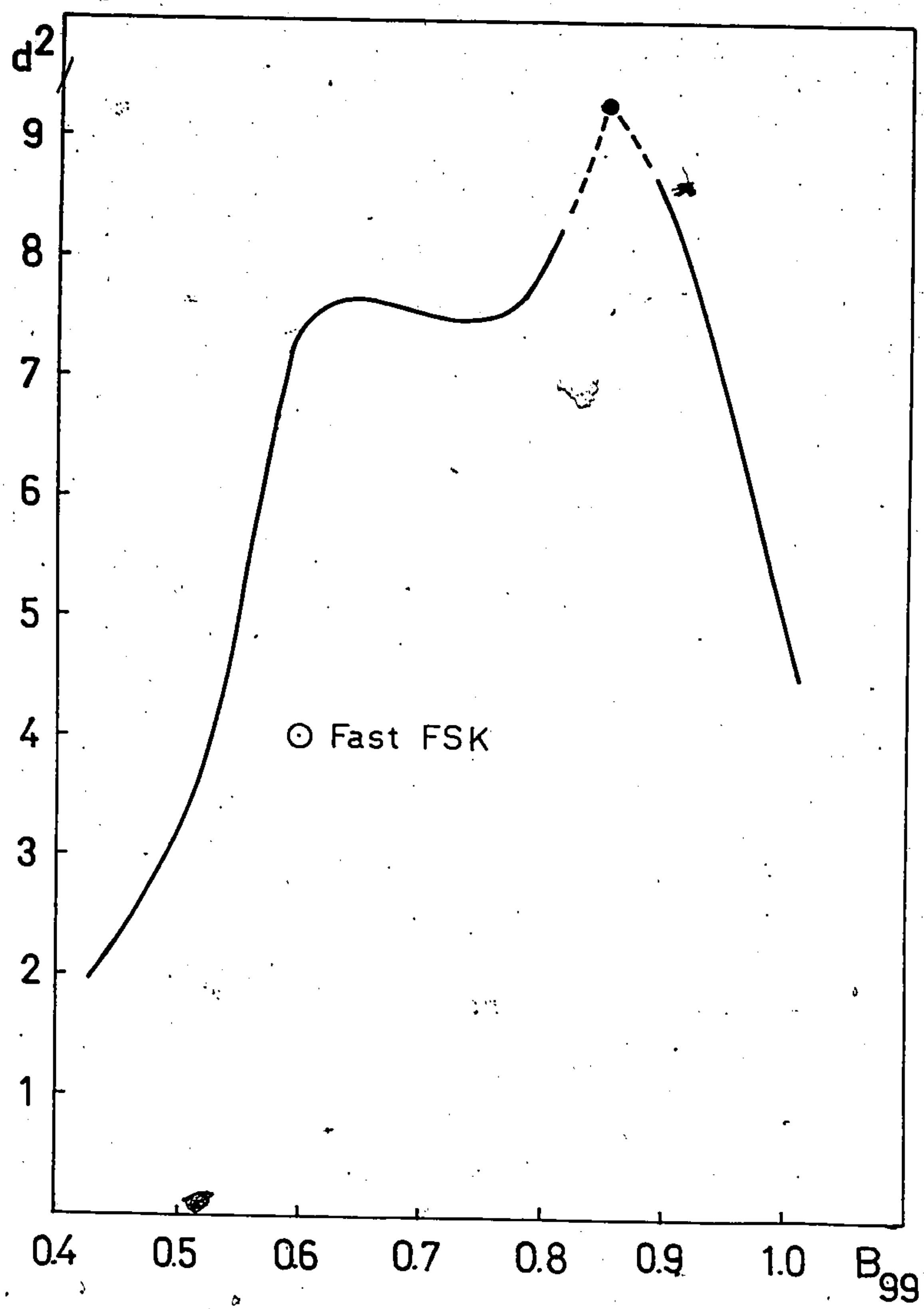

Fig. 25. MINIMUM DISTANCE VERSUS 99% BANDWIDTH.

better than Fast FSK, and multi-h coding may therefore be well suited for high-speed, high-quality data transmission.

5.1 Comparison of Multi-h Phase Coding, QPSK and Fast FSK

The power spectra of QPSK, Fast FSK and a multi-h code with the same error performance as the former two modulation methods, are shown in Fig. 26. Data for the three modulation techniques are listed in Table 5. Coding gain means gain compared to Fast FSK. The bandwidth requirements for various fractions of the total power inside the band are given, as defined in Chapter 4. Decision depth is a measure of the decoder complexity. It is defined in Chapter 2. Table 5 therefore indicates that the multi-h code yields a 12% savings in bandwidth compared to Fast FSK, and this is obtained at considerable penalty in implementation.

Table 5: Bandwidth requirements of modulation schemes with equal error performance

Modulation method	Coding gain	Bandwidths B_n n=75%	95%	99%	99.5%	Decision depth
QPSK	0 dB		0.95			1
Fast FSK	0 dB	0.29	0.46	0.60	0.80	2
Multi-h code (16/5 6)	0.06 dB	0.18	0.35	0.53	0.60	16

The band occupancy of the signals may also be compared by looking at their fractional out-of-band power W_{ob} defined as the fraction of the total power in the modulated signal s(t) which does not pass through a rectangular filter with nonzero transfer function in the frequency interval (f_c-B/T, f_c+B/T). Mathematically,

$$W_{ob} = 1 - \frac{2 \int_{-B/T}^{B/T} W(f)df}{\int_{-\infty}^{\infty} W(f)df} \tag{89}$$

Fig. 27 compares the fractional out-of-band power for QPSK, Fast FSK and the particular multi-h code. The data for QPSK are taken from [26]. As seen from Fig. 26, Fast FSK is marginally less efficient than QPSK for normalized frequencies q less than 0.5. For greater frequencies, however, Fast FSK is superior to QPSK as indicated in Fig. 27. The multi-h code is superior to QPSK and Fast FSK for all frequencies.

As shown in Fig. 26, 75% of the total power inside the band corresponds to W_{ob} = -6 dB, 95% corresponds to W_{ob} = -13 dB, 99% to W_{ob} = -20 dB, and 99.5% to W_{ob} = -23 dB.

The curve showing W_{ob} for a signal will level out for frequencies when the power spectrum either goes to zero or has a deep notch. The power spectrum of Fast FSK has its first zero for q = 0.75, and Fig. 26 shows that Fast FSK has 99.5% of its total power contained in the main lobe. This fact is also illustrated in Fig. 19.

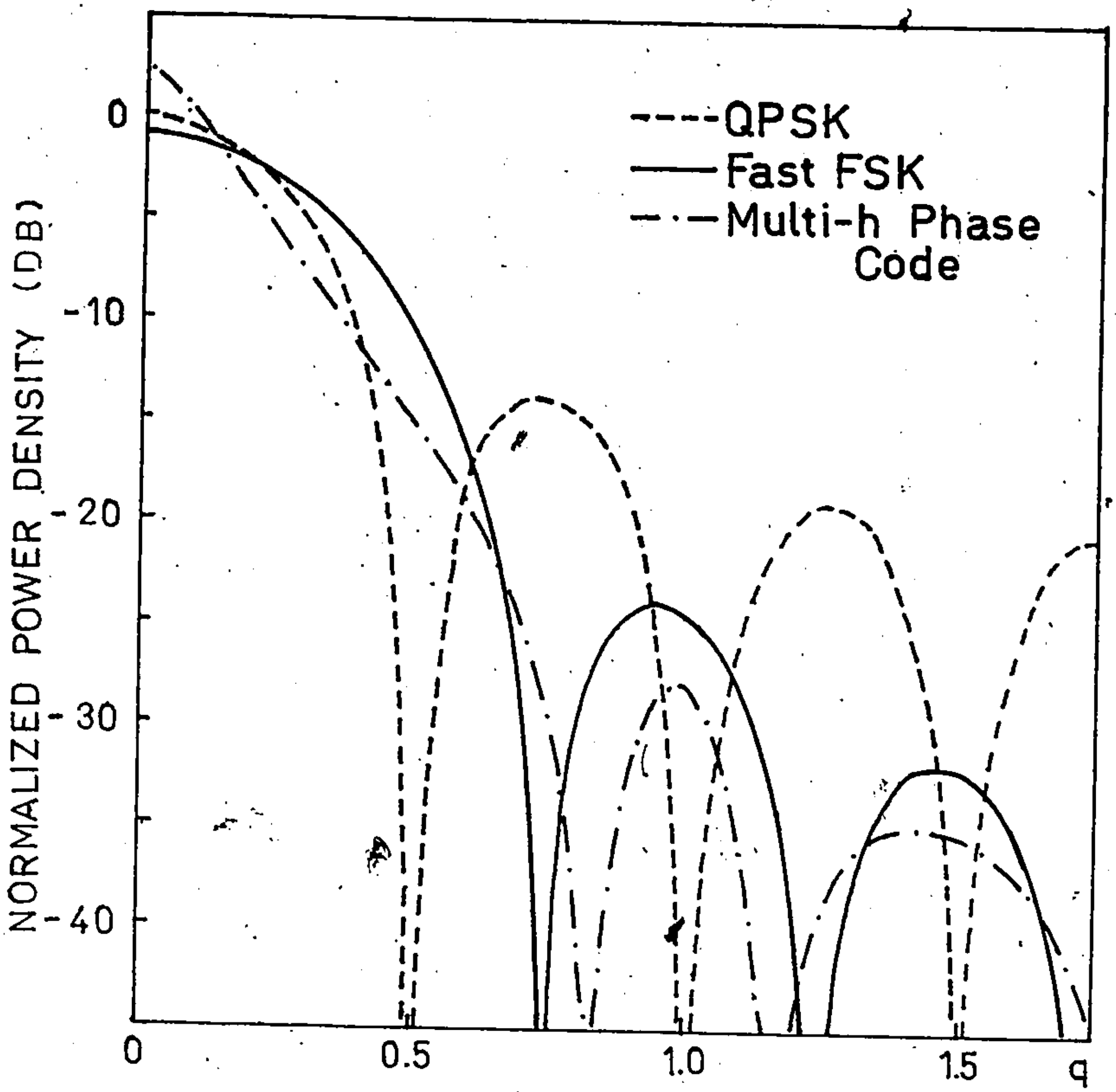

Fig. 26. POWER SPECTRA OF QPSK, Fast FSK AND MULTI-H PHASE CODING.

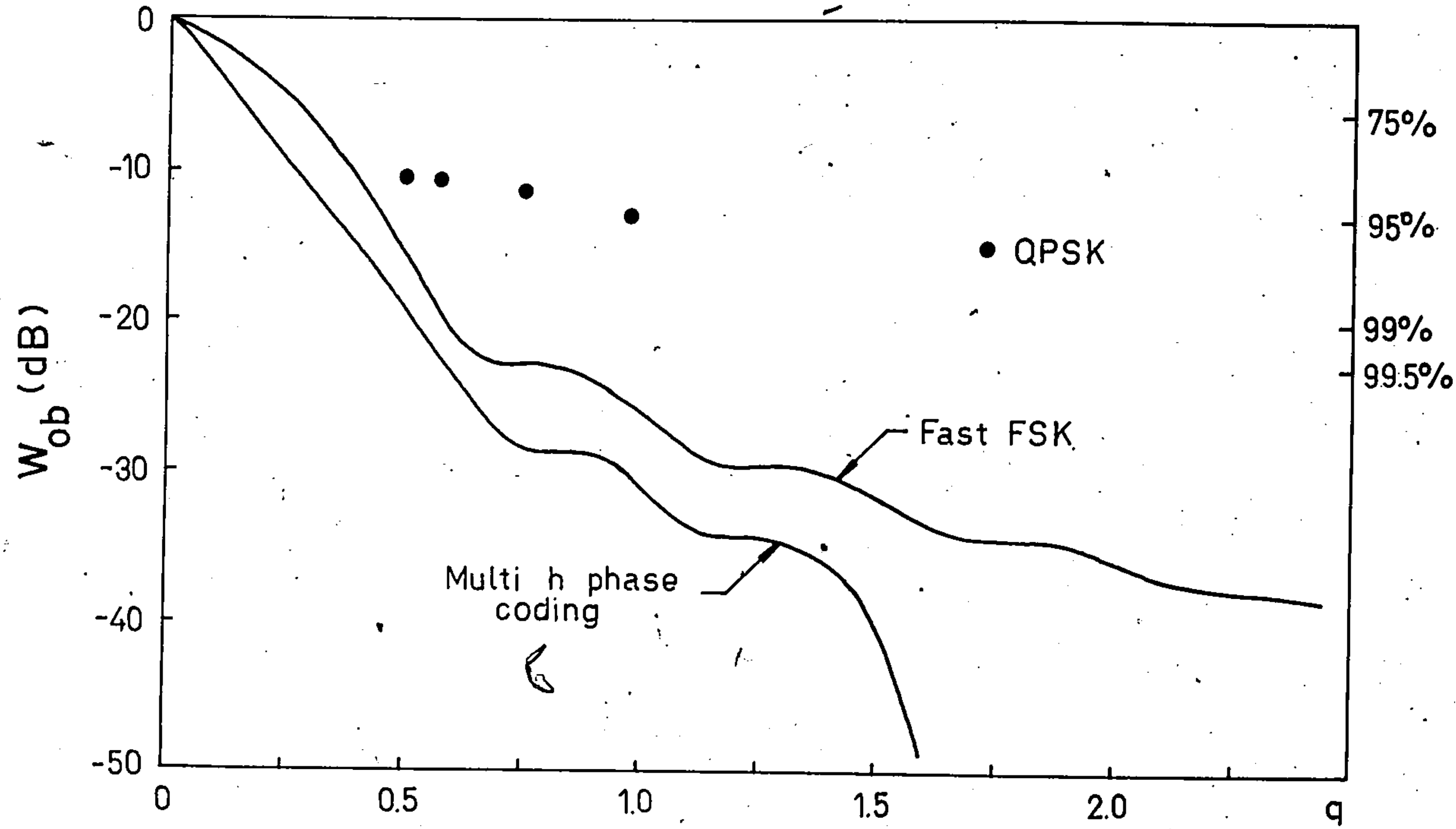

Fig. 27. FRACTIONAL OUT-OF-BAND POWERS FOR QPSK, Fast FSK AND MULTI-H PHASE CODING.

5.2 Classes of Multi-h Phase Codes

Fig. 24 shows that there are three interesting subclasses of the codes we are considering, namely

CLASS I : Codes with high coding gain, i.e. $d^2_{min} \geq 7.0$

CLASS II : Codes with better coding gain and less bandwidth needs than Fast FSK, i.e. $d^2_{min} \geq 4.0$ and $B_{99} \leq 0.60$

CLASS III: Bandwidth efficient codes i.e. $B_{99} \leq 0.55$

Data for the codes belonging to the three classes are given in Appendix E. For each code, we have specified the coding gain compared to Fast FSK, bandwidth requirements, and decision depth. Also included is the difference between the maximum value in the main lobe of the power spectrum and the maximum value in the first side lobe. This value is a measure of the filtering needed. A high sidelobe (and a small difference) requires a sharp filter in order to suppress the frequency components out-of-band.

Some general conclusions can be drawn from the data. High coding gain is obtained at the cost of complexity and bandwidth. Codes with good error performance are usually constraint 3 or 4 codes which means the encoder is complex. The decision depth is long so the decoding will be complicated, and the sidelobe is relatively high such that sharp filtering is required.

Bandwidth efficient codes trade bandwidth for coding gain and complexity although they in general are simpler to implement than codes with high coding gain.

5.2.1 Class I: Codes with High Coding Gain

Data for the best constraint 4, 3, and 2 codes, respectively, are shown in Table 6. We have also included data for two simpler codes. A 2-4 dB coding gain compared to Fast FSK is obtained at the expense of a 2% to 42% increase in band occupancy and increased complexity. As pointed out in [14], convolutional codes can give the same coding gain, but they will require wider bandwidth [37].

Table 6: Bandwidth requirements of codes with high coding gain.

Code	Coding gain	Bandwidth B_n n = 75.0%	95.0%	99.0%	99.5%	Decision Depth
16/12 10 11 8	3.66 dB	.38	.53	.85	1.00	26-38
16/10 11 12	3.36 dB	.41	.53	.89	1.03	26-27
16/8 9	2.74 dB	.30	.48	.61	.89	20
⋮	⋮	⋮	⋮	⋮	⋮	⋮
8/4 5 6	2.77 dB	.38	.53	.84	1.00	7-9
8/4 5	2.49 dB	.33	.50	.65	.94	9

The power spectra of the three 16 phases codes are shown in Fig. 28 and their fractional out-of-band-power curves in Fig. 29.

The two simpler codes have spectra as illustrated in Fig. 30. The code 8/4 5 6 has an out-of-band-power curve that closely follows the

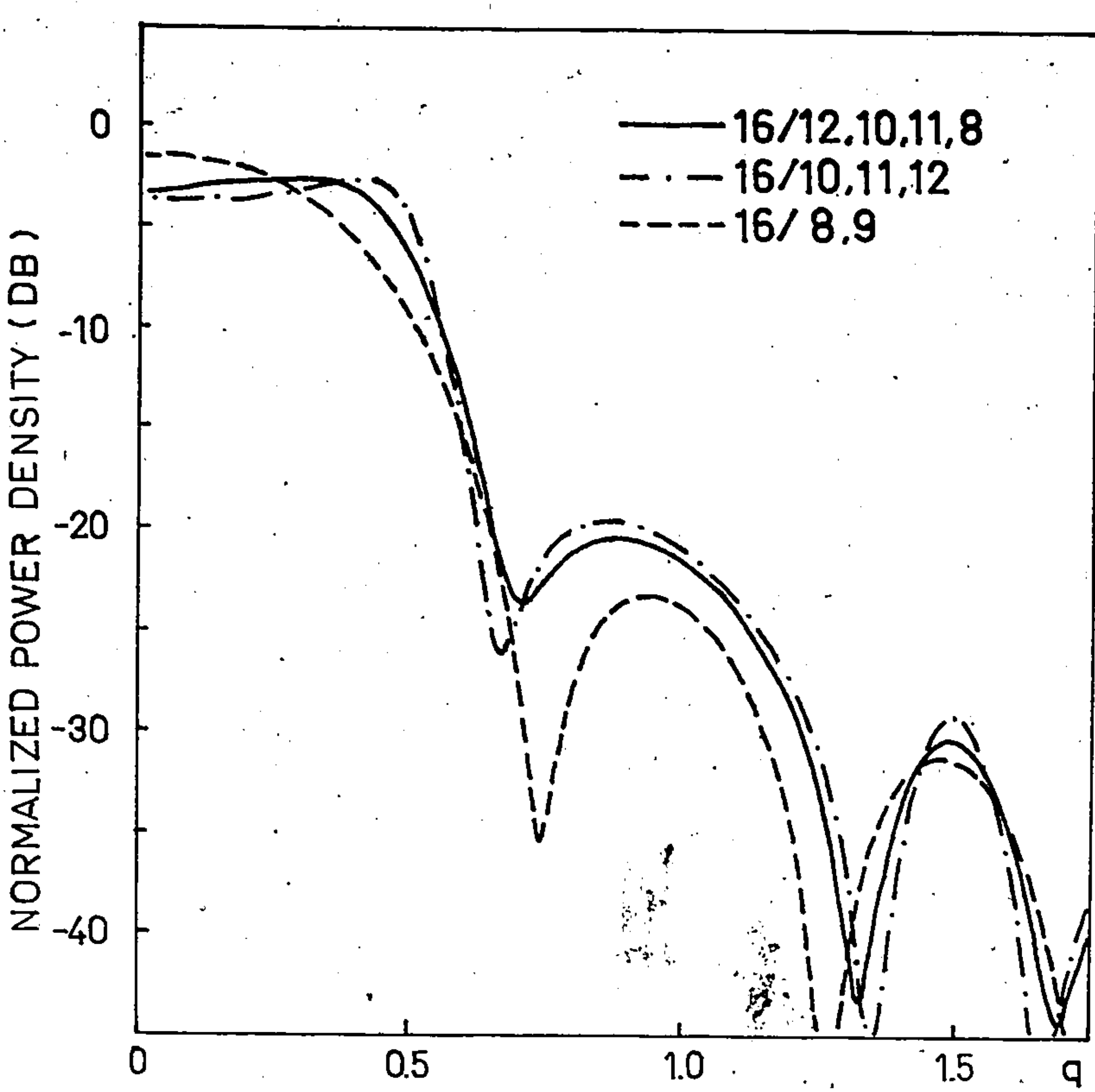

Fig. 28. POWER SPECTRA OF CODES WITH HIGH CODING GAIN.

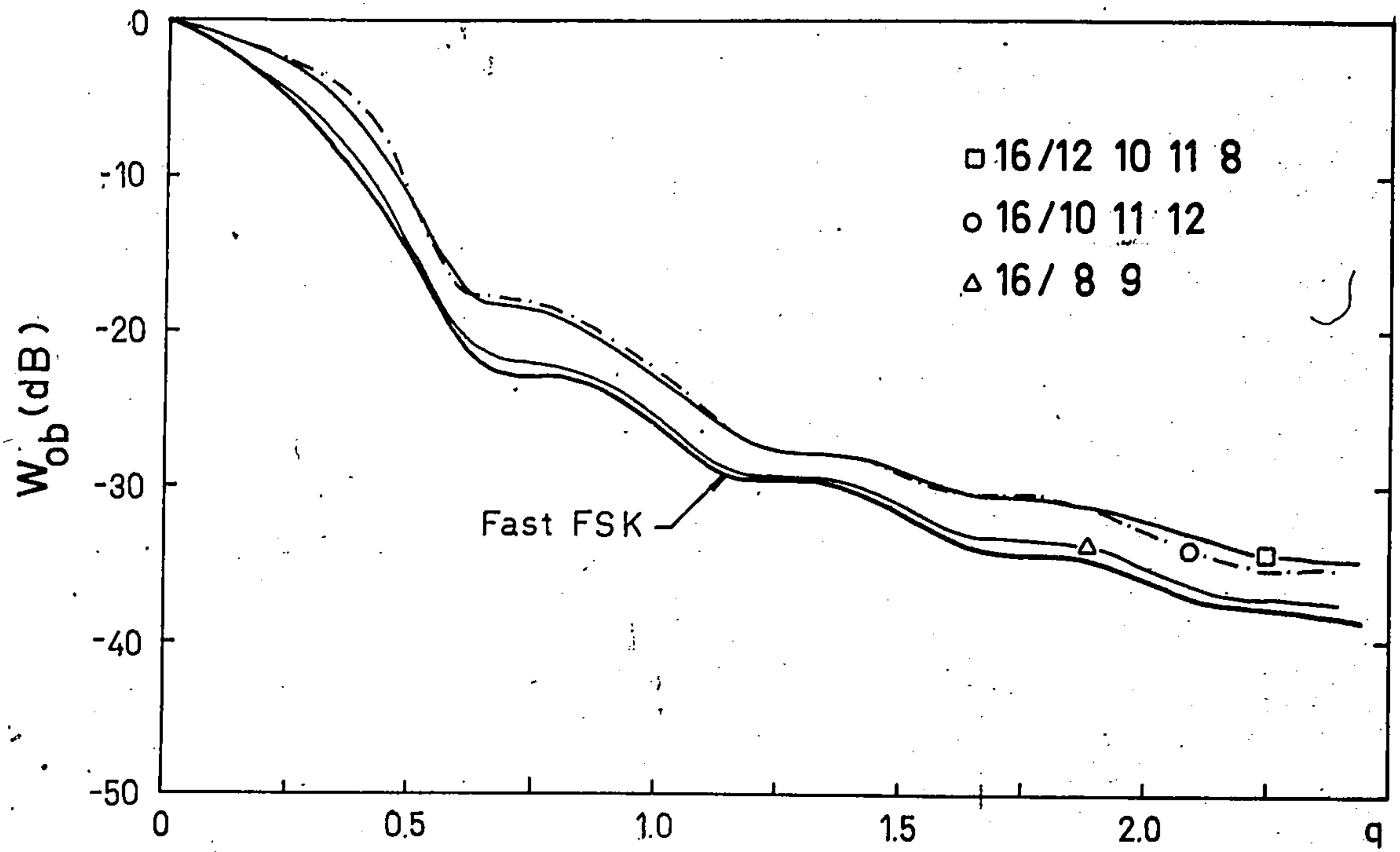

Fig. 29. FRACTIONAL OUT-OF-BAND POWERS FOR CODES WITH HIGH CODING GAIN.

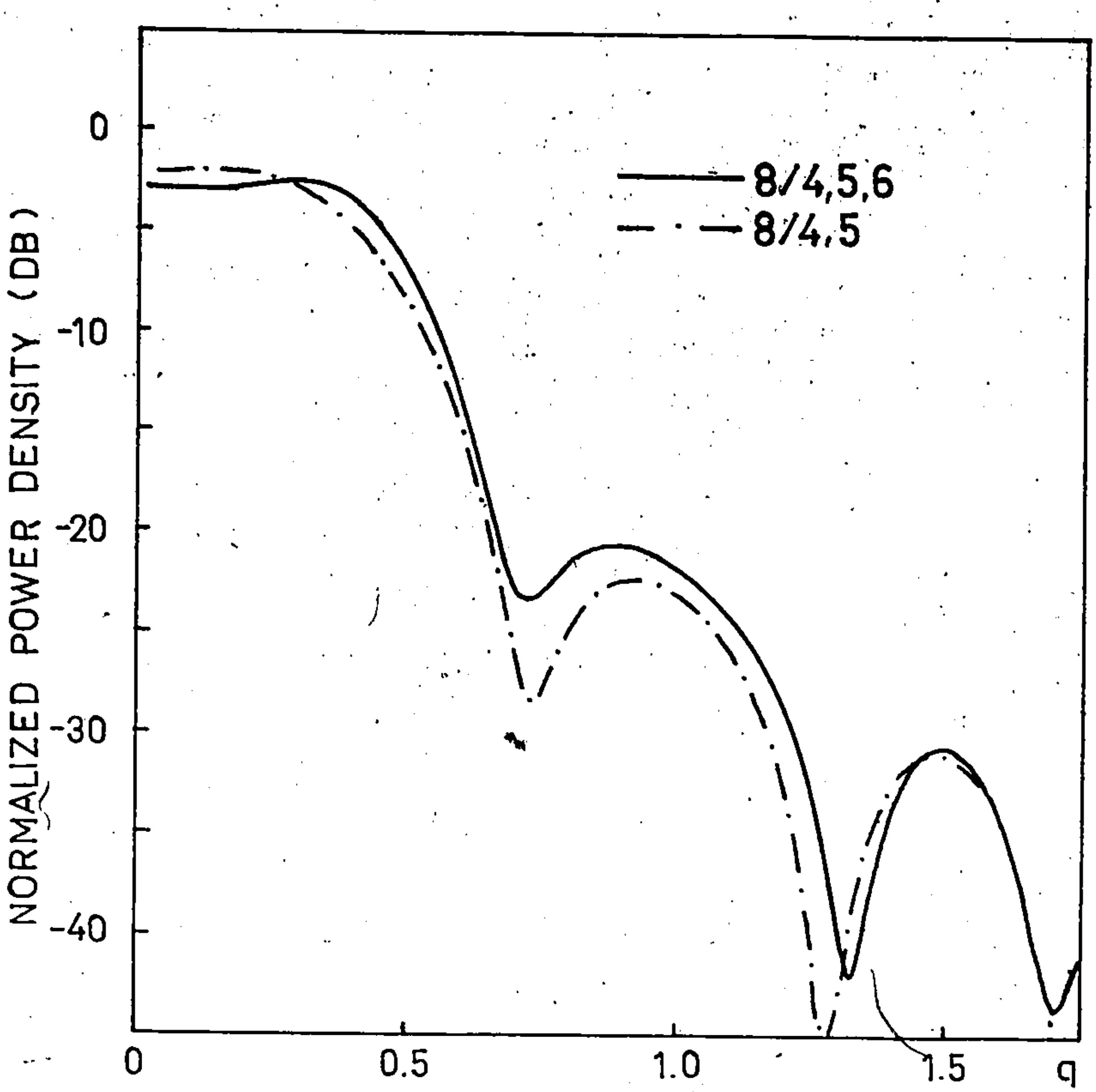

Fig. 30. POWER SPECTRA OF SIMPLE CODES WITH HIGH CODING GAIN.

curve for the constraint 4 code 16/12 10 11 8, while the curve for the code 8/4 5 shows a slightly better bandwidth efficiency.

5.2.2 Class II: Codes with higher coding gain and less band occupancy than Fast FSK

There is a multi-h code with the same bandwidth efficiency as Fast FSK and 2.19 dB higher coding gain. There is also a multi-h code with the same error performance as Fast FSK that requires 12% less bandwidth. Data for these two codes are given in Table 7, and it is seen that gain and bandwidth, respectively, are traded mainly for complexity. Codes with other trade-offs between error performance and bandwidth are listed in Table E.2. There are two simpler codes, and data for those are included in Table 7.

Table 7: Bandwidth requirements of codes with better bandwidth efficiency and error performance than Fast FSK

Code	Coding gain	Bandwidth B n = 75.0%	95.0%	99.0%	99.5%	Decision Depth
16/7 8	2.19 dB	0.26	0.45	0.59	0.68	21
8/3 4	1.45 dB	0.24	0.43	0.59	0.66	8
6/2 3	0.50 dB	0.23	0.41	0.60	0.68	6
16/5 6	0.06 dB	0.18	0.35	0.53	0.60	16

The codes in Table 7 have power spectra as shown in Fig. 31 (Fig. 25 shows the spectrum of 16/5 6), and their fractional-out-of-band powers are given in Fig. 32. The curve for 8/3 4 is not plotted, but it lies between that of 16/7 8 and that of 6/2 3.

5.2.3 Class III: Bandwidth Efficient Codes

While multi-h phase codes originally were designed for good error performance, their bandwidth efficiency seems to be of greater importance in some applications. Table 8 shows that there is a code with a bandwidth efficiency of 1.1 bits per sec per Hz, or 23% less bandwidth occupancy than Fast FSK, which requires 2.4 dB more power to give the same transmission quality.

A simpler constraint 2 code yields 1 bits per sec per Hz at an expense of 1.62 dB in coding gain as shown in Table 8.

Table 8: Bandwidth requirements of bandwidth efficient codes.

Code	Coding gain	Bandwidth B_n n = 75.0%	95.0%	99.0%	99.5%	Decision Depth
15/3 45	-2.40 dB	0.11	0.29	0.46	0.54	11
8/2 3	-1.62 dB	0.15	0.33	0.51	0.59	6
16/5 6	0.06 dB	0.18	0.35	0.53	0.60	16

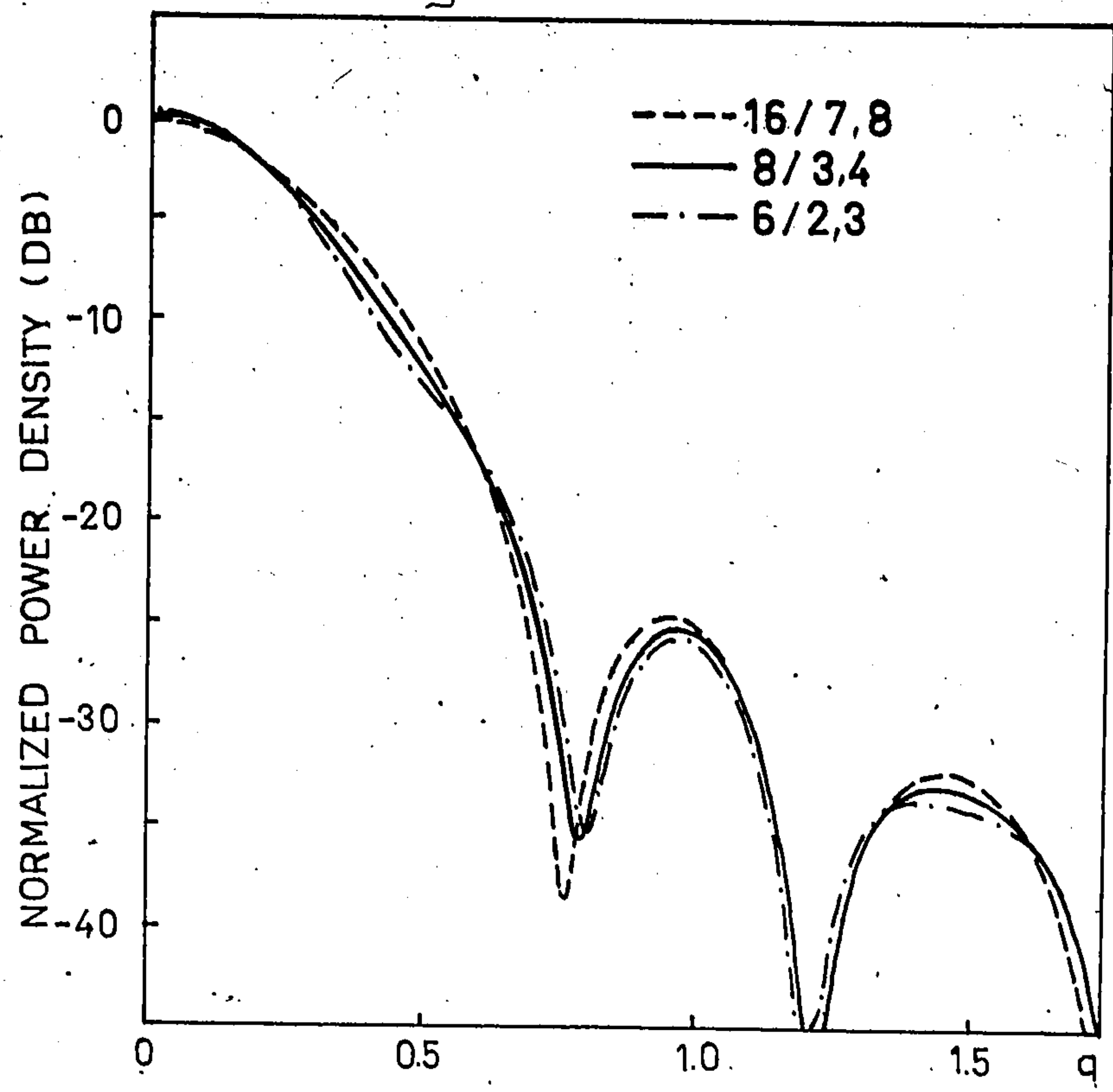

Fig. 31. POWER SPECTRA OF CODES THAT ARE BETTER THAN Fast FSK.

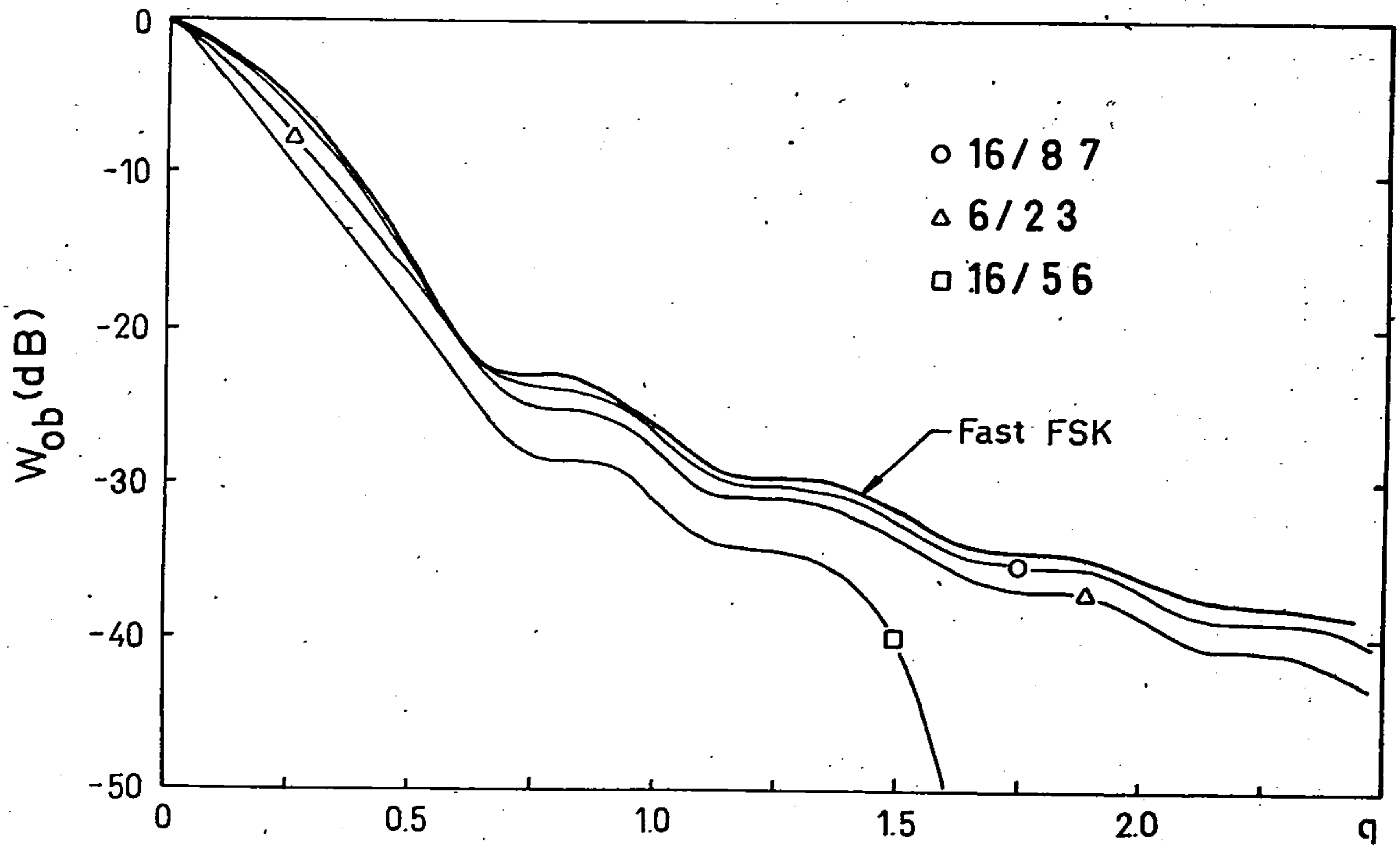

Fig. 32. FRACTIONAL OUT-OF-BAND POWERS FOR CODES THAT ARE BETTER THAN Fast FSK.

The codes have power spectra as shown Fig. 25 and Fig. 33. Their bandwidth efficiency is clearly illustrated by their fractional out-of-band powers in Fig. 34.

5.3 Use Coding Gain to Reduce Band Occupancy

We have found that there exist multi-h phase codes with a bandwidth efficiency of 1-1.1 bits per sec. per Hz and a 1.6-2.4 dB degradation in coding gain compared to Fast FSK.

However, theoretically it is possible to use multi-h phase coding for transmission of information at a still higher rate and at no expense of power.

We know that a Fast FSK signal suffers roughly 0.5-1 dB in error performance when only 95% of its total power is passed through a filter [38], and the degradation is approximately 3-4 dB when the signal is bandlimited to its 75% bandwidth [39].

We shall assume that filtering of multi-h codes results in a similar degradation of the performance. The bandwidth needs can then be reduced by passing the signal through a very narrowbanded filter and letting the achieved coding gain counteract the degradation in error performance.

Let us give a few examples. The simple 8/3 4 code can be bandlimited to B ≈ .35 which yields an efficiency of 1.45 bits per sec per Hz. The codes 6/2 3 and 8/4 5 can be bandlimited to B ≈ .40 and give 1.25 bits per sec. per Hz.

Unfortunately, filtering is likely to destroy the constant

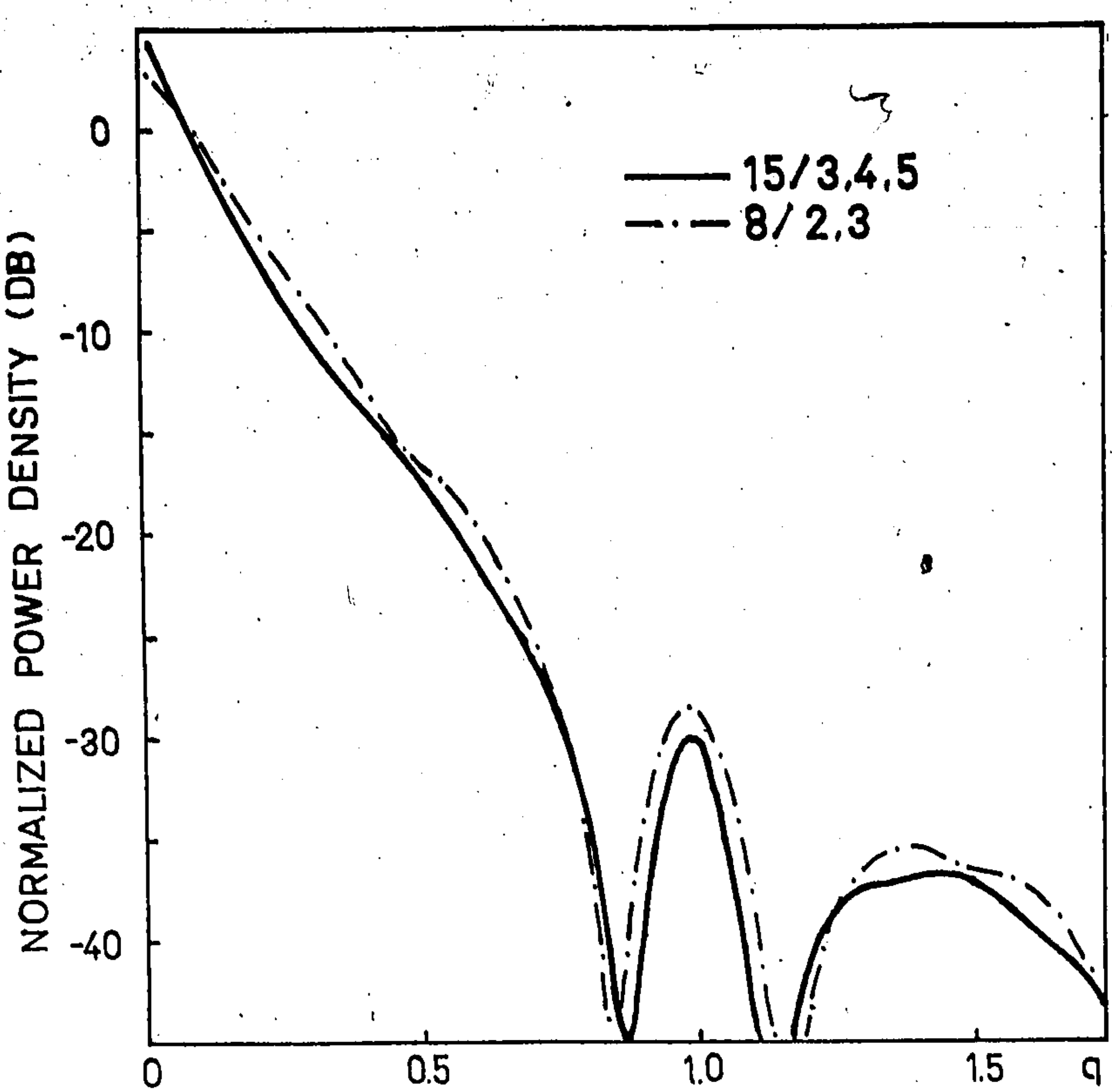

Fig. 33. POWER SPECTRA OF BANDWIDTH EFFICIENT CODES.

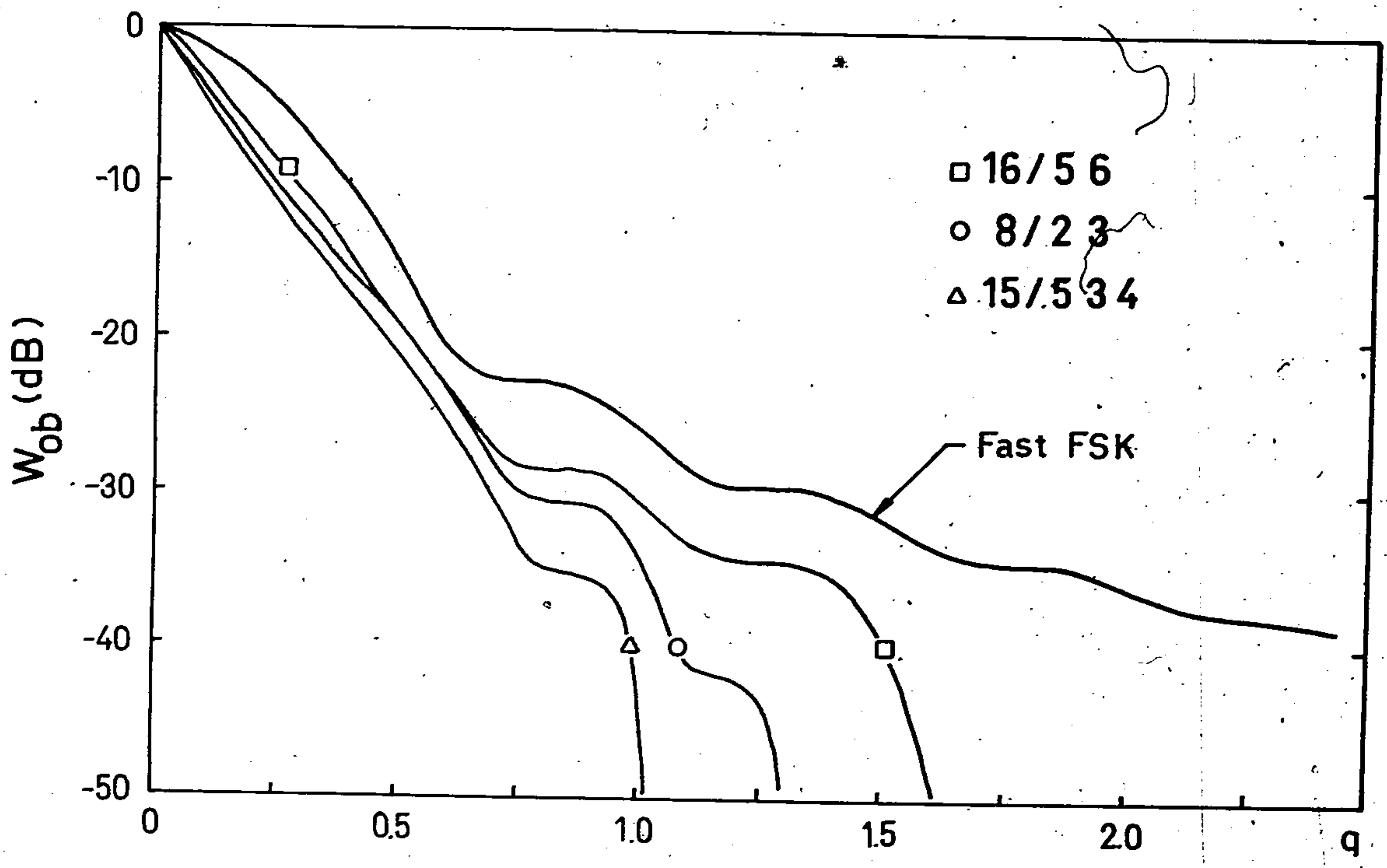

Fig . 34. FRACTIONAL OUT-OF-BAND POWERS FOR BANDWIDTH EFFICIENT CODES.

envelope. The alternative to bandwidth efficient filtered multi-h phase coding is therefore partial response signalling which yields an efficiency of 2.2 bits per sec. per Hz.

However, some multi-h codes have an efficiency of 1.25 bits per sec. per Hz when they are passed through their 95% bandwidth. These codes should be relatively immune to non-linear channel effects.

CHAPTER 6

CONCLUSION

6.1 A New Class of Bandwidth Efficient Codes with Excellent Error Performance

There are multi-h phase codes which allow for a wide range of trade-offs between band occupancy and error performance.

For example, there is a bandwidth efficient code which occupies 23% less bandwidth than Fast FSK but requires 2.4 dB more power to give the same noise immunity. And there is a code that needs 40% more bandwidth than FSK but yields the same transmission quality with a 3.7 dB savings in power. Savings in power or bandwidth are obtained at considerable penalty in implementation complexity.

The major result of this work, however, is the fact that some simple multi-h phase codes have better error performance than Fast FSK but can be passed through the same bandwidth.

This allows us to trade transmission speed for quality by filtering the transmitted signal such that the degradation in noise immunity due to loss of signal power is counteracted by the increase in coding gain.

Theoretically, bandwidth efficiencies of 1.5 bits per sec. per Hz can be obtained, but the coded signals are probably sensitive to non-linear channel effects. It seems possible, however, to transmit information over non-linear channels at a rate of 1.25 bits per sec. per Hz with the same transmission quality as for Fast FSK or QPSK for the same power.

In contrast to many coding schemes, good results do not depend on an unpractical complexity. Simple multi-h phase codes with two indices and 6 to 8 phases combine high bandwidth efficiency and good error performance, and there seems to be few or no advantages in using more indices or phases.

The power spectra of multi-h codes are computed from eqn. (65) and the most important spectral results are presented in Section 4.5.

We have followed three approaches to the problem of deriving an expression for the power spectrum, and found that approaches based on the Wiener-Khinchin Theorem, such as the Transform Technique and the Markov Chain Approach, are superior to the socalled Direct Method [28], [29]. The Transform Technique is an extension of Pelchat's spectral analysis [15] to the general multi-index case. The Markov Chain Approach [25], [26] is a well established method for spectral analysis, valid also for analysis of multi-h phase codes. We have devised a simple procedure for identifying the states of the Marov process.

6.2 Suggestions for Future Work

Although multi-h phase coding seems to be a promising modulation method for high-speed, high-quality data transmission over linear and nonlinear channels, it still remains to answer a few more questions to see if the modulation method provides a viable solution:

- How to implement the encoder and the decoder? In particular, one has to devise a simple way of extracting the required timing and phase information from the received signal.
- How will filtering degrade the error performance?
- Is multi-h coding sensitive to interference? Multi-h phase coding will be used in a multi-channel environment, and the error performance may be degraded by interference between adjacent channels. Analysis of intersymbol interference is a time-domain problem. It is therefore desirable to express the code mathematically in a linear form - if possible.

If the concept of multi-h phase coding turns out to be of practical interest, one should consider further reduction of the band occupancy by introducing shaping of the rectangular baseband pulses.

APPENDIX A

SOME PROPERTIES OF MULTI-H PHASE CODES WITH A PERIODIC PHASE TRELLIS

A.1 The Decoder has to Distinguish between S Phases

The excess phase at the end of baud i is (from eqn. (10))

$$\phi\{(i+1)T\} = \sum_{j=0}^{i} a_j \, \omega_j \, T$$

$$= \frac{\pi}{S} \{a_o L_j + a_1 L_{[j+1]} + \dots + a_i L_{[j+1]}\} \qquad (A.1)$$

where [i+j] means i+j, modulo K. We have assumed that the modulation index in the O'th baud is $h_j = L_j/S$.

When

$$\sum_{n=0}^{i} L_{[j+n]}$$

is even, the expression inside the brackets can take on the values ..., -4, -2, 0, 2, 4, ... and the possible phases are

$$\phi\{(i+1)T\} = 0, \frac{2\pi}{S}, \frac{4\pi}{S}, \dots, \frac{2\pi(S-1)}{S}; \ \Sigma L \text{ even} \qquad (A.2)$$

When

$$\sum_{n=0}^{i} L_{[j+n]}$$

is odd, the expression inside the brackets can take on the values ..., -3, -1, 1, 3, ... and the possible phases are

$$\phi\{(i+)T\} = \frac{\pi}{S}, \frac{3\pi}{S}, \frac{5\pi}{S}, \ldots, \frac{(2S-1)\pi}{S}; \ \Sigma L \text{ odd} \qquad (A.3)$$

In both cases there are S possible phases α_i and they are uniformly spaced on $[0, 2\pi]$.

Examples are given in Fig. 2b and 2c for codes with one index, and in Fig. 3 for a constraint 2 code.

A.2 The Period of the Phase Trellis

It follows from eqn. (A.2) and (A.3) that the phase-trellis has period T_s, given by

$$\begin{aligned} T_s &= K \cdot T = T_K; \quad \sum_{i=1}^{K} L_i \text{ even} \\ T_s &= 2KT = 2T_K; \quad \sum_{i=1}^{K} L \text{ odd} \end{aligned} \qquad (A.4)$$

A.3 The Number of States of the Markov Process

The number of states is equal to the number of distinct phase functions $\phi_i(t-iT)$. There are a total of $N = S$ phases when

$$\sum_{i=1}^{K} L_i \text{ even}$$

and $N = 2S$ phases when

$$\sum_{i=1}^{K} L_i \text{ odd}.$$

Since there are r = 2 paths leaving each phase, the number of states is given by

$$b = NrK \tag{A.5}$$

Fast FSK should therefore have b = 2.2.2.1 = 8 states, as found by Gronemeyer [27]. The states are shown in Fig. 9.

A.4 <u>Prove that $\sum_{s=1}^{b} p_s . q_s(t) = 0$</u> (A.6)

Consider the states with phase function of the form

$$q(t) = e^{j(\pm\omega_j t + \alpha_i)} \tag{A.7}$$

The two functions are equally probable with probability p_s. Then

$$p_s . e^{j(\omega_j t + \alpha_i)} + p_s e^{j(-\omega_j t + \alpha_i)} = 2p_s . e^{j\alpha_i} \cos\omega_j t \tag{A.8}$$

We sum over all phase functions with $\omega = \omega_j$. Thus

$$\sum_{i=1}^{N} 2 . p_s . \cos\omega_j t . e^{j\alpha_i}$$

$$= 2p_s \cos\omega_j t \sum_{i=1}^{N} (\cos\alpha_i + j\sin\alpha_i) \tag{A.9}$$

The phases α_i are uniformly spaced on [0, 2π]

$$\alpha_i - \alpha_{i-1} = \frac{2\pi}{N} = \alpha$$

Eqn. (A.9) can therefore be rewritten as

$$\sum_{i=1}^{N} 2p_s \cos\omega_j t \, e^{j\alpha_i} = 2p_s \cos\omega_j t \sum_{k=0}^{N-1} (\cos k\alpha + j\sin k\alpha) \tag{A.10}$$

The sum of the series are [40]

N > 1

$$\begin{aligned} \sum_{k=0}^{N-1} \cos k\alpha &= \cos \frac{N-1}{2}\alpha \, . \, \sin \frac{N}{2}\alpha \, . \, \operatorname{cosec} \frac{\alpha}{2} \\ \sum_{k=0}^{N-1} \sin k\alpha &= \sin \frac{N}{2}\alpha \, . \, \sin \frac{N-1}{2}\alpha \, . \, \operatorname{cosec} \frac{\alpha}{2} \end{aligned} \tag{A.11}$$

Now, $N\alpha = 2\pi$, and the sums are identically equal to zero.

N = 1

$$\Sigma \cos k\alpha = 1 \quad , \quad \Sigma \sin k\alpha = 0 \tag{A.12}$$

Next, consider all states and assume $N > 1$. Since the sums in eqn. (A.10) are zero for any group j of states having $\omega = \omega_j$, eqn. (A.6) holds.

$N = 1$ iff $S = 1$. This is satisiified only for conventional CPFSK with $h = 1, 2, 3, \ldots$.

APPENDIX B

AN EXPRESSION FOR THE POWER SPECTRUM OF CONVENTIONAL CPFSK

From eqn. (40)

$$G(f) = 2\mathrm{Re}\{F\{\frac{T-t}{T}\cos\omega t\}$$

$$+ \sum_{n=1}^{\infty} \frac{1}{T} e^{-j2\pi f(n-1)T} \cdot (\cos\omega T)^{n-1} \cdot F^2\{\cos\omega t\}\} \qquad (B.1)$$

where the function $\cos\omega t$ is zero outside the interval $0 \leq t \leq T$.

We assume that $|\cos\omega T| < 1$. The geometric series may then be replaced by its sum

$$\sum_{n-1}^{\infty} e^{-j2\pi f(n-1)T} \cdot (\cos\omega T)^{n-1} = \frac{1}{1-\cos\omega T.e^{-j2\pi fT}} \qquad (B.2)$$

From [41], we have

$$\int e^{ax}\cos bx dx = \frac{e^{ax}}{a^2+b^2}(a\cos bx+b\sin bx) \qquad (B.3)$$

and

$$\int xe^{ax}\cos bx dx = \frac{xe^{ax}}{a^2+b^2}(a\cos bx+b\sin bx)$$

$$- \frac{e^{ax}}{(a^2+b^2)^2}[(a^2-b^2)\cos bx+2ab\sin bx] \qquad (B.4)$$

Thus

$$2\mathrm{Re}\{F\{\frac{T-t}{T}\cos\omega t\}\}$$

$$= \frac{2}{T} \cdot \frac{1}{(\omega^2-4\pi^2 f^2)^2}\,[(\omega^2+4\pi^2 f^2)(1-\cos\omega T\cdot\cos 2\pi fT)-4\pi f\omega\sin\omega T\cdot\cos 2\pi fT] \tag{B.5}$$

and

$$F\{\cos\omega t\} = \frac{e^{-j2\pi fT}}{\omega^2-4\pi^2 f^2}(-2\pi jf\cos\omega T+\omega\sin\omega T) + \frac{2\pi jf}{\omega^2-4\pi^2 f^2} \tag{B.6}$$

$$F^2\{\cos\omega t\} = \frac{e^{-j4\pi fT}}{(\omega^2-4\pi^2 f^2)^2}(-4\pi^2 f^2\cos^2\omega T+\omega^2\sin^2\omega T-4\pi jf\omega\cos\omega T.\sin\omega T)$$

$$= \frac{4\pi^2 f^2}{(\omega^2-4\pi^2 f^2)^2} + \frac{e^{-j2\pi fT}}{(\omega^2-4\pi^2 f^2)^2}(8\pi^2 f^2\cos\omega T+4\pi jf\omega\sin\omega T) \tag{B.7}$$

Substituting for eqn. (B.2), (B.5) and (B.7) into eqn. (B.1), it is straight forward (but messy) to show that

$$G(f) = \frac{4}{T} \cdot \frac{\omega^2}{(\omega^2-4\pi^2 f^2)^2} \cdot \frac{(\cos\omega T-\cos 2\pi fT)^2}{\cos^2\omega t-2\cos\omega T.\cos 2\pi fT+1} \tag{B.8}$$

The power spectrum is zero when $(\cos\omega T-\cos 2\pi fT)^2 = 0$, $\omega \neq 2\pi f$. We see that the lowest positive normalized frequency q_o for which $G(f) = 0$, is given by

$$2\pi q_o = 2\pi - \pi h$$

or

$$q_o = 1 - \frac{h}{2} \tag{B.9}$$

APPENDIX C

POWER SPECTRA OF MULTI-H PHASE CODES

C.1 Some Comments on the Calculation of the Power Spectra of Multi-h Phase Codes

The two properties of the autocorrelation function $R(t_1; \tau)$ given by eqn. (47) and (53) have simplified the calculation of the power spectrum as illustrated in Fig. C.1.

The square corresponding to i=i and j=j represents the function $r_{ij}(t_1; \tau_s)$. From eqn. (44), $R(t_1; \tau)$ is the sum of all the squares.

To evaluate $R(t_1; \tau)$ for positive τ means we are considering the upper triangle of the total square, i.e. $j \geq i$.

Because of the property of eqn. (53) the contributions c and e are equal and $R(t_1; \tau)$ can be time averaged over one superbaud.

From eqn. (47), the contribution d is $C(1;T_K)$ times the contribution c. But b is not $C(1;T_K)$ times a since a lies on the diagonal (i.e. $i = j$).

Thus the autocorrelation function is uniquely defined by the terms $r_{ij}(t_1; \tau_s)$ from the cross-hatched area of Fig. C.1.

The terms $R_n'(\tau)$ and $R_n''(\tau)$ of the autocorrelation function are listed in Table C.1. These terms are defined by eqn. (54), (55), (56),

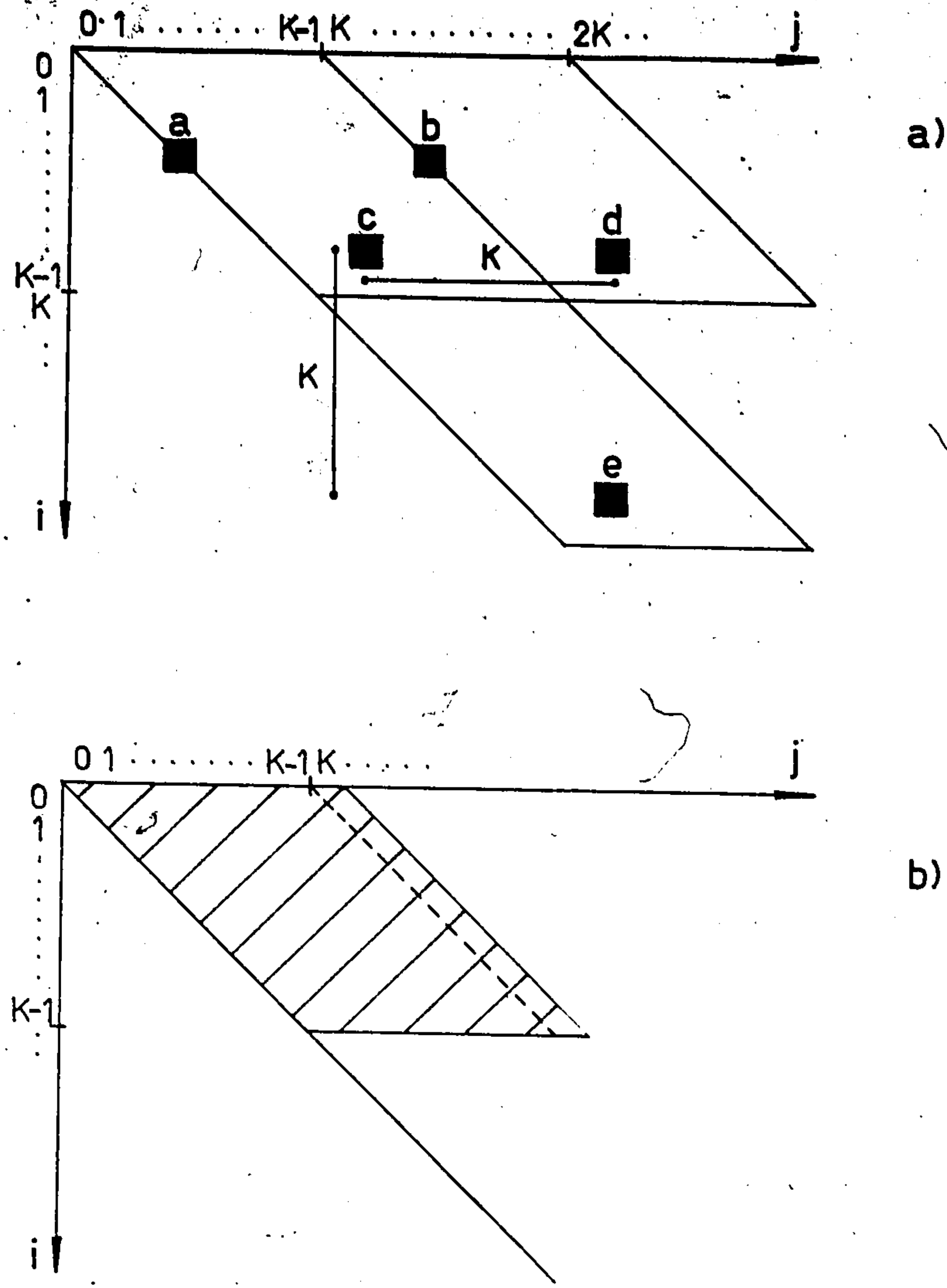

Fig. C.1.

and (58). In order to get a more compact notation, we have defined the following functions

$$A(\tau_s;\ \omega_m) = \frac{1}{T_K} \int_0^{T-\tau_s} \cos\omega_m\tau_s dT$$

$$C(\tau_s;\ \omega_m,\omega_{m+k}) = \frac{1}{T_K} \int_0^{T-\tau_s} \cos\omega_m(T-z).\cos\omega_{m+k}(\tau_s+z)dz$$

$$E(\tau_s;\ \omega_m) = C(\tau_s;\ \omega_m,\ \omega_m) \qquad (C.1)$$

$$B(\tau_s;\ \omega_m,\ \omega_{m+k}) = \frac{1}{T_K} \int_{T-\tau_s}^{T} \cos\omega_m(T-z).\cos\omega_{m+k}(\tau_s+z-T)dz$$

$$D(\tau_s;\ \omega_m) = B(\tau_s;\ \omega_m,\ \omega_m)$$

The A, B, C, D, and E functions ($0 \leq m \leq K-1$, $0 \leq k \leq K$), are defined by the r_{ij}-terms in the cross-hatched area of Fig. C.1. We have stated that all r_{ij}-terms can be derived from the $K\cdot(K+1)$ r_{ij} terms mentioned above. And Table C.1 shows that all terms $R_n'(\tau)$ and $R_n''(\tau)$ can be expressed as functions of the A, B, C, D and E functions defined in eqn. (C.1).

According to eqn. (47), the contributions to the power spectrum from the C-terms in line k may be epxressed as a geometric series. So

Table C.1. The terms $R_n'(\tau)$

	$kT \leq \tau < (k+1)T$	$T_K + kT \leq \tau < T_K + (k+1)T$	$rT_K + kT \leq \tau < rT_K + (k+1)T$
$k=0$	$\sum_{m=0}^{K-1} A\{\tau;\omega_m\}$	$\sum_{m=0}^{K-1} E\{\tau-T_K;\omega_m\} \cdot \prod_{i=1}^{K-1} \cos(\omega_{m+i}T)$	$\sum_{m=0}^{K-1} E\{\tau-rT_K;\omega_m\} \cdot \prod_{i=1}^{K-1} \cos(\omega_{m+i}T) \cdot C(1;T_K)^{r-1}$
1	$\sum_{m=0}^{K-1} C\{\tau-T;\omega_m,\omega_{m+1}\}$	$\sum_{m=0}^{K-1} C\{\tau-(T_K+T);\omega_m,\omega_{m+1}\} \cdot C(1;T_K)$	$\sum_{m=0}^{K-1} C\{\tau-(rT_K+T);\omega_m,\omega_{m+1}\} \cdot C(1;T_K)^r$
k	$\sum_{m=0}^{K-1} C\{\tau-kT;\omega_m,\omega_{m+k}\} \cdot \prod_{i=1}^{k-1} \cos(\omega_{m+i}T)$	$\sum_{m=0}^{K-1} C\{\tau-(T_K+kT);\omega_m,\omega_{m+k}\} \cdot \prod_{i=1}^{k-1} \cos(\omega_{m+i}T) \cdot C(1;T_K)$	$\sum_{m=0}^{K-1} C\{\tau-(rT_K+kT);\omega_m,\omega_{m+k}\} \cdot \prod_{i=1}^{k-1} \cos(\omega_{m+i}T) \cdot C(1;T_K)^r$
$K-1$	$\sum_{m=0}^{K-1} C\{\tau-(K-1)T;\omega_m,\omega_{m+K-1}\} \cdot \prod_{i=1}^{K-2} \cos(\omega_{m+i}T)$	$\sum_{m=0}^{K-1} C\{\tau-(T_K+(K-1)T);\omega_m,\omega_{m+K-1}\} \cdot \prod_{i=1}^{K-2} \cos(\omega_{m+i}T) \cdot C(1;T_K)$	$\sum_{m=0}^{K-1} C\{\tau-(rT_K+(K-1)T);\omega_m,\omega_{m+K-1}\} \cdot \prod_{i=1}^{K-2} \cos(\omega_{m+i}T) \cdot C(1;T_K)^r$

	$kT \leq \tau < (k+1)T$	$T_K + kT \leq \tau < T_K + (k+1)T$	$rT_K + kT \leq \tau < rT_K + (k+1)T$
$k=0$	$\sum_{m=0}^{K-1} B\{\tau;\omega_m,\omega_{m+1}\}$	$\sum_{m=0}^{K-1} B\{\tau-T_K;\omega_m,\omega_{m+1}\}\cdot C(1;T_K)$	$\sum_{m=0}^{K-1} B\{\tau-rT_K;\omega_m,\omega_{m+1}\}\cdot C(1;T_K)^r$
k	$\sum_{m=0}^{K-1} B\{\tau-kT;\omega_m,\omega_{m+k+1}\} \cdot \prod_{i=1}^{k} \cos(\omega_{m+i}T)$	$\sum_{m=0}^{K-1} B\{\tau-(T_K+kT);\omega_m,\omega_{m+k+1}\} \cdot \prod_{i=1}^{k} \cos(\omega_{m+i}T)\cdot C(1;T_K)$	$\sum_{m=0}^{K-1} B\{\tau-(rT_K+kT);\omega_m,\omega_{m+k+1}\} \cdot \prod_{i=1}^{k} \cos(\omega_{m+i}T)\cdot C(1;T_K)^r$
$K-2$	$\sum_{m=0}^{K-1} B\{\tau-(K-2)T;\omega_m,\omega_{m+K-1}\} \cdot \prod_{i=1}^{K-2} \cos(\omega_{m+i}T)$	$\sum_{m=0}^{K-1} B\{\tau-(T_K+(K-2)T);\omega_m,\omega_{m+K-1}\} \cdot \prod_{i=1}^{K-2} \cos(\omega_{m+i}T)\cdot C(1;T_K)$	$\sum_{m=0}^{K-1} B\{\tau-(rT_K+(K-2)T);\omega_m,\omega_{m+K-1}\} \cdot \prod_{i=1}^{K-2} \cos(\omega_{m+i}T)\cdot C(1;T_K)^r$
$K-1$	$\sum_{m=0}^{K-1} D\{\tau-(K-1)T;\omega_m\} \cdot \prod_{i=1}^{K-1} \cos(\omega_{m+i}T)$	$\sum_{m=0}^{K-1} D\{\tau-(T_K+(K-1)T);\omega_m\} \cdot \prod_{i=1}^{K-1} \cos(\omega_{m+i}T)\cdot C(1;T_K)$	$\sum_{m=0}^{K-1} D\{\tau-(rT_K+(K-1)T);\omega_m\} \cdot \prod_{m=0}^{K-1} \cos(\omega_{m+i}T)\cdot C(1;T_K)^r$

Table C.1. The terms $R''_n(\tau)$

may the contributions from the B-terms in the (K-1)th line. Eqn. (61) states that those two series can be combined, and the result is the kth geometric series in eqn. (62).

The D- and E-terms, as well as the other B- and C-terms, can be combined in a similar way.

C.2 Approximations of the Power Spectrum of a Multi-h Phase Code

In the limit when all the K indices are equal, eqn. (5) reduces to eqn. (41).

From this it follows that if there is a small spread in the modulation indices, the power spectrum of the multi-h code may be approximated by the spectrum of the conventional CPFSK signal with index

$$\bar{h} = \frac{1}{K} \sum_{i=1}^{K} h_i \ .$$

We also note that only A, D, and E-terms contribute to the spectrum of a conventional CPFSK signal. When the spread in the indices is small, we may consider the case when

$$\omega_{m+k} \rightarrow \omega_m \quad , \quad 1 \leq k \leq K-1 \tag{C.2}$$

and consequently,

$$\begin{aligned} C(\tau_s;\ \omega_m,\ \omega_{m+k}) &\rightarrow E(\tau_s;\ \omega_m) \\ B(\tau_s;\ \omega_m,\ \omega_{m+k}) &\rightarrow D(\tau_s;\ \omega_m) \end{aligned} \tag{C.3}$$

The power spectrum of the multi-h code may therefore alternatively be approximated by the averaged linear combination of the K spectra of the conventional CPFSK signals with modulation index h_1, h_2, ..., h_k, respectively (cfr. eqn. (65)).

APPENDIX D

MULTI-H PHASE CODING WITH UNIPOLAR (0,1) SIGNALLING

The multi-h phase code for unipolar signalling can be written as

$$s(t) = \sqrt{\frac{2E}{T}} \cdot \cos(2\pi f_c t + \Phi(t) + \alpha) \qquad (D.1)$$

where $\Phi(t)$ is the excess phase function.

The excess phase function $\Phi(t)$ for conventional CPFSK is illustrated in Fig. D.2. The unipolar signalling (cfr. Fig. D.1) results in a excess phase function that is not even around zero. Eqn. (23) is therefore not valid for unipolar signalling.

The excess phase function in Fig. D.2 may be obtained by a translation of the bipolar function $\phi(t)$ shown in Fig. 2a. Therefore,

$$\begin{aligned} \Phi(t) &= \overline{\Phi}(t) + \phi(t) \\ &= k.t + \phi(t) \end{aligned} \qquad (D.2)$$

Substitution of eqn. (D.2) into eqn. (D.1) yields

$$s(t) = \sqrt{\frac{2E}{T}} \cdot \cos\{(2\pi f_c + k)t + \phi(t) + \alpha\} \qquad (D.3)$$

which shows that the spectra of the unipolar and the bipolar code have equal shapes, but the unipolar spectrum is centered at the frequency $f = f_c + k/2\pi$.

When two or more indices are used, the function $\overline{\Phi}(t)$ is no longer linearly increasing with time and this leads to a complicated analysis.

The autocorrelation function of the modulated signal s(t) is then

$$K(t_1;\ \tau) = \frac{2E}{T} \cdot \frac{1}{2}\,\mathrm{Re}\{E[e^{j2\pi f_c\tau+\bar{\Phi}(t_1+\tau)-\bar{\Phi}(t_1)} \cdot e^{j\phi(t_1+\tau)-j\phi(t_1)}]\}$$

$$= \frac{2E}{T} \cdot \frac{1}{2}\cos\{2\pi f_c\tau+\bar{\Phi}(t_1+\tau)-\bar{\Phi}(t_1)\}.E[e^{j\phi(t_1+\tau)-j\phi(t_1)}] \tag{D.4}$$

The power spectrum of s(t) is the Fourier transform of the time averaged autocorrelation function.

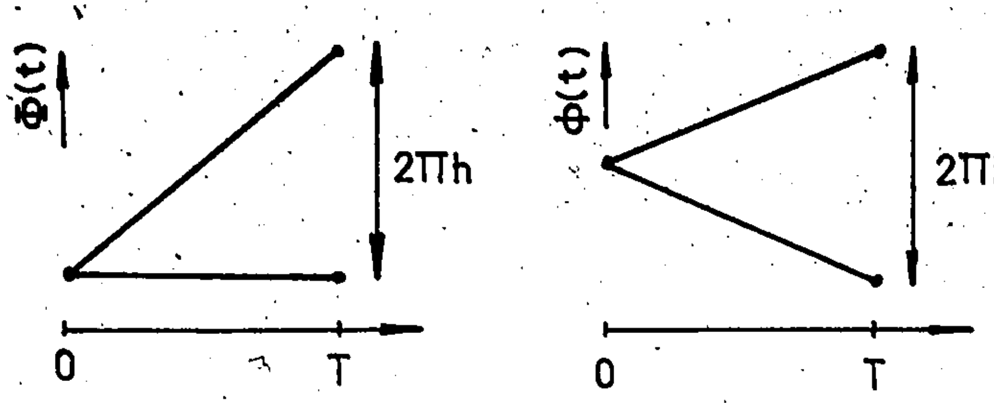

a) Unipolar b) Bipolar

Fig. D.1. UNIPOLAR AND BIPOLAR SIGNALLING.

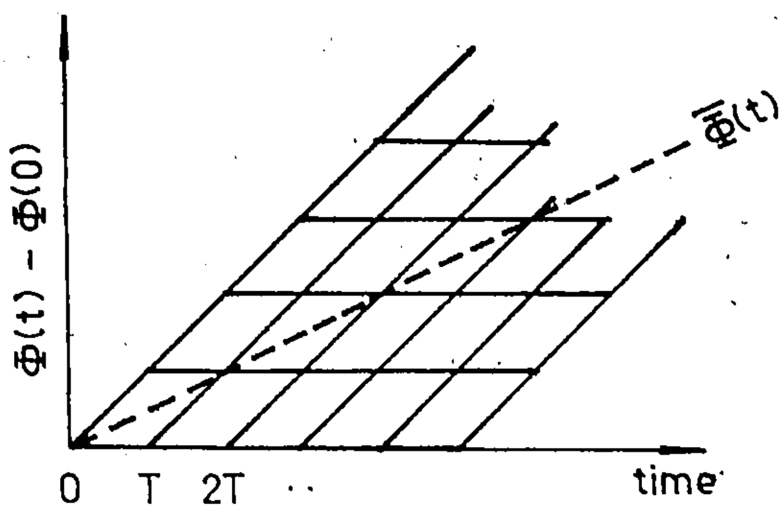

Fig. D.2. UNIPOLAR SIGNALLING, CONVENTIONAL CPFSK.

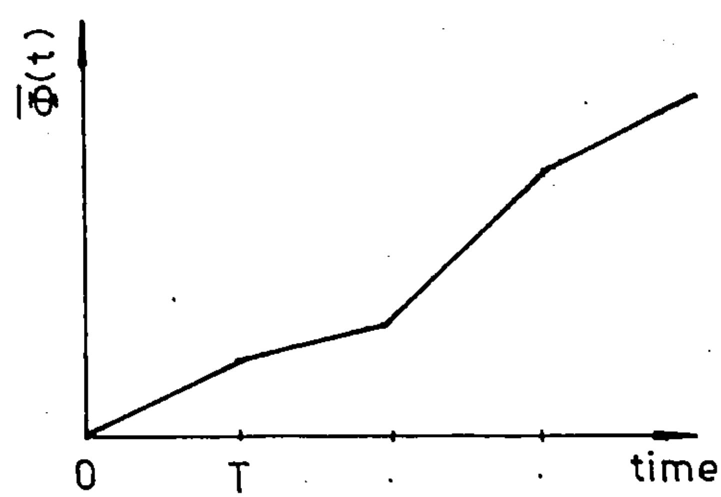

Fig. D.3. UNIPOLAR SIGNALLING, MULTI-H PHASE CODING.

APPENDIX E

LIST OF MULTI-H PHASE CODES

Coding gain means coding gain compared to Fask FSK. The *bandwidths* given are the onesided 75%, 95%, 99% and 99.5% bandwidths respectively. Bandwidth is given in normalized frequency.

Diff. is the difference between the maximum value of W(f) in the main lobe and the maximum value in the first sidelobe.

Decision depth is defined in Chapter 2. The data are obtained from [18]. For some codes, only bounds on the decision depth are available.

Table E-1: Multi-h phase codes with high coding gain.

Code	Coding gain	Bandwidths 75.0%	95.0%	99.0%	99.5%	Diff.	Decision depth
16/12 10 11 8	3.66dB	.38	.53	.85	1.00	17.7dB	26-38
16/10 11 12	3.36dB	.41	.53	.89	1.03	16.8dB	26-27
13/ 8 9 10	3.19dB	.41	.53	.90	1.03	16.7dB	17-20
16/11 12 10 8	3.16dB	.39	.53	.85	1.00	17.6dB	11-27
16/12 11 10 8	3.16dB	.39	.53	.85	1.00	17.6dB	11-34
16/ 9 10 11	3.13dB	.38	.51	.81	.98	18.1dB	24-26
14/ 8 9 10	3.13dB	.39	.53	.84	.99	17.6dB	18-20
16/12 9 10 8	3.03dB	.36	.51	.81	.98	18.6dB	28
14/ 9 10 11	2.96dB	.43	.54	.91	1.04	16.6dB	17-26
16/12 10 9 8	2.91dB	.36	.51	.81	.98	18.4dB	29-30
16/10 12 9 8	2.91dB	.36	.51	.81	.98	18.6dB	29
16/ 8 9 10	2.82dB	.33	.49	.64	.93	20.4dB	28
14/ 7 8 9	2.81dB	.34	.50	.65	.94	20.0dB	22
12/ 6 7 8	2.81dB	.34	.50	.66	.95	19.5dB	17
10/ 5 6 7	2.81dB	.35	.51	.78	.90	18.8dB	13
12/ 6 7 9	2.77dB	.36	.53	.83	.99	18.4dB	7-17
8/ 4 5 6	2.77dB	.38	.53	.84	1.00	18.1dB	7-9
12/ 6 8 9	2.77dB	.38	.53	.85	1.00	17.8dB	13-14
16/ 8 9	2.74dB	.30	.48	.61	.89	21.7dB	20
10/ 5 6 8	2.74dB	.38	.54	.86	1.01	17.7dB	11-13
10/ 6 7 8	2.74dB	.43	.54	.90	1.04	16.5dB	9-13

Table E-1, cont.

Code	Coding gain	Bandwidths				Diff.	Decision depth
		75.0%	95.0%	99.0%	99.5%		
15/ 8 9 10	2.72dB	.35	.51	.73	.96	19.0dB	18-19
13/ 7 8 9	2.71dB	.36	.51	.80	.98	18.4dB	7-18
11/ 6 7 8	2.71dB	.38	.53	.84	.99	17.8dB	7-12
14/ 7 8	2.70dB	.31	.48	.61	.90	21.5dB	20
15/ 7 9	2.65dB	.31	.48	.64	.90	21.3dB	20
12/ 6 7	2.65dB	.31	.49	.63	.90	21.2dB	16
13/ 6 8	2.60dB	.31	.49	.64	.91	21.0dB	19
16/ 7 10	2.60dB	.30	.49	.65	.90	21.2dB	20
10/ 5 6	2.58dB	.33	.49	.63	.91	20.8dB	12
16/11 12 13	2.55dB	.45	.54	.94	1.06	16.6dB	17-22
12/ 4 6 7	2.54dB	.26	.45	.63	.75	23.4dB	18
11/ 5 7	2.52dB	.31	.49	.66	.93	20.7dB	14
15/ 8 9	2.51dB	.34	.49	.63	.93	20.3dB	20
8/ 4 5	2.49dB	.33	.50	.65	.94	20.2dB	9
15/10 11	2.48dB	.43	.53	.90	1.03	16.8dB	14-19
15/ 9 11	2.48dB	.40	.53	.88	1.01	17.1dB	12
13/ 7 8	2.47dB	.34	.50	.64	.94	19.8dB	16
11/ 7 8 9	2.46dB	.44	.54	.93	1.05	16.3dB	9-16
14/ 7 9	2.43dB	.34	.50	.66	.94	19.9dB	7

Table E-2: Bandwidth efficient multi-h phase codes with high coding gain.

Code	Coding gain	Bandwidths 75.0%	95.0%	99.0%	99.5%	Diff.	Decision depth
16/ 7 8	2.19dB	.26	.45	.59	.68	24.2dB	21
16/ 6 7 8	2.10dB	.24	.43	.59	.66	25.4dB	20
14/ 6 7	2.07dB	.26	.44	.59	.68	24.4dB	19
14/ 5 6 7	1.96dB	.24	.43	.58	.65	25.8dB	16-18
10/ 4 5	1.72dB	.25	.44	.59	.66	24.9dB	11
15/ 6 7	1.67dB	.24	.43	.58	.65	25.7dB	20
16/ 6 4 7 8	1.65dB	.21	.40	.56	.64	27.2dB	7-20
15/ 5 6 7	1.53dB	.21	.40	.56	.64	27.1dB	20
12/ 4 5 6	1.47dB	.23	.41	.58	.65	26.2dB	13
8/ 3 4	1.45dB	.24	.43	.59	.66	25.3dB	8
16/ 4 6 7 8	1.45dB	.21	.40	.58	.65	27.2dB	20
13/ 5 6	1.44dB	.23	.41	.58	.65	26.2dB	15
14/ 5 7	1.28dB	.24	.43	.59	.66	25.6dB	11
16/ 6 7	1.28dB	.21	.40	.56	.64	27.0dB	21
16/ 4 7 6 8	1.21dB	.21	.40	.59	.65	27.0dB	11-20
11/ 4 5	1.12dB	.21	.40	.58	.64	26.7dB	11
16/ 5 6 7	1.07dB	.19	.39	.55	.63	28.3dB	20
14/ 5 6	.97dB	.20	.40	.56	.63	27.6dB	16
13/ 4 5 6	.89dB	.20	.39	.56	.64	27.7dB	14
16/ 5 8	.87dB	.23	.40	.60	.68	26.2dB	8

Table E-2 cont.

Code	Coding gain	Bandwidths				Diff.	Decision depth
		75.0%	95.0%	99.0%	99.5%		
15/ 5 7	.80dB	.21	.40	.58	.65	26.9dB	11
10/ 3 4 5	.78dB	.21	.40	.58	.65	26.8dB	10
16/ 4 6 7	.70dB	.18	.38	.55	.63	29.1dB	16-19
9/ 3 4	.66dB	.20	.39	.56	.64	27.6dB	8
10/ 3 5	.61dB	.21	.40	.60	.68	26.4dB	10
12/ 4 5	.54dB	.19	.38	.55	.63	28.4dB	11
15/ 5 6	.51dB	.19	.38	.55	.61	28.9dB	16
6/ 2 3	.50dB	.23	.41	.60	.68	25.9dB	6
16/ 5 7	.34dB	.20	.38	.56	.64	28.2dB	12
14/ 4 5 6	.34dB	.18	.38	.55	.61	29.1dB	14
16/ 4 6 5 8	.18dB	.19	.38	.56	.64	28.4dB	16-19
8/ 2 3 4	.07dB	.20	.39	.58	.65	27.6dB	9-10
16/ 5 6	.06dB	.18	.35	.53	.60	30.1dB	16
11/ 3 4 5	.06dB	.19	.38	.55	.63	28.6dB	10

Table E-3: Bandwidth efficient multi-h phase codes.

Code	Coding gain	Bandwidths 75.0%	95.0%	99.0%	99.5%	Diff.	Decision depth
15/ 3 4 5	-2.40dB	.11	.29	.46	.54	34.4dB	11
14/ 3 4	-2.67dB	.10	.26	.46	.54	35.8dB	8
16/ 3 4 5	-2.92dB	.11	.26	.46	.53	35.5dB	11
16/ 3 5	-3.03dB	.11	.28	.46	.55	35.3dB	11
13/ 3 4	-2.08dB	.13	.29	.48	.56	34.4dB	8
15/ 3 5	-2.50dB	.13	.29	.48	.56	34.1dB	11
16/ 4 5	-1.57dB	.13	.30	.49	.56	33.7dB	12
11/ 2 3 4	-2.48dB	.13	.30	.49	.56	33.6dB	9-10
9/ 2 3	-2.54dB	.13	.30	.49	.58	33.6dB	6
15/ 4 5	-1.08dB	.14	.31	.50	.58	32.5dB	12
10/ 2 3 4	-1.70dB	.15	.33	.50	.56	31.8dB	9-10
14/ 3 4 5	-1.84dB	.14	.31	.50	.58	33.1dB	10
16/ 4 5 6	- .68dB	.15	.33	.51	.58	31.6dB	15-16
13/ 3 4 5	-1.25dB	.15	.33	.51	.59	31.7dB	10
8/ 2 3	-1.62dB	.15	.33	.51	.59	31.4dB	6
14/ 3 5	-1.94dB	.14	.30	.51	.59	32.8dB	10

Table E-3, cont.

Code	Coding gain	Bandwidths 75.0%	95.0%	99.0%	99.5%	Diff.	Decision depth
16/ 5 6	.06dB	.18	.35	.53	.60	30.1dB	16
14/ 4 5	- .56dB	.15	.34	.53	.59	31.3dB	12
11/ 3 4	- .80dB	.15	.34	.53	.60	31.3dB	8
13/ 3 5	-1.35dB	.15	.33	.53	.61	31.5dB	10
12/ 2 4 5	-2.93dB	.15	.34	.53	.61	31.1dB	4-12
13/ 4 5	- .02dB	.18	.36	.54	.61	29.9dB	12
10/ 3 4	- .09dB	.18	.36	.54	.61	29.6dB	8
15/ 4 6	-1.13dB	.16	.35	.54	.61	30.2dB	6
16/ 5 6 7	1.07dB	.19	.39	.55	.63	28.3dB	20
16/ 4 6 7	.70dB	.18	.38	.55	.63	29.1dB	16-19
12/ 4 5	.54dB	.19	.38	.55	.63	28.4dB	11
15/ 5 6	.51dB	.19	.38	.55	.61	28.9dB	16
14/ 4 5 6	.34dB	.18	.38	.55	.61	29.1dB	14
11/ 3 4 5	.06dB	.19	.38	.55	.63	28.6dB	10
16/ 4 5 6 8	- .01dB	.19	.38	.55	.63	28.5dB	20
16/ 5 4 6 8	- .01dB	.19	.39	.55	.63	28.6dB	13-16
12/ 3 5	- .72dB	.18	.34	.55	.63	29.9dB	10

REFERENCES

[1] J.G. Smith, "A bandwidth-compressive modulation system", AIAA/CASI 6th Communication Satellite Systems Conference, Montreal, Canada, April 5-8, 1976, paper no. 76-230.

[2] J.G. Smith, "Spectrally efficient modulation", International Conference on Communications, Chigago, Ill., June 12-15, 1977, paper 3.1.

[3] M.K. Simon, "A generalization of Minimum-Shift-Keying (MSK)-type signaling based upon input data symbol pulse shaping", IEEE Trans. on Comm., vol. COM-24, no. 8, pp. 845-856 (Aug. 1976), Fig. 4.

[4] R. deBuda and H. Anto, "About FSK with low modulation index", Canadian General Electric Comp. Ltd., Report RQ69EE11, 1969.

[5] R. deBuda, "A comparison of two efficient digital modulation systems", Canadian General Electric Comp. Ltd. Report RQ74EE1, 1974.

[6] R. deBuda, "Coherent demodulation of frequency-shift keying with low deviation ratio", IEEE Trans. on Comm., vol. COM-20, no. 3, pp. 429-435 (June 1972).

[7] R. deBuda, "Fast FSK signals and their demodulation", Can. Elec. Eng. J., vol. 1, no. 1, pp. 28-34 (1976).

[8] D.M. Brady, "A constant-envelope digital modulation technique for millimeter-wave satellite systems", International Conference on Communications, Minneapolis, Minn., June 17-19, 1974, paper 36C.

[9] R.M. Fielding, H.L. Berger, and D.L. Lochhead, "Performance characterization of a high data rate MSK and QPSK channel", International Conference of Communications, Chigago, Ill., June 12-15, 1977, paper 3.2.

[10] H. Miyakawa, H. Harashima, and Y. Tanaka, "A new digital modualtion scheme - Multi-mode binary CPFSK", Proceedings 3rd International Conference on Digital Satellite Communications, Kyoto, Japan, Nov. 11-13, 1975, pp. 105-112.

[11] J.B. Anderson and R. deBuda, "Better phase-modulation error performance using trellis phase codes", Electronics Letters, vol. 12, no. 22, pp. 587-588 (Oct. 1976).

[12] J.B. Anderson and D.P. Taylor, "Trellis phase modulation coding: Minimum distance and spectral results", Electronics and Aerospace Systems Conference, Arlington, VA., Sept. 25-28, 1977.

[13] J.B. Anderson and D.P. Taylor, "A bandwidth-efficient class of signal space codes", To be published in IEEE Trans. on Inf. Theory, Nov. 1978.

[14] J.B. Anderson, D.P. Taylor, and A.T. Lereim, "A class of trellis phase modulation codes for coding without bandwidth expansion", International Conference of Communications, Toronto, Canada, June 4-7, 1978, paper 50.3.

[15] M.G. Pelchat, "The autocorrelation function and power spectrum of PCM/FM with random binary modulating waveforms", IEEE Trans. on Space Electronics and Telemetry, vol. SET-10, no. 1, pp. 39-45 (March 1964).

[16] W.R. Bennett and S.O. Rice, "Spectral density and autocorrelation functions associated with binary frequency-shift keying", B.S.T.J., vol. 42, no. 5, pp. 2355-2385 (Sept. 1963).

[17] R. deBuda, "About optimal properties of Fast Frequency-Shift Keying", IEEE Trans. on Comm., vol. COM-22, no. 10, pp. 1726-1727 (Oct. 1974).

[18] J.B. Anderson, McMaster University: Personal communication.

[19] G.D. Forney Jr., "The Viterbi algorithm", Proc. of IEEE, vol. 61, no. 3, pp. 268-278 (March 1973).

[20] A. Papoulis. Probability, random variables and stochastic processes. McGraw Hill 1965. Chapter 12.3.

[21] Reference 25, Appendix B.

[22] H.E. Rowe and V.K. Prahbu, "Power spectrum of a digital, frequency modulation signal", B.S.T.J., vol. 54, no. 10, pp. 1095-1125 (July-Aug. 1975).

[23] O. Shimbo, "General formula for power spectra of digital f.m. signals", Proc. IEE, vol. 113, no. 11, pp. 1783-1789 (Nov. 1966).

[24] O. Shimbo and T. Ohira, "A generalized formula for the power spectrum of a pulse-modulated signal and its application to PCM transmission problems", J. Inst. Elect. Comm. Eng. RS., Japan, vol. 46, no. 12, pp. 9-17 (1963).

[25] R.C. Titsworth and L.R. Welch, "Power spectra of signals modulated by random and pseudorandom sequences", Jet PRopulsion Laboratory, California, technical report no. 32-140, Oct. 1961.

[26] E. Biglieri and M.A. Marsan, "Spectral occupancy of complex PSK", International Conference on Communications, Chigago, Ill., June 12-15, paper 3.5.

[27] S. Gronemeyer and A.L. McBride, "MSK and offset QPSK modulation", IEEE Trans. on Comm., vol. COM-24, no. 8, pp. 809-819 (Aug. 1976).

[28] R.R. Anderson and J. Salz, "Spectra of digital FM", B.S.T.J., vol. 44, no. 6, pp. 1165-1189 (July-Aug. 1965).

[29] R.W. Lucky, J. Salz and E.J. Weldon Jr. Principles of data communication. McGraw Hill, 1968.

[30] Reference 15, eqn. (40).

[31] E.D. Sunde, "Ideal binary pulse transmission by AM and FM", B.S.T.J., vol. 38, no. 6, pp. 1357-1426 (Nov. 1959).

[32] S.O. Rice, "Mathematical analysis of random noise", B.S.T.J., vol. 23, no. 3, pp. 282-332 (July 1944).

[33] "System 360 Scientific Subroutine Package Version III Programmer's Manual", IBM Corp., 4th ed. 1968, p. 291.

[34] D.P. Taylor, S.T. Ogletree and S.S. Haykin, "A prototype 60 Mb/s Fast Frequency-Shift keying modem", International Conference on Communications, Philadelphia, Penn., June 14-16, 1976, pp. 51.26 - 51.30.

[35] D.P. Taylor and S.S. Haykin, "Transmission tests of a 60 Mb/s Fast Frequency-Shift Keying modem on the CTS system", International Conference on Communications, Toronto, Canada, June 4-7, 1978, paper 19.3.

[36] V.M. Ray. Interpreting FCC broadcast rules and regulations. Blue Ridge Summit, Pa.: TAB Books, 1966.

[37] J.B. Anderson and D.P. Taylor, "Bandwidth efficient modulation and coding", Communications Research Laboratory, McMaster University, report no. CRL-55, 1978.

[38] S.T. Ogletree, D.P. Taylor and S.S. Haykin, "Design and implementation of a 60 Mb/s Fast Frequency-Shift Keying modem", Communications Research Laboratory, McMaster University, report no. CRL-30, March 1975.

[39] D.P. Taylor, G. Horvai and S.S. Haykin, "Laboratory test program for the CRL 60 Mb/s Fast Frequency-Shift Keying modem", Communications Research Laboratory, McMaster University, report no. CRL-36, May 1976.

[40] I.S. Gradshteyn and I.W. Ryzhik. Table of integrals, series and products. Academic Press 1965, 4th edition, eq. 1.342.1 and eq. 1.342.2.

[41] R.S. Burington. Handbook of mathematical tables and formulas. McGraw Hill 1973, 5th edition, eq. 314 and 322.

[42] P.H. Wittke, "The autocorrelation function of the output of a nonlinear angle-modulator", IEEE Trans. on Inf. Theory, vol. IT-10, no. 1, pp. 67-72 (Jan. 1964).